COMPUTATIONAL STUDY OF POLYMER MEMBRANES FOR PROTON AND ANION EXCHANGE MEMBRANES FUEL CELLS

A Dissertation
Presented to
The Academic Faculty

by

Khaldoon Emad Abu-Hakmeh

In Partial Fulfillment
of the Requirements for the Degree
Doctor of Philosophy in the
School of Chemical & Biomolecular Engineering

Georgia Institute of Technology
December 2016

COMPUTATIONAL STUDY OF POLYMER MEMBRANES FOR PROTON AND ANION EXCHANGE MEMBRANES FUEL CELLS

Approved by:

Dr. Seung Soon Jang, Advisor
School of Materials Science and Engineering
Georgia Institute of Technology

Dr. William J. Koros
School of Chemical & Biomolecular Engineering
Georgia Institute of Technology

Dr. Thomas F. Fuller, Advisor
School of Chemical & Biomolecular Engineering
Georgia Institute of Technology

Dr. Peter J. Ludovice
School of Chemical & Biomolecular Engineering
Georgia Institute of Technology

Dr. Paul A. Kohl
School of Chemical & Biomolecular Engineering
Georgia Institute of Technology

Date Approved: August 8, 2016

To the Sabrina Oukil, Amal Ileiwat, and Emad Abu-Hakmeh

ACKNOWLEDGEMENTS

I wish to thank Dr. Seung Soon Jang and Dr. Tom Fuller for their support, guidance, and critiques of this research work. Committee member Dr. Paul Kohl and his graduate students, Lisha Liu and John Ahlfield, are recognized for their collaborative efforts in providing the experimental data for the anion exchange membranes presented in Chapter 5. Dr. Chulsung Bae of Rensselaer Polytechnic Institute is thanked for his group's involvement in synthesizing and characterizing the membranes described in Chapter 4. The use of the Keeneland Computing Facility at the Georgia Institute of Technology and the support of the Korea Institute of Energy Research are also acknowledged for the work presented in Chapter 3.

The advice given by members of the Jang and Fuller Research Groups past and present has been invaluable. Special recognition is given to Giuseppe Brunello, Ben Chun, Parveen Sood, Dr. Kichul Kim, Tapesh Joshi, and Rajiv Jaini for their professional support and camaraderie.

Thanks are given to my entire family for their continued support and encouragement. I especially thank my parents, Amal and Emad, siblings, Ahmad, Tesneam, Jenan, and Yusuf, and wife, Sabrina, for their love and optimism during my studies. Major gratitude is also expressed to my friends, Arri Ciptadi, Fayaaz Khatri, Negad Zaky, Saeed Siddiqi, Iyed Bouchamaoui, Muhammad Doukmak, and Ismail Breiwish, for their support throughout the years.

TABLE OF CONTENTS

LIST OF TABLES

LIST OF FIGURES

LIST OF ABBREVIATIONS

AEMFC	Anion exchange membrane fuel cell
AEM	Anion exchange membrane
CN	Coordination number
DFT	Density functional theory
IEC	Ion exchange capacity
LAMMPS	Large-scale Atomic/Molecular Massively Parallel Simulator
MD	Molecular dynamics
MEA	Membrane electrode assembly
MSD	Mean squared displacement
NMR	Nuclear magnetic resonance
NPT	Isothermal-isobaric ensemble
NVT	Canonical ensemble
PCF	Pair correlation function
PEMFC	Proton exchange membrane fuel cell
PEM	Proton exchange membrane
RDF	Radial distribution function

LIST OF SYMBOLS

λ	Ratio of water to ionic groups
Å	Angstrom
$g_{\text{A-B}}$	Pair correlation of atoms A and B
ρ	Density
κ	Tunneling factor
ω	Frequency for zero point energy
N_{A}	Number of A atoms
$S(\mathbf{q})$	Structure factor
$\mathbf{q}$	Scattering vector
D	Diffusivity
d	domain spacing (nm)
ξ	Local density contrast
ϕ	Local density variable
Q	Atomic charge
F	Faraday's constant

SUMMARY

Proton exchange membrane fuel cells have been a long-standing subject of interest in the automobile industry owing to their high efficiency, clean operation, and compact design. Their adoption has however been limited due to the use of expensive catalysts, membranes, and assembly and the challenges of storing hydrogen as a fuel source. This study aims to address these issues by investigating hydrocarbon-based proton exchange membranes and anion exchange membranes.

The first objective was to investigate perfluorocarbon based polymer backbones. Nafion, considered the gold-standard PEM material, was used to establish benchmarks for phase-segregation and transport properties. To improve the understanding of Nafion, the hydrated membrane was subjected to uniaxial deformation to simulate the effect of the membrane being pressed between electrodes in operating conditions. The resulting water phase was found to be better developed in the direction perpendicular to the deformation than in the stretched direction.

The second objective was to investigate the use of hydrocarbon-based polymers for use in proton exchange membrane fuel cells. Polysulfone based polymers exhibited smaller water domain sizes compared to Nafion. However, the side-chain structures of these polymer structures can be modified, effectively altering the hydrophilic properties of the resulting polymer membrane. Four different side-chain structures were simulated. The side-chains with the largest size and degree of sulfonation exhibited the best phase separation and transport properties, approaching those of Nafion. The simplest of the four studied polysulfone-based membranes was subjected to the same deformation study as

Nafion, exhibiting a similar enhancement of transport properties in the direction perpendicular to stretching.

The third objective was to investigate anion exchange membranes. First, the structure-property relationship of a polysulfone-based AEM was compared to a PEM with the same backbone. The two membranes exhibited similar phase-segregated morphologies, with significantly lower ionic transport in the anion exchange model. To address the issue of lower transport, more highly segregated nanophase structures are studied. Novel highly fluorinated anionic conducting hybrid polymers are simulated and characterized. The simulations correctly reproduced experimentally observed structure and transport property trends. Additionally, our simulations may offer insight into the underlying mechanisms driving the formation of the nanophase-segregated morphology.

CHAPTER 1

INTRODUCTION

The development of safe, reliable, and clean energy sources has been an active area of research for much of the 21st century. Growing concerns about pollution and sustainability, along with political and economic objectives, have further thrust the issue into the public conscience. Renewable sources of electricity such as solar or wind power face a number of challenges. They require large land areas and capital investment, while offering variable output, posing further challenges for energy storage. This inhibits their ability to compete commercially with current energy technologies. Electrochemical energy sources offer an alternative to non-renewable technologies without the same storage requirements. Batteries and fuel cells in particular have received significant attention for their ability to provide clean electrical power on demand. Batteries however still require energy to be stored and recharged, which also limits their convenience when compared to current technologies, particularly for transportation applications. Fuel-cell technology provides the opportunity to harness an alternative fuel source while mitigating the need to an overhaul of our energy infrastructure.

Fuel cells operate with no pollutant emissions. The use of hydrogen fuel and low operating temperature eliminate the formation of carbon dioxide and mono-nitrogen oxides. Still, the widespread adoption of fuel-cell technology has been limited. Challenges include fuel source, cost of catalysts, membranes, and assembly. The synthesis of new ionomer membrane materials has aimed to address some of these challenges. The choice of membrane can impact the type of catalyst and fuel source

required for operation. Beyond proposing and synthesizing novel membrane materials, an improved understanding of the fundamental nature of polymer electrolyte membranes is necessary. This work aims to fill address this issue, with a focus on both traditional proton exchange membrane polymers and more newly pursued anion exchange membrane polymers.

Fuel Cells

A simple fuel cell operates by oxidizing a fuel, such as hydrogen, to produce electricity and water. Initial fuel cells were used to generate power for space applications. Since, fuel cells have found applications as power sources for commercial, residential, and industrial buildings. To a lesser extent, fuel cells have also been used to power vehicles.

However, several limitations have hindered widespread adoption of fuel cells. Expensive membranes and catalysts, along with difficult hydrogen fuel storage and poor durability have prevented fuel cells from capturing a position in the transportation market. To allow fuel cells to compete within the transportation sector, lower costs and improved performance are necessary. With the increased attention and funding of fuel cell research several types of cells have received consideration. Polymer electrolyte membrane fuel cells (PEMFC) have received extensive attention for transportation applications. This is due to their solid organic polymer membrane, allowing for high specific energy and power, transportable size, and ability to operate at ambient temperatures.

Within the class of polymer electrolyte membrane fuel cells, two subclasses have been investigated. Proton exchange membrane fuel cells (also PEMFC) have received

most of the initial attention due to their high ionic transport properties, allowing for high power densities. Yet a number of factors, discussed in the following section, have limited their viability. Alternatively, alkaline anion exchange membrane fuel cells (AAEMFC or AEMFC) have begun to receive more consideration. Both PEMFCs and AEMFCs are discussed in more detail below.

Proton Exchange Membrane Fuel Cells

Proton exchange membrane fuel cells operate at moderate temperatures in comparison to others, such as solid oxide fuel cells. The primary role of the proton exchange membrane (PEM) is to separate the fuel and oxidizer compartments, while allowing protons to flow from the anode to the cathode. Internally, the PEM requires some level of hydration to conduct protons. As the polymer backbone is hydrophobic and the side chains are hydrophilic, the morphology separates into two phases. The hydrophilic phase, essential for proton transport, consists of interconnected water channels surrounding the acid groups. The complementary hydrophobic phase dictates membrane selectivity and mechanical stability. The morphology and separation of the two phases is largely determined by the ionomer. Nafion, developed by DuPont, has long been the standard for PEM fuel cells. The structure of Nafion is based on perfluorosulfonic acid. Despite high proton conductivity and mechanical stability, Nafion is costly and exhibits high fuel crossover when used with methanol. A number of ionomers have since been developed and investigated to replace Nafion, but none has yet completely succeeded.

Anion Exchange Membrane Fuel Cells

Anion exchange membrane fuel cells operate similarly to PEMFCs, but instead of conducting protons, they transport hydroxide ions in the opposite direction, from the cathode to the anode. The polymer backbones can be similar to those of PEMs, but contain cations instead of the sulfonic acid groups found in PEMs. Quaternary ammonium groups are typically used for this task. AEMFCs offer the potential to surpass their PEM counterparts as they avoid some of the limitations. Specifically, they are cheaper, as AEMFCs do not require the use of expensive catalysts due to their faster electrode reaction kinetics. AEMFCs experience lower corrosion, and are more robust to fuel sources, such as methanol and higher alcohols. The fuel versatility of AEMFCs is also advantageous, as alcohol fuels can be stored easier than hydrogen.

Despite the advantages of AEMFCs, some challenges remain before they achieve the same level of attention as PEMFCs. Notably, poor ionic conductivity due to lower anion diffusion rates is among the biggest issues in AEM research. This work aims to apply computational methods and strategies similar to those that have been success fully applied to investigating PEMs to examine novel AEM materials and elucidate the structure and transport properties of current membranes.

Present Contribution

The present study aims to study several types of membranes with respect to their suitability for use in polymer electrolyte fuel cells. First, Nafion is studied in the context of characterizing the effect of mechanical deformation of performance. This is performed to understand the nano-scale effects of deformation on performance, as polymers are squeezed between plates in a membrane electrode assembly (MEA). These simulations of

Nafion also set a benchmark for comparison with other membranes also subjected to the same deformations. Next, hydrocarbon-based membranes with varying side-chain pendants are studied. Last, anion exchange polymer membranes are compared to proton exchange polymer membranes and novel anion exchange membranes are also characterized. All of the mentioned studies are performed in view of creating a better understanding of the nano-scale structure-property relationships at play in polymer electrolyte membranes. The overall objective is to assist in informing experimental design of better-performing membranes for future fuel-cell technologies.

CHAPTER 2

SIMULATION AND ANALYSIS METHODS

Simulations

Molecular dynamics (MD) simulations have been successfully applied to study PEMs by a number of groups.[1-20] Here, all planned simulations will involve full-atomistic models of PEM and AEM systems. The simulations will be performed using the LAMMPS (Large-scale Atomic/Molecular Massively Parallel Simulator)[21, 22] MD software from Sandia National Laboratories, modified to handle the DREIDING force field.[4, 23]

Analysis

Structure and transport property characterization is necessary for useful analysis following MD simulation. In this work, relevant characteristics include local structures, nanophase-segregation, and diffusivity of water and ions. This section briefly describes characterization methods commonly used in MD studies and our own work. Newer methods and more detailed analyses are discussed in the later chapters.

Local Structure and Solvation

A radial distribution function (RDF) characterizes the local structure surrounding individual species and provides insight into the extent of solvation of important moieties, such as the sulfonate (PEM) or quaternary ammonium (AEM) groups. Shown in Equation 1, the pair correlation function $g_{A-B}(r)$ indicates the relative probability of finding *B* atoms at a distance *r* from *A* atoms, averaged over the equilibrium trajectory.

$$g_{A-B}(r) = \left(\frac{n_B}{4\pi r^2 \Delta r} \right) \Big/ \left(\frac{N_B}{V} \right) \qquad (1)$$

Specifically, n_B is the number of *B* particles located at a distance *r* from particle *A* in a shell of thickness Δr. N_B is the total number of *B* particles in the system, while *V* is the system volume. From the RDF, several useful conclusions can be drawn. Assuming only pairwise interactions between atoms, the thermodynamic properties of the system can be calculated. The structure factor can also be calculated as the Fourier transform of the RDF. Additionally, the coordination number, signifying the number of *B* atoms surrounding atom *A* can be calculated by integrating the RDF radially, as shown in Equation 2. The integration limits are defined as the minima surrounding given peaks in the RDF.

$$CN = \int_0^{r_0} 4\pi\rho g(r) r^2 \, dr \qquad (2)$$

The area of the peak, representing the coordination number, describes the solvation shell of *B* atoms, like water, around species *A*, like sulfonate or ammonium.

Transport and Diffusion

Mean Squared Displacement

Efficient fuel cell operation is reliant on facile transport of ions through the polymer membrane. For macroscopic analysis, ion conductivity, water diffusivity, and electro-osmotic drag describe the relevant transport properties for a given polymer membrane. In MD simulation, the simplest assessment of transport properties can be achieved by measuring the movement of ions over the course of an equilibrium MD

simulation. Similar study of the movement of water is also indicative of ion transport if ions are well solvated. The mean squared displacement, (MSD) defined as the ensemble average of the square of displacement as a function of time, is commonly used in MD simulation to calculate transport properties. The MSD is calculated over the time interval $dt_0 \leq dt \leq dt_{max}$. The anisotropic MSD is calculated using the following algorithm:

$$MSD(dt) = \frac{\sum_{t=0,T-dt,s} \sum_{i=1,N} \left| r_i(t+dt) - r_i(t) \right|^2}{\sum_{t=0,T-dt,s} (N)} \qquad (3)$$

Where *s* is the time origin step, N is the number of particles, T is the length of the trajectory, dt_0 is the single frame interval, dt_{max} is the maximum MSD time, and *r(t)* are the coordinates at time *t*. Individual components of the MSD are calculated using only the relevant components of the coordinate vectors. This provides the six components of the MSD, in addition to the isotropic average. The diffusion coefficient, *D*, is obtained from the linear region of the MSD from the limit in Equation 4.

$$D = \lim_{t \to \infty} \frac{1}{6t} \left\langle \left(r(t) - r(0) \right)^2 \right\rangle \qquad (4)$$

Here, $r(t)$ and $r(0)$ are the positions of a water molecule at time *t* and the beginning of the simulation. The diffusion constant is proportional to the slope of the linear asymptote of the MSD plot. For 3D diffusion, the proportionality constant is 6. For 2D diffusion, the proportionality constant is 4. This treatment of transport is inherently simple and only accounts for vehicular diffusion.

Grotthuss Mechanism

Further to the vehicular diffusion of protonated water (hydronium), protons also hop along sequences of proximate water molecules through Grotthuss diffusion. The Grotthuss mechanism has also been proposed as a possible method of transport for hydroxide in the anion exchange membrane.[24-26] Several methods have been developed to calculate the contribution of Grotthuss diffusion in simulated membranes, which requires calculating the forces required to break and form bonds. This has been demonstrated using quantum mechanics,[27, 28] reactive force fields,[29, 30] multistate empirical valence bond models[31], and by several other methods.[16, 31-36] However, such methods need to be carefully selected, as the proposed systems are too large for quantum methods and not parameterized for use with reactive force fields.

Calculating the diffusion coefficient of the hopping mechanism required a quantum mechanical approach. The dynamic evolution of the intermolecular distances between water molecules affects proton conduction. Thus, quantum mechanical transition state theory (TST) is used as shown in the following equation:

$$k_{ij}(r) = \kappa(T,r)\frac{k_B T}{h}\exp\left(-\frac{E_{ij}(r) - 1/2h\omega(r)}{RT}\right) \qquad (5)$$

Here, κ(T,r) and ω(r) are the tunneling factor and the frequency for the zero point energy correction. These values are obtained from previous publications in literature.[37, 38] E(r) is the energy barrier for a proton to be transferred from donor to acceptor in water at a distance r. The proton hopping energy barrier is calculated for fixed distances between donor-acceptor oxygen pairs by quantum mechanics. This establishes the energy

distribution as a function of distance between the donor-acceptor pair. The Poisson-Boltzmann self-consistent reaction field model is used to correct the effect of the solvent, before the energy barrier is recalculated.[39, 40] Using the tunneling results and the donor-acceptor pair distances, the proton hopping diffusion coefficient is obtained from the following equation:

$$D_{hopping} = \frac{1}{6Nt} \int_0^{t\to\infty} \sum_i^N \sum_j^M k_{ij} r_{ij}^2 P_{ij} dt \qquad (6)$$

Here, N is the number of protons and P_{ij} is the probability that a proton will jump from hydronium ion i to water j. The distance of the donor-acceptor pairs is determined from the MD simulation trajectory at equilibrium and defined as r_{ij}. The calculated hopping diffusivity, added to the previously described vehicular diffusivity, gives the proton diffusivity. The total diffusivity can then be used to calculate the ionic conductivity.

Conductivity

Ionic conductivity for either protons or hydroxide anions is calculated using the Nernst-Einstein equation as shown below:

$$\sigma = \frac{D_{ion,total} c z^2 F^2}{RT} \qquad (7)$$

The ion concentration and charge are denoted by c and z, respectively. F and R represent the Faraday and gas constants. T is the temperature in Kelvin.

Nanophase-Segregation and Water Channels

Structure Factor

Nanophase-segregation describes the extent of separation between the hydrophilic and hydrophobic components of the hydrated polymer membrane. In PEMs, the extent of nanophase-segregation largely affects the ionic transport. Increased segregation generally corresponds to more developed water channels, leading to better transport of both water and protons. Transport in AEMs is expected to be analogous to PEMs. Prior to developing any novel understanding of transport in AEMs, assessing the extent of separation alongside PEMs is important in understanding any possible dependence. Thus, a highly segregated and well-defined water phase should correlate with facile water and ionic transport.

To characterize nanophase-segregation, the structure factor is calculated as shown in Equation 8. Here, the angular brackets denote a thermal statistical average. ξ^i represents a local density contrast, $\mathbf{q}$ is the scattering vector, $\mathbf{r}_{ij}$ is the vector between two species *i* and *j*.

$$\mathbf{S}(\mathbf{q}) = \left\langle \sum_{r_i} \sum_{r_j} \exp\left(i\mathbf{q}\cdot\mathbf{r}_{ij}\right)\left(\xi^i\xi^j - \langle\xi\rangle^2\right) \right\rangle \Big/ L^3 \qquad (8)$$

Commonly used in small angle scattering experiments, (SAXS and SANS) the structure factor has been used computationally to characterize polymers,[41, 42] including hydrated polymer membranes. [4, 8, 12, 20] Though experimental use of the structure factor measures the electron density contrast or deuterium density contrast, the computational application introduces an artificial density contrast to determine whether a

site is occupied by a hydrophilic or hydrophobic entity. The structure factor is spherically averaged as shown in Equation 9.

$$S(q) = \sum_{|\mathbf{q}|} \mathbf{S}(\mathbf{q}) \Big/ \sum_{|\mathbf{q}|} 1 \qquad (9)$$

Here, $q = (2\pi / L)n$, where n = 1, 2, 3, L denotes for given n, a spherical shell $n - 1/2 \le qL/2\pi \le n + 1/2$. Practically, the maximum peak of the structure factor profile gives the characteristic correlation length, corresponding to the extent of nanophase-segregation. It is important to note that due to the periodicity of simulated systems, the structure factor profiles are only considered for q values greater than 1.

Anisotropic Structure Factor

The general expression above calculates the structure factor of an isotropic structure from the Fourier transform of the RDF. This version is a spherically averaged measure of particle arrangement in real space. However, in non-cubic systems, the development of anisotropic features is expected. To evaluate these features, the structure factor must be calculated along the direction specific reciprocal space vectors, **k**. The simplest directions to evaluate are (100), (010), and (001). The anisotropic structure factor is computed from the following equation:

$$S(\mathbf{k}) = \frac{\left\langle \sum_{i=1}^{N} \sum_{j=1}^{N} \exp(-i\mathbf{k}\mathbf{r}_i) \exp(i\mathbf{k}\mathbf{r}_j) \right\rangle}{N} \qquad (10)$$

Here, **k** is the scattering vector, $\mathbf{r}_i$ and $\mathbf{r}_j$ are the position vectors of atoms i and j, and N denotes the number of atoms. The angular brackets denote an ensemble average.

CHAPTER 3

PERFLUOROCARBON BASED PROTON EXCHANGE MEMBRANES

The work presented here was published in Materials Performance and Characterization.[43]

The deformation of hydrated Nafion 117 is implemented using full-atomistic molecular dynamics simulation method to elucidate how the mechanical deformation affects the structure and transport of hydrated Nafion membrane. First, Nafion 117 membrane is equilibrated with 20 weight percent water content through an annealing procedure. The simulated characteristic correlation length and the diffusion coefficient of water and hydronium ions are analyzed for comparison with those observed in experiments. Then, the equilibrated Nafion membrane is deformed uniaxially up to 300% of strain with a constant strain rate. The change in nanophase-segregation of hydrated Nafion during the deformation process is characterized using a directional structure factor as well as the pair correlation function in order to achieve fundamental understanding of the relationship of such structural change as a function of strain with the proton transport. It is found from the pair correlation analysis that the sulfonate distribution and sulfonate-hydronium correlation becomes stronger through the deformation while the hydronium ion solvation and the internal structure of water phase are not dependent on the deformation. From the directional structure factor profile, it is found that the long-range correlation is developed in the perpendicular direction to the extension. In the initial study, the diffusion of water and hydronium ions were enhanced by 30 % and 2 %,

respectively, after the deformation. To better understand the effect of deformation on proton transport, an extended equilibrium simulation was carried out before and after the stretching. The directional components of the diffusion were also considered. In the extended simulation, the vehicular diffusivities of water and hydronium ions were improved by 32 % and 12 %, respectively, following uniaxial deformation. The directional diffusivity was also found to depend on the direction of drawing. The diffusivity of water parallel to the draw direction was found to decrease by 1 % while improving by 42 % in the through-plane directions.

Introduction

Proton exchange membrane (PEM) fuel cells have been subject to extensive study as alternative powers sources to thermal devices that combust non-renewable fuels.[44-49] Specifically, Nafion (Figure 1has been studied extensively as a candidate material for PEMFC applications. The choice of Nafion is attributed to its high proton conductivity, desirable thermal, chemical, and mechanical stability. However, high cost, efficiency, and durability have hindered the widespread use of Nafion in PEM fuel cells.

Experimental studies have attempted to improve the performance of Nafion in PEM fuel cells by physical or chemical treatment methods.[50] In particular, the uniaxial pre-stretched treatment of recast Nafion shows 33-48% higher power densities compared to Nafion 117 in direct methanol fuel cell operation, along with reduced methanol permeability,[51] suggesting further investigation into the underlying mechanism for the improved performance could provide better understanding of Nafion in the context of PEM fuel cell applications. The study claims the difference in methanol permeability is associated with the morphology difference in the stretched membranes. Rod-like polymer

aggregates, present in Nafion solution, may be better aligned prior to elongation, and thus, improve the stretched membrane nanostructure, with fewer molecular-level defects, better polymer chain packing, and greater polymer crystallinity following annealing.[51]

Molecular dynamics simulations have been successfully used to study PEM systems.[2, 4, 8, 12, 13, 15-18, 20, 52-55] Although molecular dynamics does not allow for a full-scale study of fuel cell operation, it has provided detailed molecular level information on the nanophase-segregated structure and proton transport in PEMFC systems. Previous studies have used molecular dynamics (MD) simulation techniques to characterize polymer electrolyte membranes including Nafion,[4] Dendrion,[16, 20] S-PEEK,[8, 12] sulfonated polystyrene,[54] and sulfonated sulfone.[55] These studies have mainly focused on elucidating the relationship between nanophase-segregation and transport properties, whose primary conclusion was that proton conduction improves as a function of nanophase-segregation, due to the prevalence of well-developed water channels with a tight hydrogen-bonding network. Similarly, MD simulations should also be able to characterize the nature of the nanophase-segregation and transport properties in uniaxially stretched Nafion. Previously, the effect of uniaxial stretching has been studied using coarse-grained molecular dynamics simulation.[56] In this context, the conductivity was found to increase in the direction of stretching, while hydrophilic regions were elongated in the same direction and side-chains oriented perpendicular to the stretching axis.[56] To our knowledge, however, no further computational study has been implemented to examine the mechanical deformation treatment of Nafion in the context of PEM fuel cells. Additionally, no study implementing mechanical deformation via full-atomistic MD has been found.

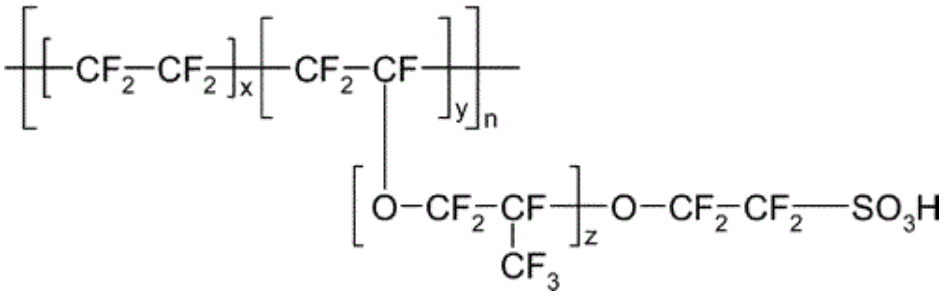

Figure 1: Chemical structure of Nafion polymer (x = 7, y = 1, and z = 1).

In this study, full-atomistic MD simulations were performed to investigate the effect of uniaxial deformation on the nanophase structure and transport properties of Nafion. For this, the strain of 300 % was induced onto amorphous phase of Nafion with 20 wt. % of water content. Our focus is on characterizing 1) the structural change in nanophase-segregation and 2) the corresponding change in transport properties in the membrane.

Modeling and Simulations

All simulations were carried out using fully atomistic models consisting of 1100 EW Nafion, water, and hydronium ions. The composition of the Nafion system is summarized in Table 1.

Force Field and Simulation Parameters

We used the DREIDING force field [23] to describe the intramolecular and intermolecular forces in the hydrated Nafion membrane. The force field is the same as previously used to study Nafion,[4] Dendrion,[16, 20] S-PEEK,[8, 12] sulfonated polystyrene,[54] and sulfonated sulfone,[55] as well as various molecular systems.[57, 58] Water was described using the F3C force field.[59] The force field for hydronium ion has been used since it was developed for the simulation study of the hydrated Nafion 117

membrane.[4] The force field parameters used are the same as reported in their original papers.[23, 59, 60] The DREIDING force field has the form:

$$E_{total} = E_{vdW} + E_{Q} + E_{bond} + E_{angle} + E_{torsion} + E_{inversion} \qquad (11)$$

where E_{total}, E_{vdW}, E_{Q}, E_{bond}, E_{angle}, $E_{torsion}$ and $E_{inversion}$ are the total, van der Waals, electrostatic, bond stretching, angle bending, torsion and inversion energy components, respectively. The individual atomic charges were assigned through Mulliken population analysis using B3LYP and 6-31G** in Jaguar.[61] Electrostatic interactions were calculated using the Particle-Particle Particle-Mesh (PPPM) method.

Table 1: Composition of hydrated Nafion 117 system and simulation conditions

Polymer	**Nafion (PEM)**
Molecular weight (Number of monomeric unit/chain)	11473 (10)
Equivalent weight	1147.3
Number of sulfonate	10/chain
Number of atoms	18728
Water content (wt %)	20
Number of water molecule	2392
Number of water molecule/sulfonate (λ_S)	15
Density (g/cm^3) at 353.15 K	1.62
Number of chains	16
System dimension (a=b=c)	61.86 ± 0.09 Å

Model Construction and Equilibration

Hydrated Nafion 117 membranes consisting of 16 chains were constructed with 20 wt % of water content. The total number of atoms was 18728 and the number of water molecules and hydronium ions were 2392 and 160, respectively. The initial Nafion structure was built using the Amorphous Builder module in the Cerius2 software package.[62] Since this initial structure may contain unstable confirmations, the initial structure of amorphous Nafion membrane was equilibrated using the annealing procedure as previously used for various membranes.[4, 8, 12, 16, 20, 54, 55] The annealing procedure utilizes a systematic variation of the temperature and volume to accelerate the equilibration of the structure. Please refer to the reference[4] for detailed information of the annealing procedure.

Molecular Dynamics Simulations

Full-atomistic MD simulations were performed using LAMMPS (Large-scale Atomic/Molecular Massively Parallel Simulator)[22] software developed by Sandia National Laboratory, with modifications to handle the DREIDING force field. The equations of motion were integrated using the Verlet algorithm[63] with a time step of 1.0 fs. The Nose-Hoover thermostat[64, 65] for the isothermal-isobaric ensemble (NPT) simulations used a damping relaxation time of 0.1 ps and a dimensionless cell mass factor of 1.0. In this study, the equilibrium MD simulations were conducted to equilibrate the structure before and after the deformation.

The non-equilibrium MD simulation of uniaxial deformation was performed to investigate the effect of deformation on the nanophase-segregated structure and transport properties of Nafion 117. The uniaxial deformation was applied up to 300 % strain at

T=353.15 K for 1 ns, indicating that the strain was applied uniformly across the simulation box with the constant strain rate of 0.000186 Å/fs, and correspondingly the atomic coordinates were rescaled to the new box dimensions at each time step. This procedure was employed for the uniaxial deformation in x, y and z-axis directions independently. As the strain of 300 % was used in experimental study,[66] we also employed the same strain for comparison. Following the 1 ns deformation simulation, each system was allowed to equilibrate for 5 ns via NPT. The results from each direction were statistically averaged. The initial and final structures of the hydrated Nafion membrane are shown in Figure 2.

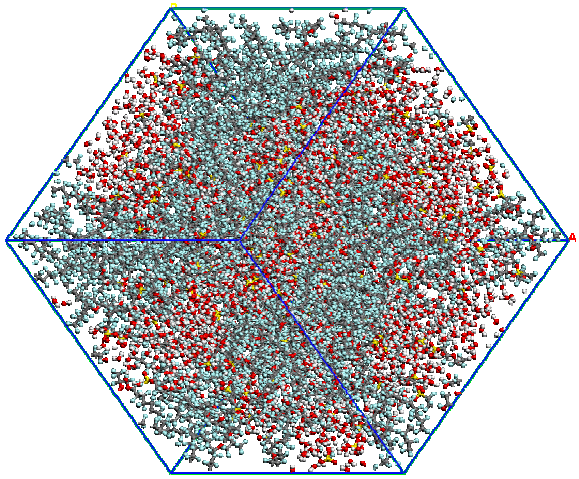

(a) Initial structure

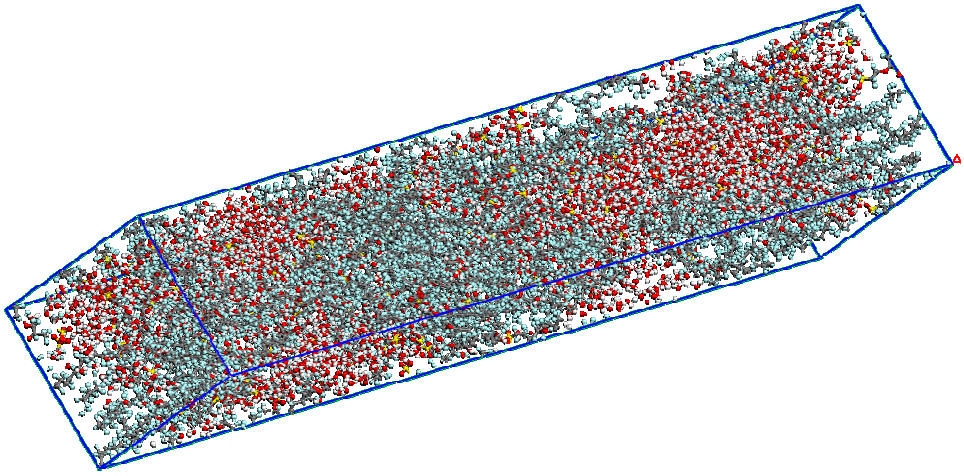

(b) Deformed structure

Figure 2: Simulated Structure of hydrated Nafion 117 membrane (a) before deformation and (b) after uniaxial deformation with 300% strain deformation in z-axis direction. Gray and green colors denote carbon and fluorine, respectively, and red and white colors denote oxygen and hydrogen, respectively.

Results and Discussion

Nanophase-Segregated Structures

Distribution of Sulfonate Groups

Proton transport in polymer electrolyte membranes occurs as hydronium cations diffuse through the water channels. The water channels in Nafion have been previously characterized[4] and determined to be more conducive for proton transport as the channels become more connected and its internal structure approaches that of bulk water phase. The structure of water channels remains critical to the proton transport in stretched Nafion. Thus, the effect of mechanical deformation on the internal structure of water channels is one of the primary interests in this study. Here, we consider the sulfonate groups of the Nafion as an essential factor in determining the nanophase-segregation in the hydrated membrane since water molecules should gather around the hydrophilic sulfonate groups to solvate them, and thereby form water channels. To investigate the

distribution of the sulfonate groups, we calculate the pair correlation function (PCF) that is a time-averaged probability of finding sulfonate groups at a distance *r* from a sulfonate group:

$$g_{S-S}(r) = \left(\frac{n_S}{4\pi r^2 \Delta r} \right) / \frac{N_S}{V} \qquad (1)$$

where n_S is the number of sulfonate groups located at a distance *r* in a shell of thickness Δr from a sulfonate group, N_S is in the total sulfonate groups in the system, and *V* is the total volume. For direct comparison, the quantity of $g_{S-S}(r)$ is multiplied with the number density of sulfonate group (ρ_S) in a unit cell system.

Figure 3 shows the pair correlation of the sulfonate group pair, $g_{S-S}(r)$, before and after the deformation of Nafion. The sulfonate-sulfonate PCF shows a broad peak ranging from approximately 5-10 Å both before and after the deformation, suggesting that the sulfonate groups are likely to be found near each other at a higher relative probability for this range of distances. While the overall profiles show a similar trend, the maximum peak positions differ. The undeformed structure shows a PCF peak around 8 Å while the deformed structure has larger intensity at 5-7 Å and at 10-15 Å, indicating that the distances among sulfonate groups becomes diversified more as the membrane is uniaxially stretched. The sulfonate-sulfonate PCF showed good agreement with both profile shapes and peak locations reported in previous studies.[4, 10, 18, 52] Furthermore, the profiles and peak locations of the other PCFs reported in this study show similar agreement with literature.

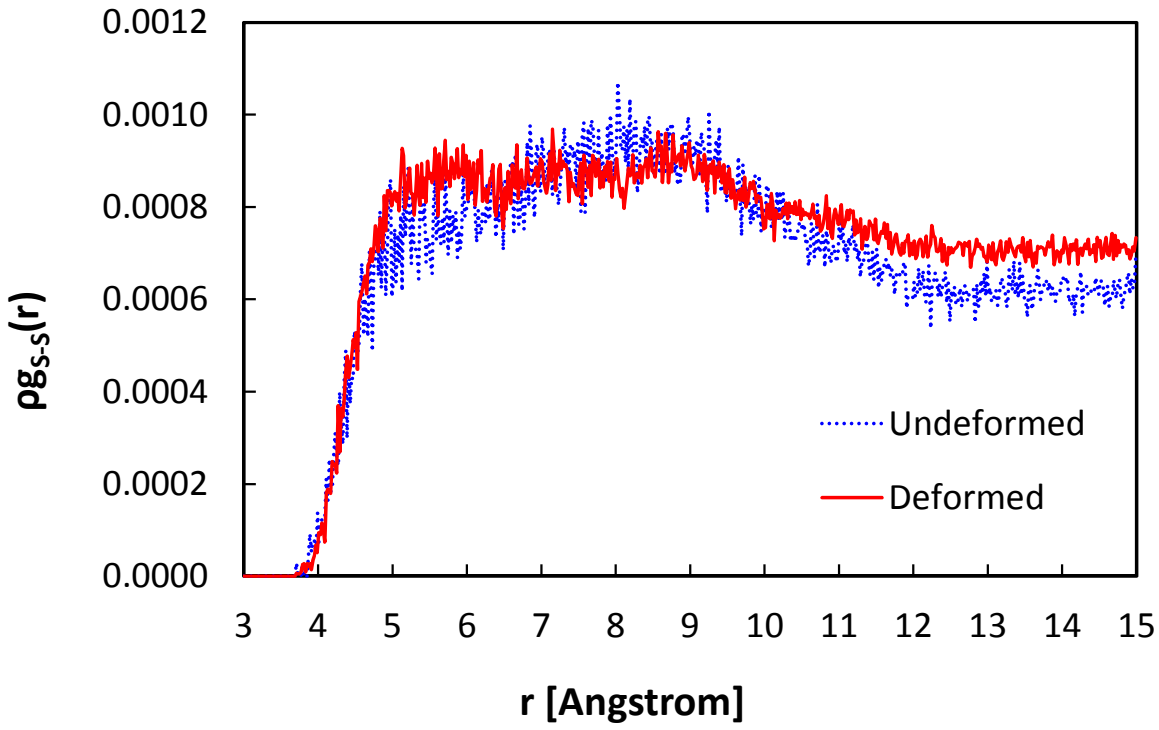

Figure 3: Pair correlation function of sulfur-sulfur, $\rho g_{S-O(water)}(r)$, in hydrated Nafion.

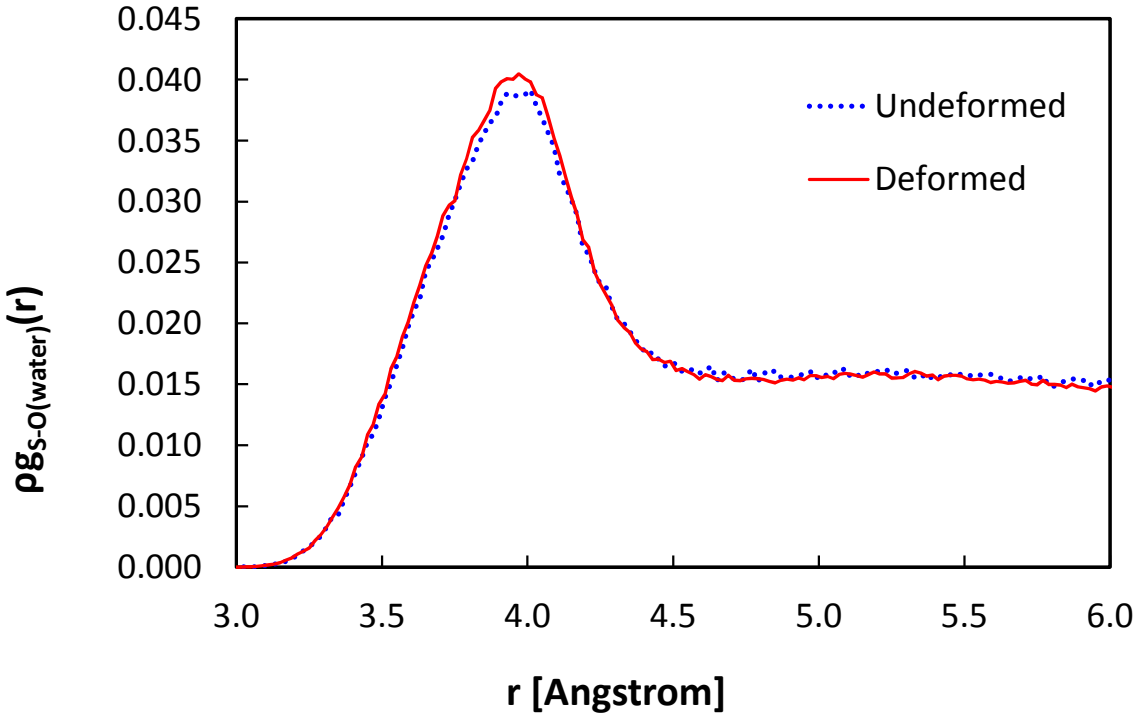

Figure 4: Pair correlation function of sulfur-oxygen, $\rho g_{S-O(water)}(r)$, in hydrated Nafion.

Solvation of Sulfonate

The effect of deformation on the solvation of the sulfonate groups of Nafion can be studied using the PCF of the sulfur (sulfonate) - oxygen (water) pair, $\rho g_{S-O(water)}(r)$, shown in Figure 4. The first solvation shell is ranged from 3.0 Å to 4.75Å, observed both prior to and following deformation. The two distribution profiles similarly exhibit a significantly smaller second peak at 5.25 Å. The identical peak position of PCF indicates that the deformation does not affect the strength of the molecular interaction between the hydrophilic sulfonate groups and the water molecules. However, the peak intensities of the two distributions show slight difference, presenting that the sulfonate groups in the deformed membrane are more solvated by water compared to those in the undeformed membrane. The higher intensity implies a greater probability of a water molecule being located at a particular distance from a sulfonate group. To quantify this observation, the coordination number (CN) is calculated by integrating the first solvation shell of the sulfonate group (Figure 4). From Table 2, it was found that the water CN of sulfonate group in the deformed membrane (6.91) is slightly larger than that in the undeformed membrane (6.79). We think this difference might be caused by the closer proximity of the sulfonate groups after the deformation.

Table 2: Coordination numbers

	Nafion
Model	**S - O (H_2O)**
	CN (S)
Undeformed	6.79

Deformed	6.91

Model	**O (H_3O^+) - O (H_2O)**
	CN (H_3O^+)
Undeformed	3.45
Deformed	3.44

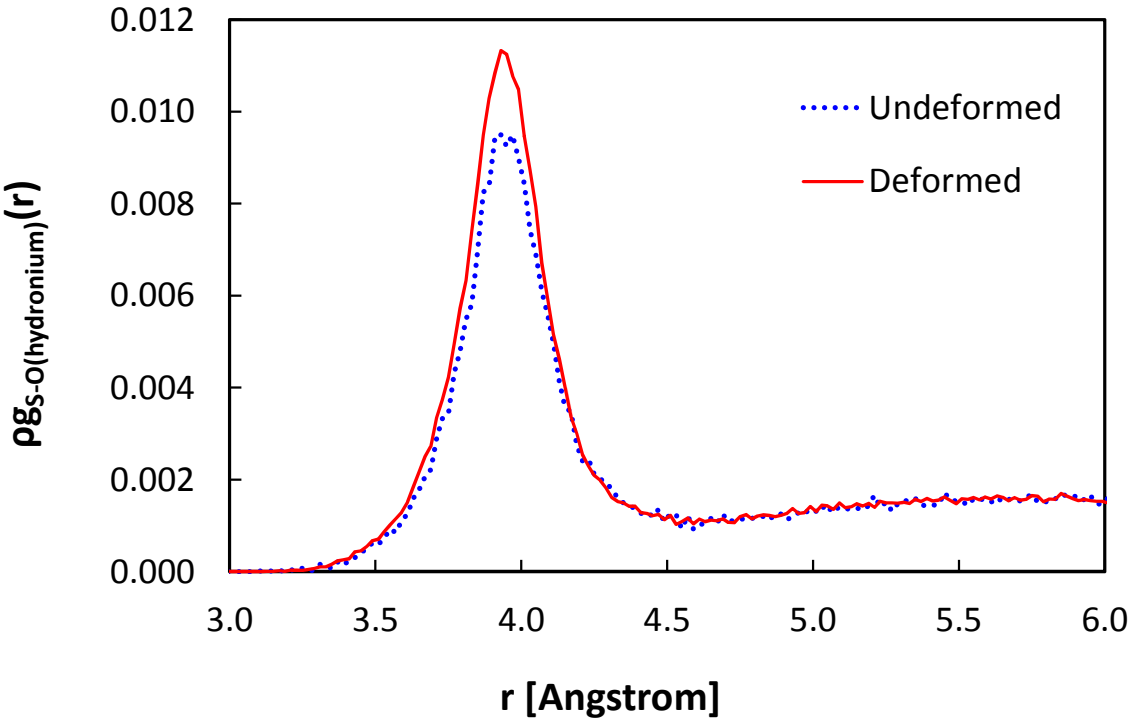

Figure 5: Pair correlation function of sulfur-oxygen, $\rho g_{S-O(hydronium)}(r)$, in hydrated Nafion.

Correlation between Sulfonate and Hydronium Ions

The PCF of the sulfonate-oxygen (hydronium) pair, $\rho g_{S-O(hydronium)}(r)$ is also analyzed (Figure 5) both before and after the deformation, showing that the primary peak is located at ~4.0 Å. It is found that the deformed system has stronger correlation between sulfonate and hydronium ions while the curves overlap for the remainder of the

profile outside of the primary peak area. Considering that $\rho g_{S-O(hydronium)}(r)$ is similar when the sulfonate groups are solvated by water to a similar extent, this is not an expected result. We think that a clue can be found from the previous analysis for $\rho g_{S-S}(r)$: since the sulfonate groups gather closely, the hydronium ions would also get correlated with other sulfonate groups. In order to confirm this explanation, we need to analyze the solvation of the hydronium ions with water, discussed immediately below.

Solvation of Hydronium Ions

As mentioned in the discussion of the sulfonate-hydronium pair correlation, we need to investigate the solvation of hydronium ions by water for a complete understanding of the behavior of hydronium ions in the deformed Nafion membrane. Figure 6 shows that $\rho g_{O(hydronium)-O(water)}(r)$ is very similar at the peak position (~2.6 Å) before and after the deformation, which is confirmed quantitatively by the water CN of hydronium ions: 3.45 and 3.44 for the undeformed and the deformed membrane, respectively. This result indicates that the hydronium ion solvation is not affected by the deformation, which is a strong evidence that the enhancement of $\rho g_{S-O(hydronium)}(r)$ is just due to the enhanced proximity of sulfonate groups. If not, the solvation of hydronium ions would be reduced as $\rho g_{S-O(hydronium)}(r)$ becomes enhanced.

Internal Structure of Water Phase

Internal structure of the water phase in hydrated polymer membranes is of critical importance to proton transport. This has been established by previous studies, confirming that improved connectivity of the hydrophilic phase leads to better proton transport, approaching the behavior observed in bulk water. The proton transport is partially aided

by the hydrogen-bonding network that is less developed in hydrated membranes in comparison to the bulk water phase.[67-72] Figure 7 shows that the PCF of the water-water pair is not sensitive to the mechanical deformation of the membrane: the peak position is identical (~2.8 Å), indicating that the water phase holds a very similar local structure via the deformation.

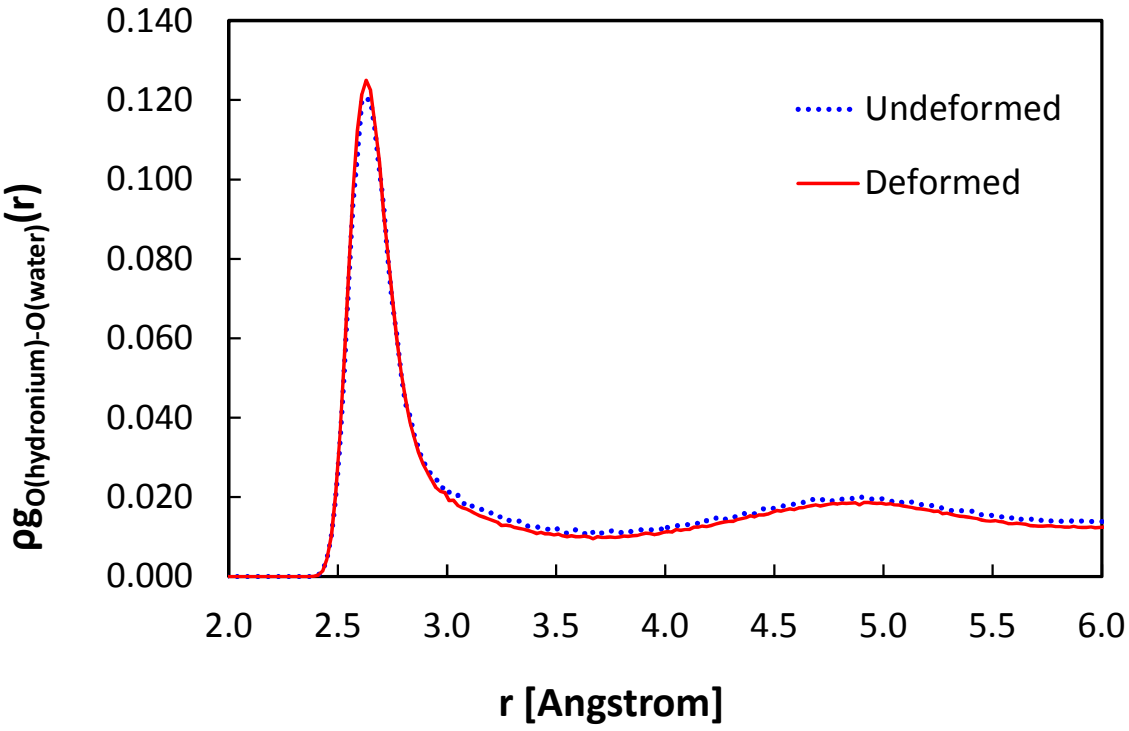

Figure 6: Pair correlation function of oxygen-oxygen, $\rho g_{O(hydronium)-O(water)}(r)$, in hydrated Nafion.

One of the factors affecting the local structure in the water phase would be the composition of the system. Since the composition of the hydrated membrane is the same before and after the deformation, this simulation result means that the water phase holds its internal hydrogen bonding network to the same level although the water channels are rearranged during the deformation. The water CN is calculated as 4.01 and 3.98 for the

undeformed and the deformed membrane, respectively, which is smaller than the water CN (4.5) for the bulk water.

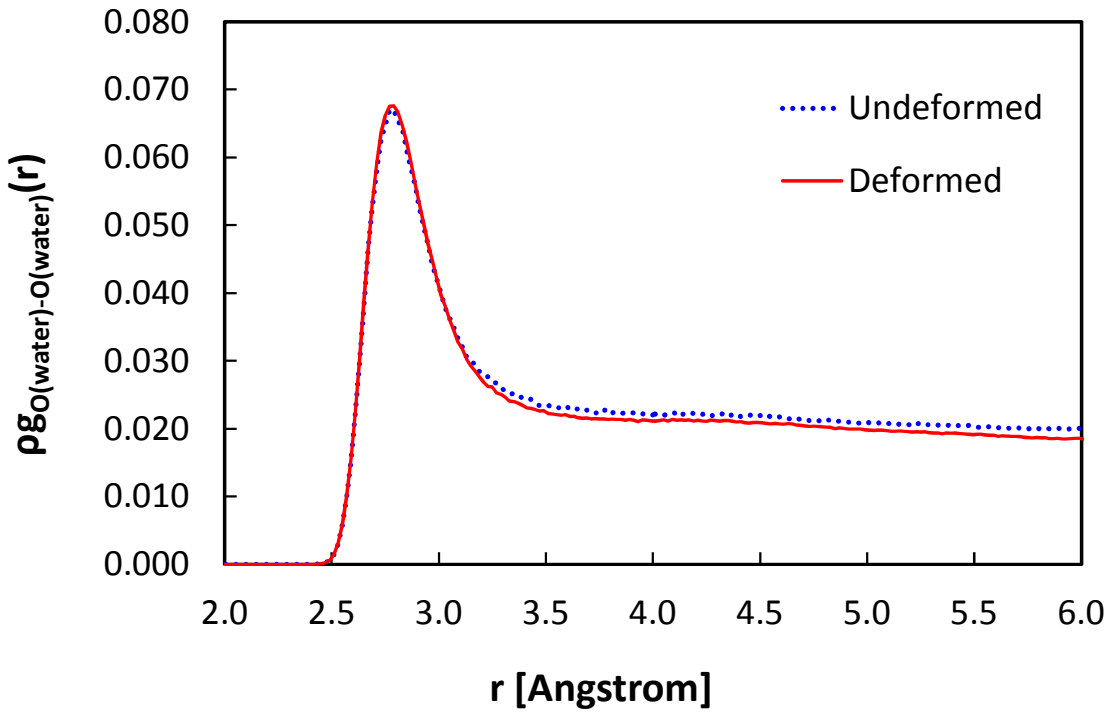

Figure 7: Pair correlation function of oxygen-oxygen, $\rho g_{O(water)-O(water)}(r)$, in hydrated Nafion.

Extent of Nanophase-Segregation

The nanophase-segregation of the hydrated polymer membrane describes the extent to which the hydrophilic and hydrophobic phases are separated. As the nanophase-segregation proceeds, the water phase develops its internal structure more with better hydrogen bonding network. There has been a consensus that a greater extent of nanophase-segregation is desired to facilitate the proton transport. Therefore, it is crucial to quantitatively characterize the effect of mechanical deformation on the nanophase-segregation of Nafion. For this, the structure factor,[73] $S(\mathbf{k})$ is calculated as a function of **k** vector from the Fourier transform of the pair correlation, which is defined as[74]

$$S(\mathbf{k}) = \frac{\left\langle \sum_{i=1}^{N} \sum_{j=1}^{N} \exp(-i\mathbf{k}\mathbf{r}_i) \exp(i\mathbf{k}\mathbf{r}_j) \right\rangle}{N} \qquad (10)$$

where $\mathbf{k}$ is the scattering vector, $\mathbf{r}_i$ and $\mathbf{r}_j$ are the position vectors of atoms i and j, respectively, and N denotes the number of atoms. The angular bracket in Equation 10 means an ensemble average.

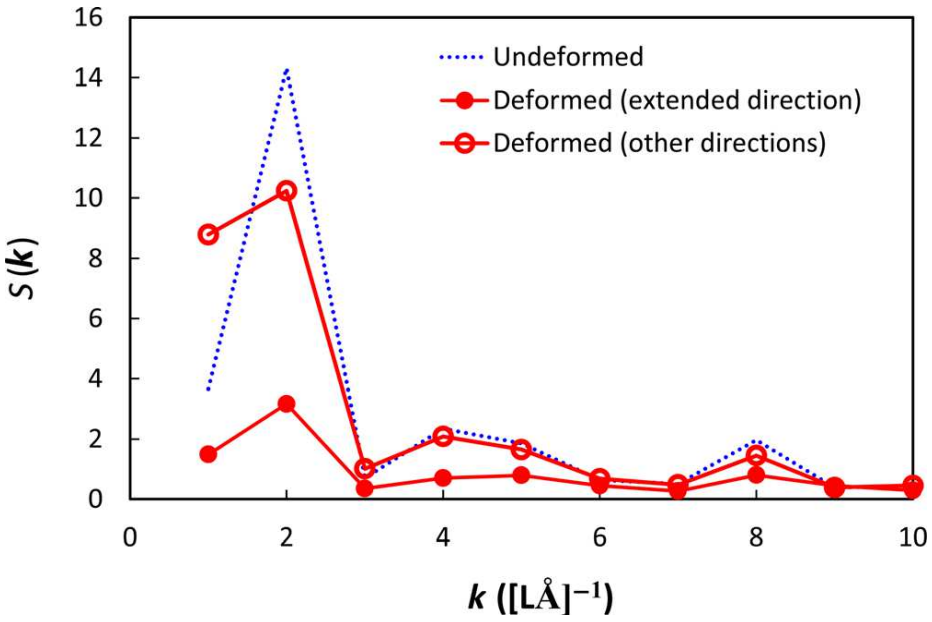

Figure 8: Structure factor profile for hydrated Nafion before and after deformation

It is noted that the structure factor for the isotropic structure that is calculated from the Fourier transform of the PCF, is a spherically averaged measure of particle arrangement in in real space. In this simulation study, however, the structure is uniaxially extended, which would develop anisotropic feature in the hydrated membrane. In order to evaluate the effect of such uniaxial deformation, therefore, the directional structure factor was calculated along the direction of specific reciprocal space vectors, **k**, such as (100),

(010), and (001). These directions are chosen based on the deformation direction during our MD simulations.

Figure 8 shows the structure factor profile calculated from hydrated Nafion before and after deformation. The structure factor profiles are calculated as a function of the scattering vector, **k**. Before the deformation, the strongest peak is found at k=2 $[LÅ]^{-1}$ whereas its intensity is significantly decreased after the deformation, especially in the direction of extension. We think this change in the structure factor profile indicates that the nanophase-segregated structure is significantly deformed and rearranged during the uniaxial extension, and thereby the long range correlation along the extended direction is suppressed very much. The other directions perpendicular to the extended direction also shows a small reduction in their intensity in Figure 8, meaning that the nanophase-segregated structure in the hydrated Nafion membrane loses some portion of the long range correlation at k=2 $[LÅ]^{-1}$ during the deformation. Instead, it should be noted that the longest range correlation in our structure factor profile analysis at k=1 $[LÅ]^{-1}$ is increased more than 2 folds. We believe this is very clear evidence that the nanophase-segregated structure develops greatly in the perpendicular direction to the extended direction, implying a more developed water phase correspondingly, since the enhanced segregation and developed water phase are desirable for transport properties in the membrane.

Transport Properties

Perhaps most indicative of the performance of proton exchange membranes is the water and proton transport properties. Previous studies have established that water and hydronium ion diffusion are enhanced in more nanophase-segregated structures, where

water molecules approach a bulk water-like structure.[69, 75] Such diffusion enhancement of water and hydronium ions is mostly due to the higher phase-segregation in membrane and well-developed hydrogen bonding network in water phase. Here, we use the mean squared displacement (MSD) of both water and hydronium ion molecules, calculated from the last one nanosecond of an equilibrated deformed Nafion structure for comparison to the MSD from the undeformed membrane. The diffusion coefficients, *D*, are then obtained from the linear region of the MSD using the following limit:

$$D = \lim_{t\to\infty} \frac{1}{6t} \left\langle \left(r(t) - r(0) \right)^2 \right\rangle \quad (4)$$

where $r(t)$ and $r(0)$ are the positions of a water molecule at time t and zero, respectively. In this case, the diffusion coefficient is proportional to the slope of the linear asymptote of the MSD plot. The MSD plot for water molecules is shown in Figure 9, and the estimated diffusion coefficient of water is presented in Table 3. The vehicular diffusion coefficient of hydronium ions is also calculated using the same way used for water molecule. The MSD plot for hydronium is shown in Figure 10. The hopping diffusion coefficient is calculated using the quantum mechanical energy barrier and transition state theory as described our previous works.[20]

Table 3: Diffusion coefficients (D) of water and hydronium ions

	D ($\times 10^{-5}$ cm^2/s)			
Simulation	**Water**	**Hydronium**		
		Vehicular	**Hopping**	**Total**
Undeformed	0.3699	0.1278	0.2435	0.3713
Deformed	0.4823	0.1407	0.2376	0.3784

First, the diffusion coefficient of water shows a clear dependency on the deformation, which is consistent with the development of nanophase-segregation in the

membrane. In other words, the water phases are connected more through the deformation, which increases the long-range correlation in the membrane and thereby the water diffusion becomes greater by 30 %.

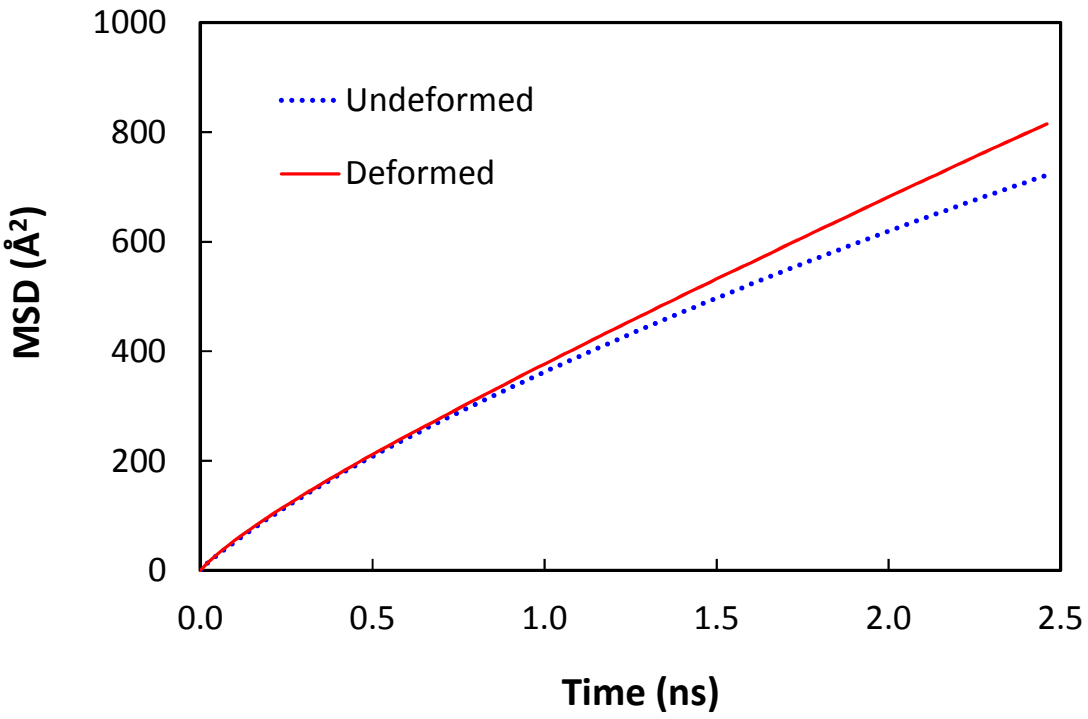

Figure 9: Mean squared displacement of water in Nafion before and after deformation.

On the other hand, the hydronium ion diffusion does not increase much: the vehicular diffusion coefficient is increased by 10 % while the hopping diffusion coefficient is decreased by 2.4 %. Therefore, the overall change is 2 % increase due to the deformation. The calculated diffusion coefficients demonstrate qualitative agreement regarding the vehicular component of diffusion of water and hydronium ions with previous studies.[4, 52]

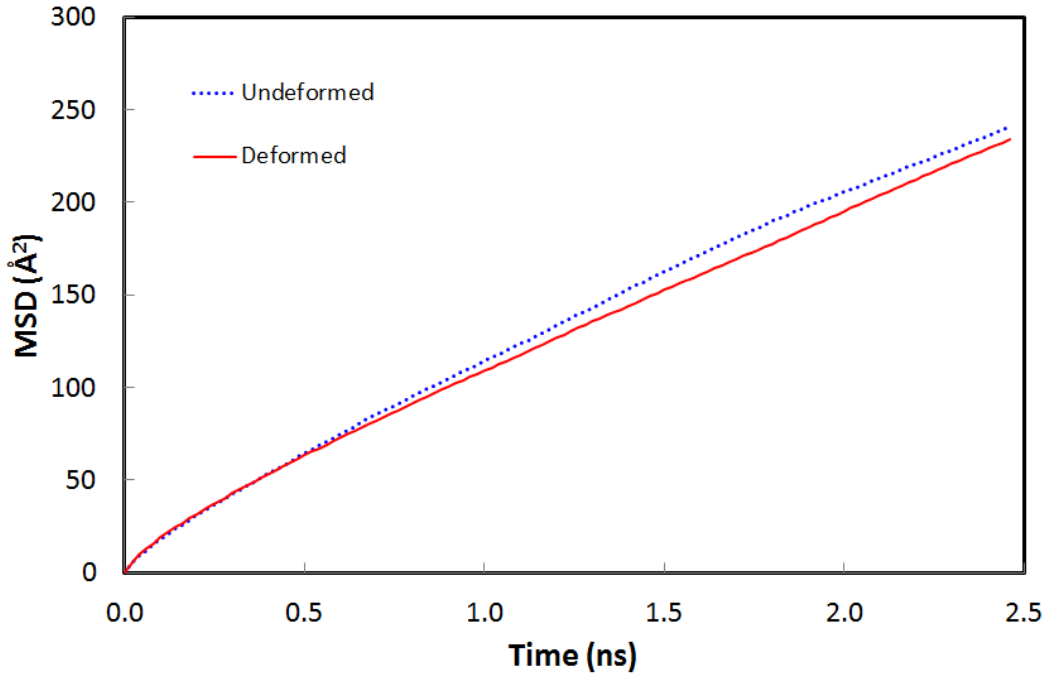

Figure 10: Mean squared displacement of hydronium ions in Nafion before and after deformation.

Directional Transport Properties

To confirm whether hydronium diffusion is unaffected by deformation an additional 15 ns simulation was performed following the initial equilibration simulation for each deformed structure. To account for the effect of the deformation, an anisotropic Mean Squared Displacement is calculated, accounting for the six directional components along with the isotropic average. Of particular interest are the in-plane and through-plane diffusion of water and hydronium. These diffusivities are calculated and averaged for the three stretching directions as shown in Table 4. The results of the 15 ns simulation show agreement with the initial 5 ns study and the nanophase development indicated by the structure factor. The diffusivity of water improves significantly in the direction perpendicular to drawing, while showing little change in the parallel direction. The effect of deformation on hydronium transport remains inconclusive. Similar to the original

simulation, the vehicular diffusion is enhanced in both the in-plane and through-plane directions. However, no significant difference is observed between these two directions.

Table 4: Vehicular directional diffusion coefficients (D) of water and hydronium ions from extended MD simulation

	D ($\times 10^{-5}$ cm^2/s)	
Simulation	**Water**	**Hydronium**
Undeformed	0.1547	0.0959
Deformed (in-plane)	0.1536	0.1230
Deformed (through-plane)	0.2665	0.1023

Currently, our simulation does not fully explain the increase of diffusion observed in experiment.[51] Thus, it is suggested to investigate the hydrated membrane using large-scale simulation methods such as coarse-grained MD simulation.

Summary

We performed molecular dynamics simulations of hydrated Nafion polymer electrolyte membrane to evaluate the effect of uniaxial mechanical deformation on the structure and transport properties. All simulations were performed using fully atomistic models of hydrated Nafion membranes with 20 wt. % water content at 353 K. The system was deformed uniaxially in each of the x, y, and z-directions for 1 ns, and then re-equilibrated for 5 ns via NPT MD simulations which provided statistical data for analysis.

The distribution of sulfonate was analyzed using the PCF of the sulfur-sulfur pair, showing a decrease in distance among sulfonate groups via the deformation. The PCF of the sulfonate-water pair suggested that sulfonate is more solvated in the deformed membrane. It was also discovered from the PCF of the sulfonate-hydronium pair that the correlation between sulfonate and hydronium ions becomes stronger without affecting the water-water correlation and hydronium-water correlation. Thus, it was concluded that the

uniaxial deformation induced the structural change in the membrane, especially the sulfonate distribution. The other local structures in the membrane such the correlations for the hydronium-water pair and the water-water pair as do not seem to undergo significant change.

The extent of the nanophase-segregation was also investigated using directional structure factor profile. It was found that the long-range correlation was developed in the perpendicular direction to the extension through the nanophase-segregation. The improved long range correlation implies better continuous water phase throughout the membrane, and therefore, advantageous for proton transport.

Last, transport properties were assessed by calculating the mean squared displacement of both water and hydronium ions. After the deformation, the water diffusion was enhanced by 30 % while the hydronium ion diffusion was so by only 2 %, which is less than the experimental observation. Extended MD simulations also confirmed these results. The diffusivity of water parallel to the draw direction was found to show insignificant change while improving in the through-plane directions, suggesting that transport properties are enhanced in the direction perpendicular to deformation. For further investigation, it is suggested to utilize large-scale simulation methods in order to fully elucidate the effect of mechanical deformation of the membrane on the structural and transport properties.

Previous experimental results report improved PEMFC performance in stretched membranes, citing increased power density and reduced methanol permeability. While the scope of our simulations cannot capture these full-scale results, the changes observed in our deformed membrane, specifically, more nanophase-segregation and water

transport, suggest improved PEMFC performance as well. We do acknowledge that our methodology, namely, uniaxial deformation, is not conducted in the same manner of pre-stretching and recasting with appropriate solvents as demonstrated experimentally. We also cannot comment on the stability of a membrane deformed in this manner. However, our simulations do demonstrate that membrane deformation can be advantageous in fuel cell applications.

CHAPTER 4

HYDROCARBON BASED PROTON EXCHANGE MEMBRANES

To address the high cost and performance limitations of Nafion and other perfluorinated sulfonic acid ionomers, a number of sulfonated aromatic polymers have been synthesized and studied. Molecular dynamics simulations were used to study hydrocarbon-based proton exchange membranes systems. Inherently, these systems typically do not exhibit the same ionic conductivities as perfluorinated backbone based membranes. One strategy to improve the ionic conductivity is to engineer membranes with well-connected water channels. To initiate changes in the nanoscale morphology of the membrane, the backbone or side chain structures can be modified. A number of studies have investigated various backbones including polystyrenes,[76] poly(phenylene)s,[47] poly(arylene ether ketone)s,[55, 77-85] poly(arylene ether sulfone)s,[45, 55, 81, 83-86] and polyimides[87-89]. Less attention has been dedicated to clarifying the effect of side-chains on structure and transport properties. Here, extensive study was conducted to investigate the role of superacidic side chain structures on aromatic polymer fuel cell membranes. This work was part of a broader collaborative effort with experimental research groups and expanded upon earlier computational study of similar polymer membrane systems. Here, proton-conducting superacidic polymer membranes with varying pendant acidic sulfonate moieties were simulated via full-atomistic molecular dynamics. For comparison with fluoropolymer-based PEMs, one representative polymer was selected and subjected to the same deformation procedure described earlier in Chapter 3.

The work presented here was published partially in *Macromolecules*.[90] This study was performed in collaboration with experimental partners at Rensselaer Polytechnic Institute and The Pennsylvania State University. Our collaborator provided the experimental results presented here and requested our insight to help explain the behavior of the newly synthesized polymers presented. Synthetic details not immediately pertinent to this work are included in the appendix.

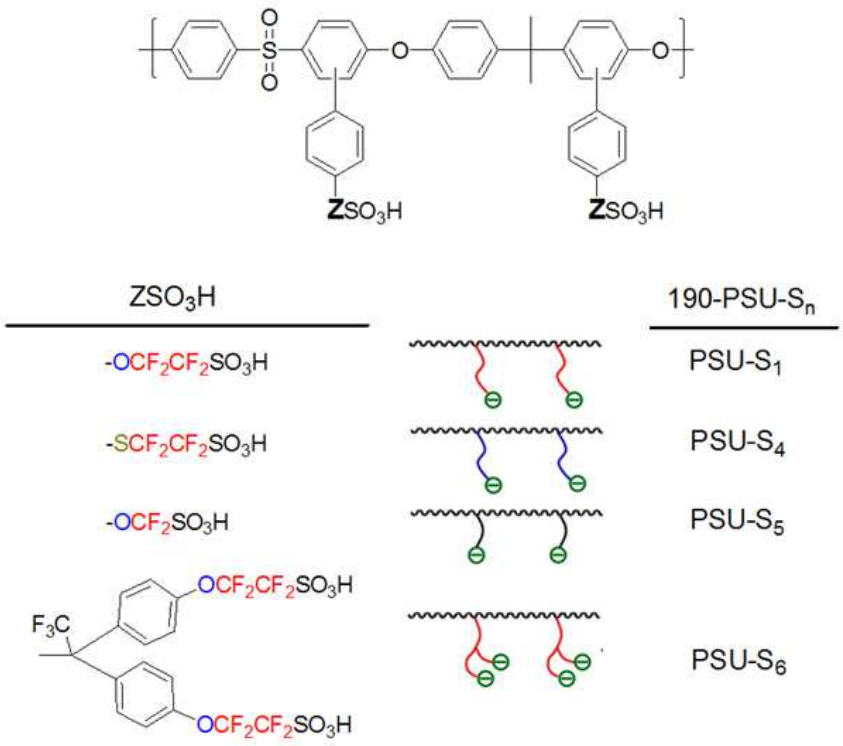

Figure 11: Aromatic polymer backbone and superacidic fluoroalkyl pendants

Proton-conducting superacidic polymer membranes with different fluoroalkyl sulfonate pendants on an aromatic polymer were synthesized via C–H borylation and Suzuki coupling reactions. Variation in chemical structures of pendant sulfonates and

their effects on membrane properties including water uptake, ion exchange capacity (IEC), morphology and proton conductivity were systemically investigated. Chang et al. [90] found the membrane containing the short –OCF2SO3H pendant (PSU-S_5) showed a smaller hydrophilic domain size and lower proton conductivity than those containing the longer pendants –OCF2CF2SO3H (PSU-S_1) and –SCF2CF2SO3H (PSU-S_4) because of the short chain's less favorable aggregation and lower acidity. Sulfone linkage-containing fluoroalkyl sulfonate (–SO2CF2CF2SO3H) was found not to be suitable for PEM applications as it easily undergoes desulfonation. Polymer membrane with branched fluoroalkyl sulfonate pendants (PSU-S_6) gave larger ionic domain size, more uniform hydrophilic channels, and higher proton conductivity than polymer membrane with linear pendant chains (PSU-S_1).

Introduction

Increasing concerns about the environmental impact of our heavy dependence on fossil fuels have motivated research on alternative clean energy technologies. Proton exchange membrane (PEM) fuel cells, which are comprised of a cathode, an anode, and a PEM, generate electricity cleanly via electrochemical reactions of hydrogen and oxygen, and give water as the only byproduct.[91-95] The development of perfluorosulfonic acid ionomers, such as Nafion®, has greatly contributed to fuel-cell technologies, and these materials are still widely used as the benchmark membrane in fuel cells. Due to its perfluorinated polymer structure and superacidic pendant side chain, Nafion possesses high proton conductivity as well as good chemical stability. However, Nafion is still not an ideal PEM material, and its drawbacks (e.g., high cost, low operation temperature and high methanol crossover) mean that development of alternative PEMs is needed for

successful adoption of fuel cells as reliable energy generators.[96-99] Over the past decades, extensive efforts have been devoted to the development of hydrocarbon-based PEMs, and many aryl and alkyl sulfonated polymers have been described.[100-106] In general, these sulfonated aromatic polymer PEMs swell excessively on hydration and give much lower proton conductivity than Nafion when relative humidity (RH) is reduced. If a PEM provides good proton conductivity at high temperature (above 100 °C) and low RH, it can bring many desirable advantages to the fuel-cell system, such as high electrode reaction kinetics, good tolerance toward carbon monoxide impurity, and simplified water management.[98, 103, 107-109] To achieve this, creation of well-connected hydrophilic channels within PEMs through architectural controls of polymer morphology has been pursued over the past decade. For example, several sulfonated multi-block copolymers[110-112] and graft polymers[113-116] show significantly higher proton conductivities at low RH conditions than conventional randomly sulfonated polymers due to the facilitated proton transport within the hydrophilic channels.

Previously, our groups suggested strong acidity-driven enhancement of proton conductivity as an alternative approach to high performance PEMs. To investigate the acidity effect of sulfonates, our collaborators synthesized polystyrenes and polysulfones functionalized with fluoroalkyl sulfonate, aryl sulfonate, and alkyl sulfonate pendants and compared their membrane performances. Among them fluoroalkyl sulfonated polymers demonstrated significantly higher proton conductivities especially at low RH than those with less acidic sulfonated polymers.[54, 55] We attributed these observations to the fact that that the fluoroalkyl sulfonated groups of superacidic polymers have better proton dissociation and the resulting ionic species tend to attract more water molecules.

Morphological differences among polymers functionalized with different sulfonate groups were found to be insignificant, supporting the conclusions that proton conductivity enhancement of superacid PEMs is not morphology-driven but is an acidity-driven effect. Similar improvements in performance of superacidic PEMs have been reported by other groups too.[117-122] While there are still different opinions on the ideal chemical structure of PEM, we believe fluoroalkyl sulfonate is the best side chain structure for a PEM because it can promote proton conductivity at low RH without the need to increase ion exchange capacity (IEC), which would induce more water absorption and sacrifice the membrane's mechanical properties. To date, however, there are very few examples of hydrocarbon-based superacidic polymers with different structures. To begin to fill this important gap in our knowledge of PEM membrane materials, our collaborators have now synthesized polysulfones functionalized with different fluoroalkyl sulfonated pendants and systematically studied the effects of their structures on proton conductivity, water properties and morphology.

Computational simulations of the superacidic PEMs were performed to understand the sulfonated structure–fuel cell membrane property relationships. The study sought to establish a relationship between the acidity and chemical structure of several ionic pendant groups and the properties of PEMs at the molecular level. Notably, attention was given to the dissociation and acidity of the ionic groups and the nanophase-segregated morphology, as the development of water channels is critical to membrane transport properties. Initially, full-atomistic molecular dynamics simulations were conducted with water contents of 10 and 20 wt % at 353.15 K. However, due to the wide variation in water uptake observed experimentally, additional simulations were carried

out reflecting the measured water content. These corrected systems were used for the analyses presented here.

Computational Models and Methods

Force Field and Simulation Parameters

We used the DREIDING force field [23] to describe the intramolecular and intermolecular forces in the hydrated polysulfone-based membranes. The force field is the same as previously used to study Nafion,[4] Dendrion,[16, 20] sulfonated poly(ether ether ketone),[8, 12] and sulfonated polystyrene,[54] as well as various molecular systems.[57, 58] Water was described using the F3C force field.[59] The force field for hydronium ion has been used since it was developed for the simulation study of the hydrated Nafion membrane.[4] The force field parameters used are the same as reported in their original papers.[23, 59, 60] The form of the potential energy used is:

$$E_{total} = E_{vdW} + E_{Q} + E_{bond} + E_{angle} + E_{torsion} + E_{inversion} \quad (11)$$

where E_{total}, E_{vdW}, E_{Q}, E_{bond}, E_{angle}, $E_{torsion}$ and $E_{inversion}$ are the total, van der Waals, electrostatic, bond stretching, angle bending, torsion and inversion energy components, respectively. The individual atomic charges were assigned through Mulliken population analysis using B3LYP and 6-31G** in Jaguar.[61] The Particle-Particle Particle-Mesh (PPPM) method was used to calculate electrostatic interactions.[21]

The annealing and equilibration MD simulations were performed using the LAMMPS (Large-scale Atomic/Molecular Massively Parallel Simulator) code developed by Plimpton at Sandia National Laboratories.[123] The code was used with some modifications to integrate our force fields.[4] The equations of motion were integrated

using the velocity Verlet algorithm with a time step of 1.0 fs. The Nose-Hoover temperature thermostat for the NVT and NPT simulations used a damping relaxation time of 0.1 ps and a dimensionless cell mass factor of 1.0.

Construction and Equilibration of Amorphous Membrane

Using a full atomistic simulation method, we investigate the nanophase-segregated structure and transport properties hydrated polysulfone membranes at 353.15 K. The simulated hydrated membrane systems consist of four chains of polysulfone ionomers and water molecules with 24–37 wt % as summarized in Table 5. The degree of polymerization and the degree of sulfonation were set to 40 and 200, respectively. The sulfonated units were selected randomly from 40 repeating units in the backbone and all of the sulfonic acid groups are assumed to be ionized as assumed in the previous studies.

Table 5: Composition of hydrated PSU membranes and simulation parameters

Ionomers	PSU-S_1	PSU-S_4	PSU-S_5	PSU-S_6
Molecular weight per chain (Daltons)	39362	40642	35362	73682
Equivalent weight	492	508	442	461
Dimension of simulation cell (Å)	64.36	64.75	62.39	80.21
Number of sulfonate groups per chain	80	80	80	160
Density (g/cm3) at 353.15 K	1.23	1.30	1.26	1.31
Water content [a] (wt %)	24	29	29	37
λ [b]	6.8	8.5	7.3	9.6

[a] The water content in each simulation was set to the experimental value for the water uptake
[b] λ = number of water molecules per sulfonate group

The initial amorphous structures of hydrated polysulfone ionomers were constructed using the Amorphous Builder of Cerius2.[124] Since such initial structures of polymeric materials may include unstable conformations, they were equilibrated using the annealing procedure as used in the previous studies of Nafion,[4] Dendrion[16, 20] and sulfonated poly(ether ether ketone)[11] membranes, which accelerates the attainment

of equilibrium by driving the system repeatedly through 5 cycles of thermal annealing (between 300 and 600 K) and volume annealing (between densities of 0.5 to 1.1 times the expected density). This procedure aims to help the system escape from various local minima and promote the migration of species required for phase-segregation in heterogeneous systems, whose detailed steps are described in the previous publications.

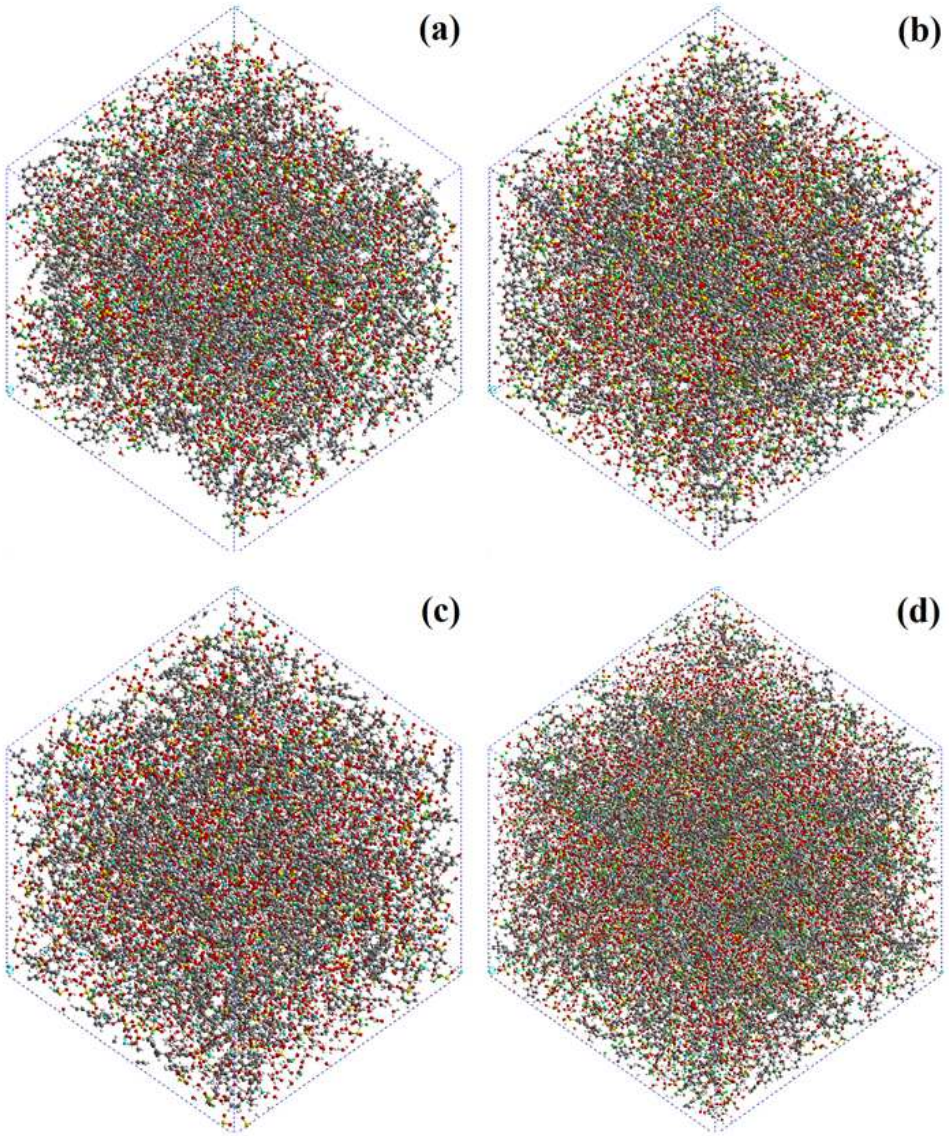

Figure 12: Equilibrated PSU structures (a) PSU-S_1, (b) PSU-S_4, (c) PSU-S_5 and (d) PSU-S_6

After finishing the *annealing cycles*, a 100ps NVT MD simulation and a subsequent 5 ns NPT MD simulation were performed at 353.15 K to finalize the annealing procedure. Then, another 15 ns NPT simulations were performed at 353.15 K for data collection.

Results and Discussion

Experimental Results of Hydrocarbon Ionomers

The synthesis and experimental characterization of the PSU polymers presented here were performed by the Bae Research Group at RPI and the Hickner Research Group at Penn State.[90]

Table 6 summarizes the membrane properties of the fluoroalkyl sulfonated PSUs. The NMR-based IEC values (IECNMR) were estimated from the 1H NMR spectra using the integral ratio of the methyl pendant groups of PSU-Sn-Ar and the isopropylidene group of the polymer backbone. IECs were also measured from titration (IECtitr), and they matched well with the IECNMR values (1.9–2.2 mequiv/g). Between the two IEC measurement methods, IECNMR values would be better reflective of the final polymer structure because IECtitr values are sensitive to remaining water content of hygroscopic membranes in the dried state. Titration may also not be able to have good access to the buried sulfonate groups within the hydrophobic domains.

Table 6: Properties of Fluoroalkyl Sulfonated PSUs and Comparison with Nafion

Sulfonated polymer[a]	IEC (mequiv/g)		Water uptake[d]	λ[e]
	NMR[b]	titr[c]		
PSU-S_1	1.97	1.83	24	6.8
PSU-S_4	1.91	1.96	29	5.8

PSU-S_5	2.19	1.99	29	7.3
PSU-S_6	2.13	2.23	37	9.6
Nafion 112		0.86	15	9.7

[a] All sulfonated PSUs contain average of 1.9 sulfonic acid groups per repeating unit (190 mol %). [b] IEC calculated from polymer structure based on the integral ratio of 1H NMR spectrum of 3,5-dimethylphenol protected sulfonated PSU. [c] IEC measured by titration. [d] Water uptake (%) = (Wwet – Wdry)/Wdry, where Wdry and Wwet are the weights of dried and wet membranes, respectively. Water uptake of wet membrane was measured at 30 °C and 98% RH. [e] Hydration number (i.e., molar ratio of water molecules per sulfonate group) at 98% RH.

Figure 13 shows the humidity-dependent water uptake values and hydration numbers (i.e., the number of water molecules per mol SO3H). As shown in Table 6, the water uptake values of the PSU membranes generally follow the trend of IEC values except for PSU-S_5. Although PSU-S_5 and PSU-S_6 have comparable IECNMR, the water uptake and hydration number of the former were significantly smaller in comparison to the latter. Although all PSU-Sn of Table 6 have superacidic fluoroalkyl sulfonated side chains, PSU-S_6 had consistently higher water uptake and hydration numbers than other sulfonated PSU membranes.

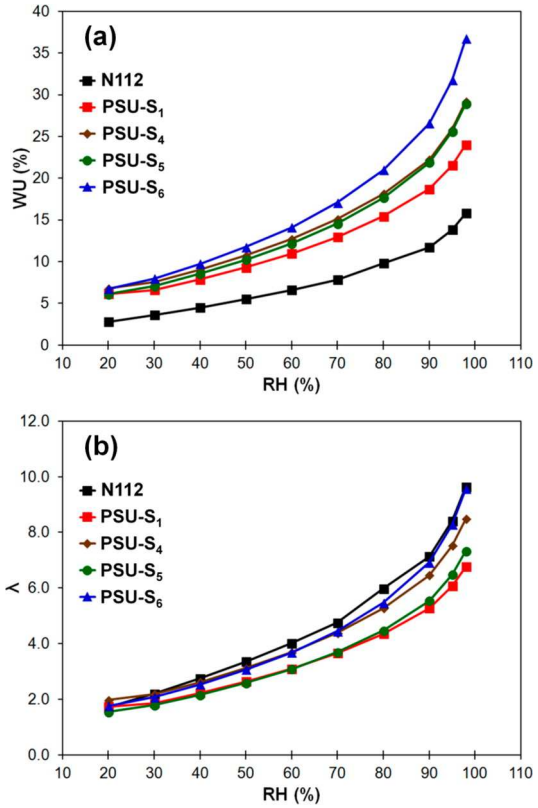

Figure 13: Water uptake (a) and hydration number (b) of fluoroalkyl sulfonated PSUs versus relative humidity at 30 °C. These measurements were obtained by from experimental measurements performed by our collaborators.[90]

In-plane proton conductivities of the sulfonated PSU membranes and Nafion 112 were measured as a function of RH at 100 °C, and the data are shown in Figure 14. Among sulfonated PSU membranes, PSU-S_6 gave the highest conductivity over a wide range of humidity and showed values even higher than Nafion at 50% RH or above. Although PSU-S5 has higher IECNMR and greater water uptake than PSU-S_1 (2.19 vs 1.97 mequiv/g and 29 vs 24% for IECNMR and water uptake, respectively), this sample had lower proton conductivity than PSU-S1. Noticeably, PSU-S_5 gave significantly lower conductivity than all other PSU membranes over the entire RH range. This inferior performance might be due to the presence of the shorter fluoroalkyl chain (−OCF2−)

which has weaker electron-withdrawing ability and, as a result, led to a lower degree of dissociation of the sulfonate group. Thus, we can conclude that at least two CF2 groups are needed to obtain the desired superacidic functionality of the sulfonate, which has been demonstrated computationally by Yeh et al.[125]

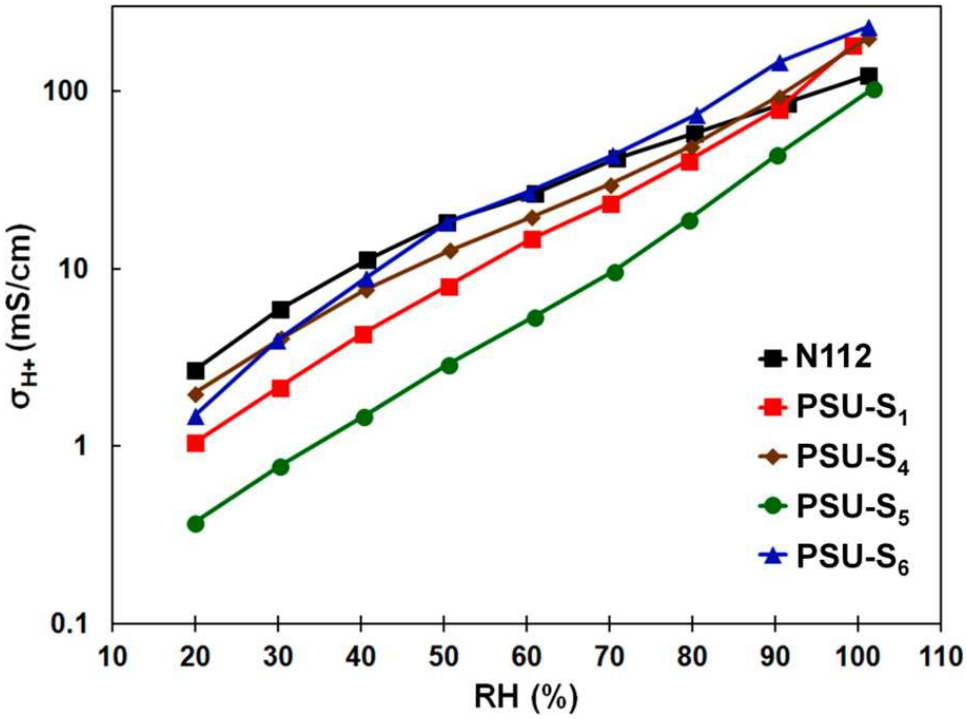

Figure 14: Proton conductivity of sulfonated PSUs versus relative humidity at 100 °C. These measurements were obtained by from experimental measurements performed by our collaborators.[90]

PSU-S_1 and PSU-S_4 have almost the same IECNMR (1.97 vs 1.91 mequiv/g); however, the latter polymer absorbed more water and had higher proton conductivity than the former. The only difference in chemical structure between the two polymers is the linkage to the fluoroalkyl group: thioether (−SCF2CF2−) for PSU-S_4 versus ether (−OCF2CF2−) for PSU-S_1. Because sulfur atom is larger and has a higher polarizability

than oxygen atom, it is possible that PSU-S_4 with a thioether linkage might absorb more water molecules than PSU-S_1 with an ether linkage, giving enhanced proton conductivity.

Morphology

The morphology of sulfonated PSU membranes was studied by transmission electron microscopy (TEM) and small-angle X-ray scattering (SAXS). For the TEM characterization, membranes were stained with lead acetate.[126] Therefore, the dark and light areas in the images represent the hydrophilic and hydrophobic domains, respectively (Figure 15). All fluoroalkyl sulfonated PSU membranes showed distinct phase separation. The hydrophilic domains range from 1 to 3 nm, which are smaller than those of Nafion 112 (3 to 5 nm). This difference may be due to a combination of less hydrophobic and more rigid backbone structure and shorter pendant chains of PSU-Sn compared to those of Nafion. Compared to PSU-S_1, PSU-S_6 with branched pendant chains showed larger hydrophilic domains while PSU-S_5 with a short tethered chain had smaller hydrophilic domains in the TEM images. This trend might be ascribed to the shorter side chains of the S5-polymer and its less favorable aggregation behavior of the hydrophilic sulfonate head groups. However, it is difficult to draw definite conclusions about overall morphological structure from the TEM images because they give only a small representation of the morphology of a limited sample area of the membrane.

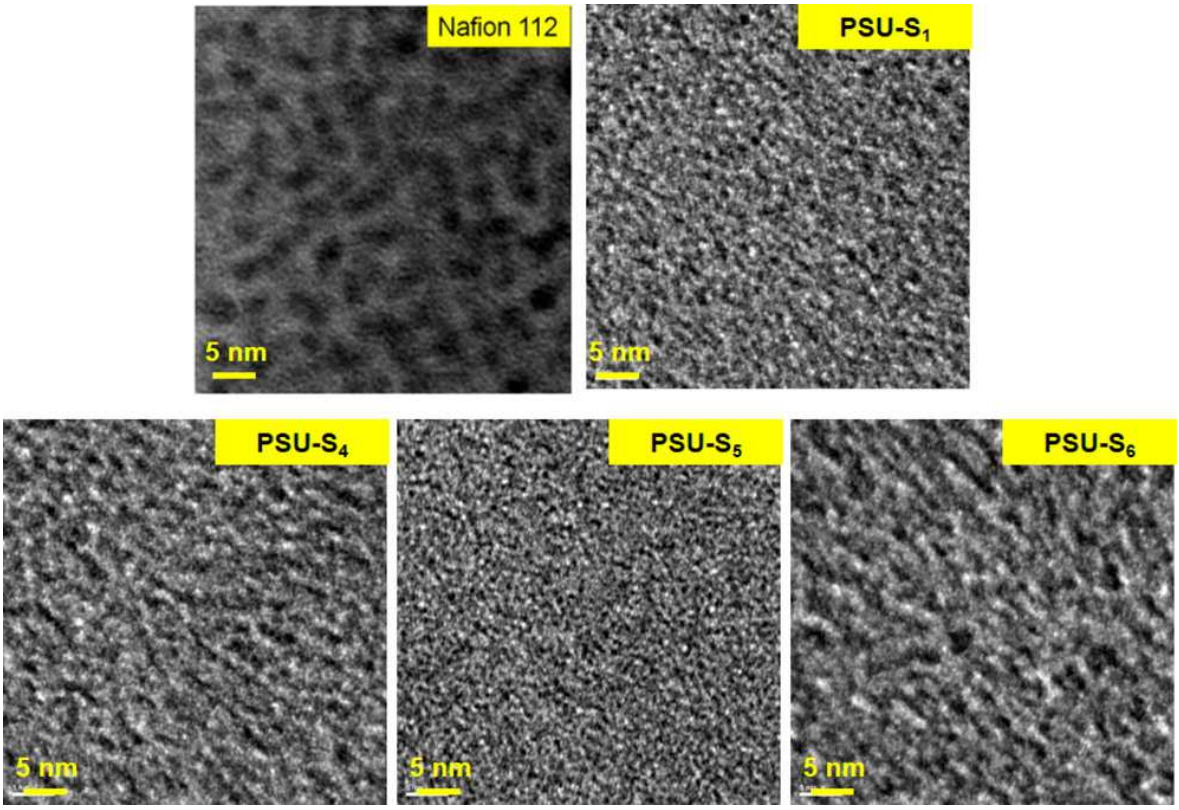

Figure 15: TEM images of Nafion 112 and superacidic sulfonated PSU membranes.[90]

To complement the localized morphology study of TEM, the average nanoscale morphology in bulk of the sulfonated PSU membranes was studied using SAXS. Because the X-ray beam of our in-house SAXS is about 0.4 mm in diameter (defined by the second pinhole from the rotating anode), these measurements reflect averaged morphology of the membranes over a relatively large area as compared to the TEM measurements. Figure 16 shows the SAXS profile for PSU-S_1, -S_4, -S_5, and -S_6 in their sodium salt form. Both H+ and Na+ forms of the membranes were analyzed but the membranes in Na+ form showed a more pronounced pattern of phase separation (i.e., peaks in Na+ form were narrower than those in H+ form) and gave higher intensity peaks owing to the greater electron density of sodium compared to hydrogen.

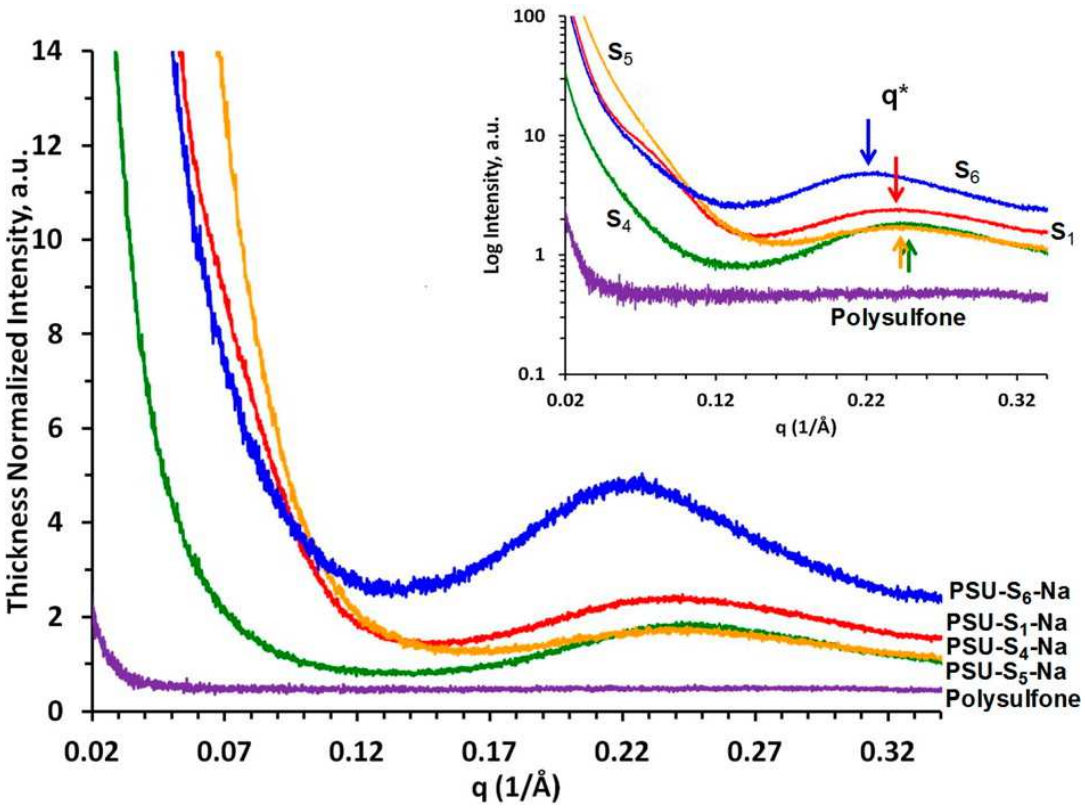

Figure 16: SAXS profiles for PSU-S_1 (red), PSU-S_4 (green), PSU-S_5 (orange), PSU-S_6 (blue), and unfunctionalized PSU (purple) in sodium salt form. Data in the inset are plotted on a logarithmic scale.[90]

SAXS data allows the quantitative comparison of the overall interdomain spacing distance based on the position of the correlation peak, q*. As shown in Figure 16, unfunctionalized PSU did not show any sign of phase separation in the q-regions from 0.5 to 3.4 nm^{-1}, while broad-yet-distinct interdomain correlation peaks were present in all functionalized PSU membranes. These phase-separated ionic domains were likely to be formed by the self-assembly of fluoroalkyl sulfonated pendant groups along the hydrocarbon PSU backbone chain in the bulk membranes.

Table 7: Interdomain Spacing (d) of Sulfonated PSU Membranes

Polymer [a]	q^{*} [b] (1/Å)	d [c] (nm)
PSU-S_1	0.24	2.61

PSU-S_4	0.24	2.61
PSU-S_5	0.24	2.61
PSU-S_6	0.22	2.80

[a] Sulfonated polymer in Na+ form. [b] Value at peak maximum. [c] Calculated from q* using $d = 2\pi q^{-1}$.

As indicated by the solid arrows in the inset of Figure 16, PSU-S6 exhibited a distinct peak maximum at a lower q value than any of the other PSU membranes. This lower q* value reflects a larger distance between the ionic domains, as calculated from the peak maxima using the equation $d = 2\pi q^{-1}$ (listed in Table 7). The larger domain spacing for the PSU-S_6 sample presumably resulted from its bulky and branched fluoroalkyl sulfonate group. The larger d-spacing in PSU-S6 (2.80 nm) correlates well with the larger size and branched structure of the S_6 relative to S_1, S_4, and S_5. Furthermore, because PSU-S_6 has two sulfonate groups per repeat unit instead of just one, it could create greater localized charge density and larger domains with greater d-spacing, resulting in stronger SAXS scattering contrast upon phase separation. Most importantly, these morphology data suggest that PSU-S_6 has more uniform ionic channel size and a distinct phase separation of hydrophilic domains since its scattering peak is narrower and more intense than the other samples. According to the SAXS data in Table 7, all other functionalized polymers (i.e., PSU-S_1, -S_4, and -S_5) have a shorter and almost identical interdomain spacing of 2.61 nm. This is probably because they all have broader peaks with lower intensity in the SAXS profile. Although the morphology structures of PSU-S1, -S4, and -S5 from TEM analysis are slightly different each other, they all could be characterized by a wide distribution of different sizes of interdomain spacing between ionic channels. Such a wide distribution of domain sizes is likely to result in the

development of “bottleneck” regions in the ionic channels, leading to lower conductivity compared to that of PSU-S_6.

Simulation Results of Superacid Polysulfones

The experimental data above demonstrate differences in membrane properties but offer no mechanistic insight. We investigated the effect of acid strength on nanophase-segregated structure and transport properties using molecular dynamics simulations. We elected to simulate all four of the synthesized polymers, PSU-S1, -S4, -S5, and -S6. Despite the identical backbone structure, the higher concentration of sulfonic groups and bulkier pendant group in the PSU-S6 system required special attention. Results obtained at 20 wt % hydration conditions were consistent with experimental observations only for PSU-S_1, -S_4, and -S_5. For accurate comparison with PSU-S_6, all of the membranes were re-simulated with a water content matching the experimental water uptake. We believe that a comparison of the simulated properties provides a theoretical understanding of the effect of acidity on structure and transport properties in proton exchange membranes.

We investigated the nano-scale structures of PSU-S_1, PSU-S_4, PSU-S_5 and PSU-S_6 using full-atomistic molecular dynamics (MD) simulation method, which was used in our previous studies of sulfonated poly (arylene ether sulfone)[55] and other polymers.[54, 127-132] To understand the effect of the pendant superacidic groups, a polysulfone backbone with the same degree of sulfonation (200 mol%) was selected. The materials and simulation parameters are listed in Table 5. The water contents of the simulated polymer system were set to be the same as the experimental water uptakes of Table 6 to mimic the experimental conditions of hydrated membranes.

Structure Factor Profile Analysis

To quantitatively analyze the effect of sulfonate head group on the nanophase-segregated morphology of the materials, we calculated the structure factor, S(**q**), as used in previous studies of hydrated polymer membranes.[38-40] S(**q**) is defined as:

$$\mathbf{S}(\mathbf{q}) = \left\langle \sum_{r_i} \sum_{r_j} \exp\left(i\mathbf{q}\cdot\mathbf{r}_{ij}\right)\left(\xi^i \xi^j - \langle\xi\rangle^2\right) \right\rangle / L^3 \quad (8)$$

where the angular bracket denotes a thermal statistical average, ξ^i represents a local density contrast, $(\phi_A^j - \phi_B^j)$, $\boldsymbol{q}$ is the scattering vector and $\boldsymbol{r}_{ij}$ is the vector between the sites *i* and *j*. While SAXS and SANS experiments rely on scattering length density contrast, the structure factor is calculated from an artificial density contrast as follows. The local density variables are ϕ_A^j and ϕ_B^j: where ϕ_A^j is equal to 1 if the site *j* is occupied by a hydrophilic entity such as water or sulfonate group and equal to 0 otherwise, and ϕ_B^j is equal to 1 if the site is occupied by hydrophobic entities such as the polysulfone backbone or equal to zero otherwise. The quantity S(q) is spherically averaged as follows:

$$S(q) = \sum_{|\mathbf{q}|} \mathbf{S}(\mathbf{q}) / \sum_{|\mathbf{q}|} 1 \quad (9)$$

with q = $(2\pi/L)$n, where $n = 1,2,3,\cdots$ denotes that, for a given n, a spherical shell is taken as $n-1/2 \leq qL/2\pi \leq n+1/2$.

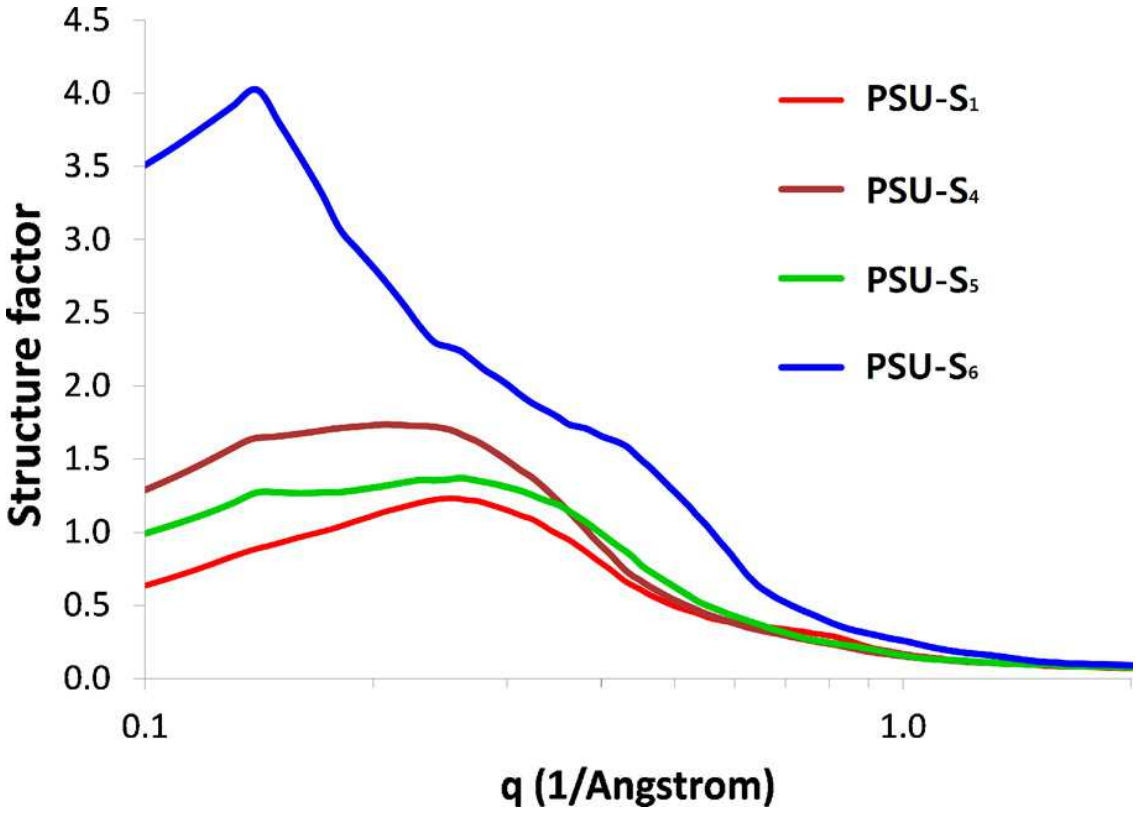

Figure 17: Structure factor profiles calculated from PSU- S1 (red), PSU- S4 (brown), PSU- S5 (green), and PSU- S6 (blue) with experimental water uptake. The interdomain spacings calculated from qmax are 2.4 nm, 2.5 nm, 2.3 nm and 3.5 nm for PSU-S1, PSU-S4, PSU-S5, and PSU-S6, respectively.

The simulated structure factor profiles in Figure 17 show that the calculated interdomain spacing *d* are 2.4 nm, 2.5 nm, 2.3 nm and 3.5 nm for PSU-S_1, PSU-S_4, PSU-S_5, and PSU-S_6, respectively. These values are calculated from the $q_{max} = 2\pi/d$. Although our simulated d values are slightly smaller than those measured from the SAXS experiments (Figure 16 and Figure 17), both data present a consistent conclusion: PSU-S_1, PSU-S_4, and PSU-S_5 have similar *d* values and PSU-S_6 has a significantly larger *d* value than those of the mono-sulfonated PSUs. Due to the difference in electron-withdrawing ability of the pendant groups (–CF_2CF_2– vs. –CF_2–), more acidic PSU-S_1

and PSU-S_4 can form better-developed nanophase-segregation with a larger d spacing than less acidic PSU-S_5.

Another point to note is the unique nanophase-segregation behavior of PSU-S_6, which has the largest d spacing in both SAXS and simulation. Considering the acidity of sulfonate in PSU-S_6 will be similar to that in PSU-S_1, the highest proton conductivity and the largest d spacing of the former suggest that the branched sulfonate side chain of PSU-S_6 can generate better developed water channel compared to the rest of the mono-sulfonated polymer membranes in this study.

Dissociation of Sulfonate Groups

The proton dissociation from sulfonate group can be interpreted as a measure of the acidity strength in hydrated polymer membrane. Thus, in order to investigate the extent of proton dissociation from each sulfonate group, we calculated the pair correlations of sulfonate-hydronium pair, $\rho g_{\text{S-O (hydronium)}}$. The definition of pair correlation function, $g_{A\text{-}B}(r)$, is the probability density of finding B atoms at a distance r from A atoms averaged over the equilibrium trajectory as shown in equation 1:

$$g_{A-B}(r) = \left(\frac{n_B}{4\pi r^2 \Delta r} \right) / \left(\frac{N_B}{V} \right) \quad (1)$$

where n_B is the number of B particles located at a distance r in a shell of thickness Δr from particle A, N_B is the number of B particles in the system, and V is the total volume of the system.

The pair correlation for the sulfonate-hydronium pair in Figure 18 indicates the effect of acidity on local structure. The more acidic PSU-S_6 can more readily dissociate and has the lowest pair intensity.

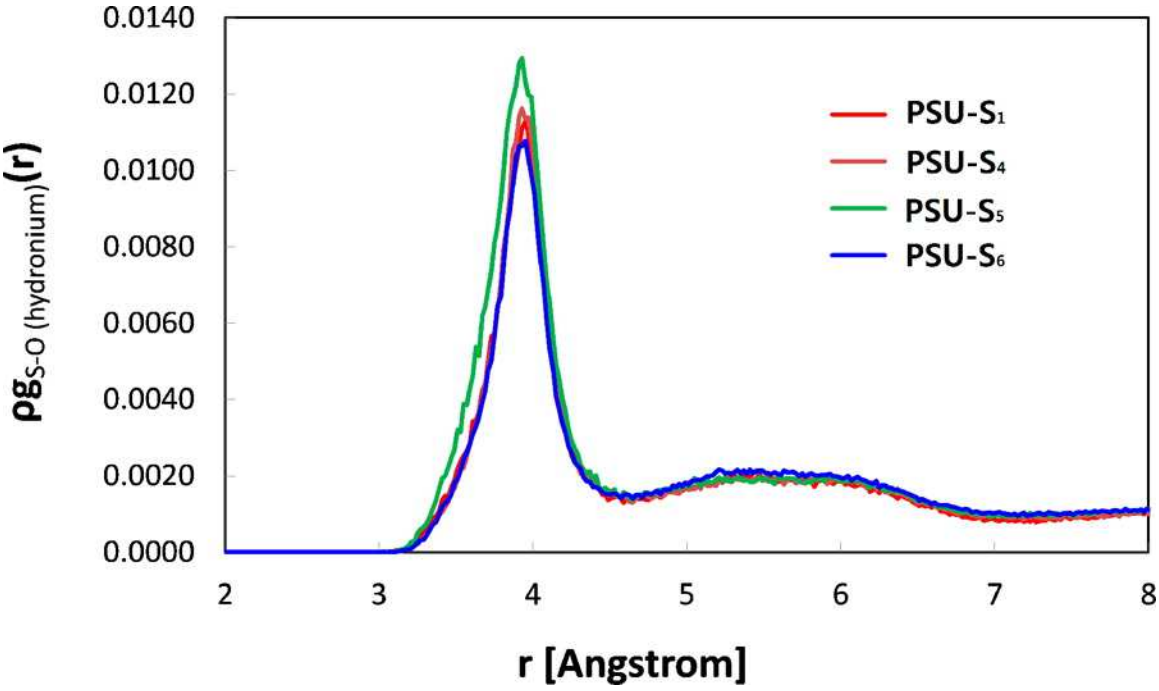

Figure 18: Calculated pair correlation functions of sulfonate–hydronium ion in PSU-S1 (red), PSU-S4 (brown), PSU-S5 (green), and PSU-S6 (blue). Water content was set to match experimental water uptake.

The $\rho g_{\text{S-O (hydronium)}}$ data in Figure 18 showed that PSU-S_1 and PSU-S_4 have a similar sulfonate-hydronium correlation while PSU-S_5 and PSU-S_6 have the most and the least correlations, respectively. These simulation results agree well with our structure factor profiles and SAXS data which indicate that the order of nanophase-segregation is PSU-S_6 > PSU-S_1 ≈ PSU-S_4 > PSU-S_5. The least electron-withdrawing –CF_2– group seems to impart the lower acidity, more tightly bound water molecules and less developed nanophase segregated structures for PSU-S_5 than other sulfonated PSUs in this study. Overall, we found the acidity difference in a series of superacidic PSU-S_n membranes is well reflected in the structure factor and the pair correlations of sulfonate-hydronium.

Transport Properties

As previously described, the diffusivity can be calculated from the slope of the MSD obtained from MD simulation. The following equation is used to calculate the diffusivity.

$$D = \lim_{t\to\infty} \frac{1}{6t} \left\langle \left(r(t) - r(0) \right)^2 \right\rangle \quad (4)$$

where $r(t)$ and $r(0)$ are the positions of a water molecule at time t and zero, respectively. The calculated diffusion coefficients only represent the vehicular diffusion of water and hydronium. The classical MD simulations performed do not account for secondary mechanisms of transport, including proton hopping for hydronium. The vehicular diffusivities of water and hydronium are shown in Table 8.

Table 8. Vehicular diffusion of equilibrated PSU-based membranes with experimental levels of hydration

	D ($\times 10^{-5}$ cm^2/s)	
	Water	**Hydronium**
PSU-S1	0.0913	0.0094
PSU-S4	0.1363	0.0252
PSU-S5	0.0889	0.0132
PSU-S6	0.2237	0.0402

The calculated diffusivities show a clear agreement with the observed experimental results and calculated nano-phase segregation. For water, the diffusion coefficient ordering is PSU-S_6 > PSU-S_4 > PSU-S_1 > PSU-S_5. This trend is slightly different for hydronium, with the rankings as follows: PSU-S_6 > PSU-S_4 > PSU-S_5 > PSU-S_1. Overall, these trends agree with the conductivities calculated experimentally.

Deformation

Following the publication of this work, additional simulations were conducted to investigate the effect of mechanical deformation on hydrocarbon-based PEMs. For comparison with fluoropolymer-based PEMs, one representative polymer was selected and subjected to the same simulation procedure described earlier in Chapter 3. PSU-S_1 was selected for comparison with Nafion. For direct comparison, a level of hydration of 20 wt % was used for both systems. The PSU-S_1 similarly showed little change in the local structure following deformation. However, the anisotropic structure factor Figure 19) shows a similar trend as observed in Nafion. The intensity is shown to decrease following deformation, with no apparent peak at the main position of q = 1. 5 $[LÅ]^{-1}$ in the direction parallel to extension. In directions perpendicular to stretching, the intensity of the calculated structure factor is nearly the same as for undeformed PSU-S. We believe this is very clear evidence that the nanophase-segregated structure develops greatly in the perpendicular direction to the extended direction, implying a more developed water phase correspondingly, since the enhanced segregation and developed water phase are desirable for transport properties in the membrane. Still, a direct comparison to Nafion is necessary to determine how deformed PSU-S_1 would perform in a PEM.

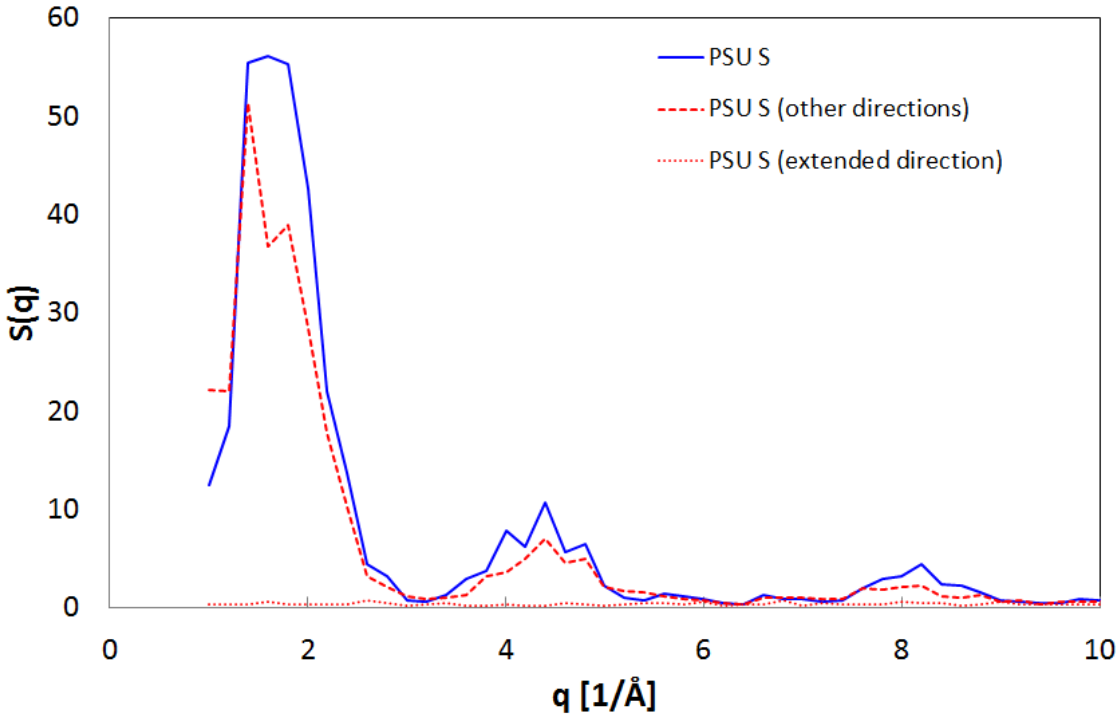

Figure 19: Structure factor profile for PSU-S with 20 wt % water content.

The calculated vehicular diffusivities of water and hydronium for undeformed and deformed Nafion and PSU-S_1 following 5 ns of equilibrium MD are shown in Table 9. The overall diffusivities are shown to improve for both Nafion and PSU-S_1 following deformation. Similarly, the water diffusivities are shown to be lower in the direction parallel to drawing compared to the perpendicular directions. This further supports the hypothesis that conductivity is improved through-plane in deformed polymer membranes.

Table 9. Vehicular diffusion coefficients (D) of water and hydronium ions

	D ($\times 10^{-5}$ cm^2/s)					
Simulation	**Water**			**Hydronium**		
	Total	**Def Perp.**	**Def Ext.**	**Total**	**Def Perp.**	**Def Ext.**
Undeformed Nafion	0.3699	0.1911	0.1726	0.1278	0.0692	0.0534
Deformed Nafion	0.5592	0.2909	0.2570	0.1506	0.0737	0.0785
Undeformed PSU-S	0.0913	0.0462	0.0446	0.0094	0.0038	0.0064
Deformed PSU-S	0.5850	0.3627	0.1521	0.0124	0.0073	0.0039

Conclusions

We have studied a series of superacidic polymers containing different fluoroalkyl sulfonate groups and systematically investigated the structural influence of sulfonic acid pendant (e.g., side chain length, linear vs. branched structure, ether vs. thioether linkage) on PEM properties (e.g., water uptake, IEC, proton conductivity, and morphology). The membrane containing short –OCF2SO3H pendant showed smaller hydrophilic domain size and lower proton conductivity than the membrane containing –OCF2CF2SO3H because of its less favorable aggregation of sulfonate groups and lower acidity. Sulfone (–SO2–) linkage-containing fluoroalkyl sulfonate is not suitable for PEM applications because it easily undergoes desulfonation. The polymer membrane with –SCF2CF2SO3H pendant chains (PSU-S4) absorbed more water and showed enhanced proton conductivity than the polymer with –OCF2CF2SO3H chains (PSU-S1), possibility due to higher polarizability of sulfur than oxygen. In contrast to unfunctionalized polysulfone, all sulfonated polymers exhibit ordering peaks from the aggregation of ionic domains. Among them, the polymer with branched sulfonate sidechain structure (PSU-S6) produced larger interdomain size and more distinct phase separation behavior compared to other linear fluoroalkyl sulfonated polymers. These results suggest that not only the superacidity of fluoroalkyl sulfonic acid but also the shape of sulfonate groups (e.g., linear vs. branched side chains) can play a significant role in determining proton conduction in fuel cell membrane. This present work significantly broadens the scope of hydrocarbon-based superacidic polymers as alternative PEM of Nafion, and the structure-properties study of sulfonic acid pendants can be an important guide for the future PEM and ionomer development for fuel cell technology.

CHAPTER 5

ANION EXCHANGE MEMBRANES

Polymer electrolyte membrane fuel cells, especially proton exchange membrane (PEM) fuel cells have been extensively studied to harness hydrogen as an alternative to fossil fuels, for applications such as automobiles.[44-49] However, the high cost in the production of PEM fuel cells has remained as a drawback to their commercialization, due to costs of the membrane, bipolar plates, assembly, and the use of precious noble metal catalysts such as platinum. In this context, anion exchange membrane (AEM) fuel cells have received significant attention since AEM can in principle allow the use of a non-platinum metal catalyst, such as nickel, in an alkaline environment. Consequently, the cost of AEM fuel cells in high volume is projected to be substantially lower compared to PEM fuel cells. PEM fuel cells have a history of achieving up to 70% electrical efficiency in NASA's Project Gemini in the 1960s,[133] which is due to the improved kinetics for oxygen reduction and fuel electro-oxidation in alkaline environment.[134-137] Subsequently, alkaline fuel cells were used in Apollo-series missions. The switch from membrane fuel cells was made to address the poor stability of the polymer electrolyte membrane. In addition, since the electro-osmotic drag force generated by the anion transport occurs in the opposite direction to the crossover of aqueous fuel, the fuel waste and related voltage reduction can be overcome. Therefore, AEM fuel cells are more robust to fuel and catalyst source.

We hypothesize that the ionic conduction through AEM strongly depends on the formation of water channels because the hydroxide anion (OH^-) is transferrable through such water channels. In order to achieve an enhanced ionic conduction, therefore, a three-

dimensional network of water channels in the polymer electrolyte membrane should be formed as a prerequisite. Besides, regarding the transport of OH^- through such water channels, it has been expected that the OH^- diffusion in AEM occurs via similar mechanisms to the proton (H^+) diffusion in PEM. Although the diffusion of H^+ and OH^- in bulk water has been well discussed and summarized by Tuckerman and his co-workers,[138, 139] to our knowledge, the nanophase-segregated structure and the corresponding OH- transport in AEM system have not been investigated thoroughly either by experiment or by simulation.

In this context, molecular dynamics (MD) simulation techniques have provided detailed information on the ionic transport, especially the proton transport through the PEM system. In previous studies, our group has used MD simulations to characterize various PEMs, such as Nafion,[4] Dendrion,[20] S-PEEK,[12] sulfonated polystyrene,[11] sulfonated sulfone,[55] mainly focusing on the relationship between nanophase-segregation and transport properties. The lesson from these studies is that the proton conduction is enhanced as a function of the nanophase-segregation because the key requirements for high proton conduction, such as the well-connected water channels and tight hydrogen-bonding network, are developed more through the nanophase-segregation.

Polysulfone-Based Anion Exchange Membrane

In this study, we investigated two types of polysulfone-based membranes (quaternary ammonium-functionalized anion exchange membrane and sulfonated proton exchange membrane) using molecular dynamics simulations to compare their nanophase-segregated structures and transport properties. We performed full-atomistic MD

simulations to elucidate the relationship between the nanophase-segregated structure and transport properties in quaternary ammonium-functionalized polysulfone-based AEM (PSU-A, Figure 20a). In order to objectively analyze the difference between AEM and PEM, we also simulated sulfonated polysulfone-based PEM (PSU-S, Figure 20b) as a counter system in which we used the same simulation conditions, such as molecular weight, degree of polymerization, degree of functionalization, equivalent weight, and extent of hydration (water content), listed in Table 10. Following the equilibrium MD simulation of each polymer membrane, the systems were then deformed following the same stretching procedure described in in Chapter 3 for Nafion. Here, we aim to understand how deformation affects the phase-segregated morphology both along and perpendicular to the direction of stretching. This ultimately provides a more complete picture of the structure-property relationships in PSU-based membranes.

We found that although the distribution of ionic groups on the polymer backbone is similar for both types, the quaternary ammonium groups and hydroxide ions in the anion exchange membrane were more solvated by water compared to the sulfonate groups and hydronium ions in the proton exchange membrane.[6] Correspondingly, better solvation of the ammonium groups and hydroxide ions led to a less matured hydrogen-bonding network in the water phase, especially at low water content condition. Through analyzing the nanophase-segregation of the membranes, a similar characteristic correlation length was found for both membranes, whereas the concentration contrast between the polymer domain and water phase was more distinct in the anion exchange membrane compared to the proton exchange membrane. Within such nanophase-segregated structures, it was found that the diffusion of hydroxide is ~ 6 % and ~ 11 % of

that of hydronium at 10 wt % and 20 wt % of water content, respectively, which might be due to the strong correlation at ~ 4 Å among the hydroxide in the anion exchange membrane. Uniaxial stretching of both the proton and anion exchange membranes confirmed the same trends as Nafion, where the undeformed model showed the strongest peak indicating a higher degree of phase segregation. The intensity is similarly decreased after the deformation, especially in the direction of stretching.

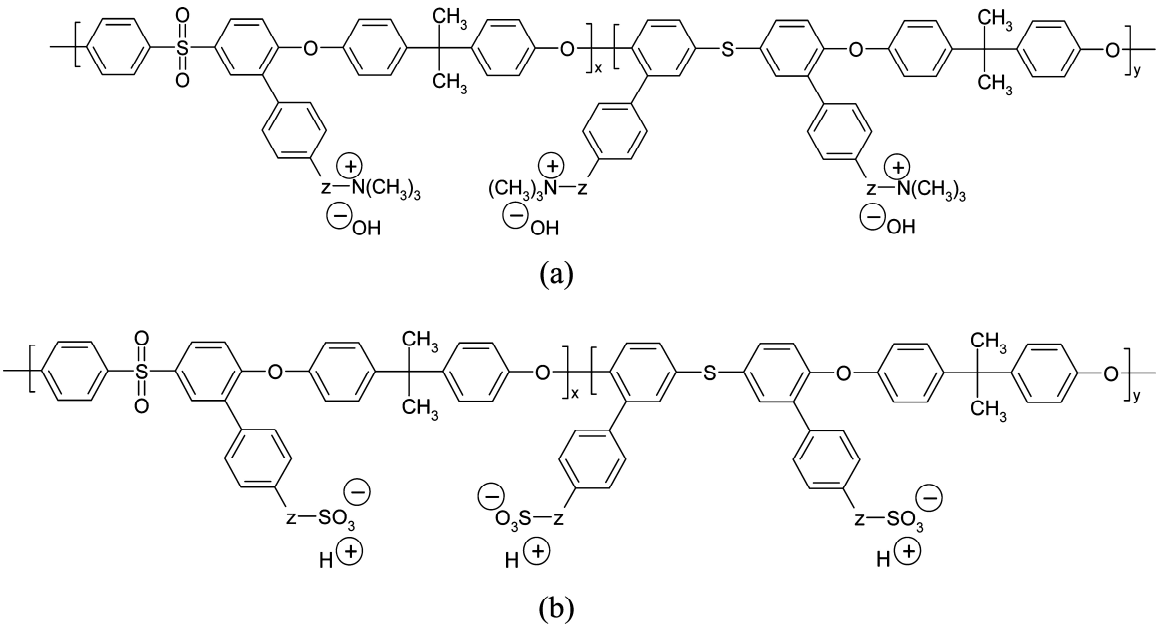

Figure 20: Chemical Structures of model polymers: (a) quaternary-ammonized polysulfone, PSU-A, and (b) sulfonated polysulfone, PSU-S.

Computational Models and Methods

All simulations were carried out using full-atomistic models of PSU-A and PSU-S with 10 wt % and 20 wt % of water content. The compositions of the PSU-A and PSU-S systems are summarized in Table 10.

Table 10: Composition of hydrated PSU-A and PSU-S systems and simulation conditions

Polymers	PSU-A (AEM)		PSU-S (PEM)	
Molecular weight	23286		23484	
Equivalent weight (daltons)	582		587	
Degree of polymerization	30		30	
Number of quaternary ammonium	40/chain		0	
Number of sulfonate	0		40/chain	
Water content (wt %)	10	20	10	20
Number of water molecule/ammonium (λ_N)	3.6	8.1	0	0
Number of water molecule/sulfonates (λ_S)	0	0	3.7	8.2
Density (g/cm^3) at 353.15 K	1.1192 ±0.0037	1.1774 ±0.0034	1.1922 ±0.0040	1.2455 ±0.0043

Force Field and Simulation Parameters

For this study, we used DREIDING[23] force field as previously used to study Nafion, and Dendrion as well as various molecular systems such as hydrogel,[57, 140-144] liquid-liquid and liquid-air interfaces[58, 145] and molecular self-assembly.[146]The water was described using the F3C force field.[59] These force field parameters were reported in the original papers[23], [59, 60]and in our previous study on hydrated Nafion. Thus the force field has the form:

$$E_{total} = E_{vdW} + E_Q + E_{bond} + E_{angle} + E_{torsion} + E_{inversion} \quad (11)$$

where E_{total}, E_{vdW}, E_{Q}, E_{bond}, E_{angle}, E_{torsion} and $E_{\text{inversion}}$ are total energies, van der Waals, electrostatic, bond stretching, angle bending, torsion and inversion components,

respectively. The individual atomic charges were assigned through the Mulliken population analysis using B3LYP and 6-31G** in Jaguar.[61] The Particle-Particle Particle-Mesh (PPPM) method[21] was used to calculate the electrostatic interactions.

Molecular Dynamics Simulation

All the MD simulations were performed using the MD code LAMMPS (Large-scale Atomic/Molecular Massively Parallel Simulator)[123] from Sandia National Laboratories with modifications to handle our force fields.[4] The equations of motion were integrated using the velocity Verlet algorithm[147] with a time step of 1.0 fs. The Nose-Hoover temperature thermostat[64, 65] for the NVT and NPT MD simulations used a damping relaxation time of 0.1 ps and a dimensionless cell mass factor of 1.0. To simulate OH^-, we developed a force field using the Hessian-biased singular value decomposition (HBSVD) method[148, 149] as summarized in Table 11 to reproduce the quantum mechanical vibrational frequency (3600.49 cm^{-1}) calculated using B3LYP and 6-311G**++ in Jaguar. The van der Waals, electrostatic, and bond energies described in equation 11 are calculated individually as described by equations 12, 13, and 14, respectively, in the original DREIDING paper.[23] The van der Waals non-bonded interactions (equation 12) are the Lennard-Jones 12-6 type expression. Here, D_0 is the van der Waals well depth and R_0 is the van der Waals bond length. Electrostatic interactions (equation 13) are calculated for non-bonded atoms. Interactions between bonded atoms or atoms involved in angle terms are assumed to be contained the bond and angle interactions. The bond interaction (equation 14) is described as a simple harmonic oscillator.

$$E_{vdW}(R) = D_0\left\{\left(\frac{R_0}{R}\right)^{12} - 2\left(\frac{R_0}{R}\right)^{6}\right\} \quad (12)$$

$$E_Q{}^a = 322.0637\sum_{i>j}\frac{Q_i Q_j}{\varepsilon R_{ij}} \quad (13)$$

$$E_{bond}(R) = \frac{1}{2}K_b(R - R_0)^2 \quad (14)$$

Table 11: Force Field used for hydroxide anion.

E_{vdW}	H (H_OH)	R_0[b]	0.9000	D_0[c]	0.0100
	O (O_OH)	R_0	3.5532	D_0	0.1848
E_Q	Q_{H_OH}	0.1135	Q_{O_OH}	-1.1135	
	(Q_{H_H3O}	0.4606)	(Q_{O_H3O}	-0.3819)	
E_{bond}	O_OH – H_OH	R_0	0.9665	K_b[d]	1042.3896

[a] Q_i and Q_j are atomic charge of atom *i* and *j*, respectively. ε = 1.
[b] Å for R_0. [c] kcal/mol for D_0. [d] kcal/mol/Å^2 for K_b.

Construction of Amorphous Membrane

We built hydrated PSU-A membranes consisting of four chains with 10 wt % and 20 wt % of water content (Table 10). The degree of polymerization, the molecular weight, and the equivalent weight of the PSU-A chain are 30, 20969 daltons, and 524 [units], respectively. We also built hydrated PSU-S membranes using approximately the same values for those simulation variables with the PSU-A membrane for direct comparison (Table 10). The only difference between PSU-A and PSU-S is the ionic group attached onto the polymer chain: ammonium for PSU-A and sulfonate for PSU-S.

Therefore, we can directly investigate the effect of such ionic groups on the nanophase-segregation and transport properties.

The initial amorphous structures of hydrated PSU-A and PSU-S systems were constructed in a three dimensional periodic cell using the Amorphous Builder of Cerius2. Since such initial structures of polymeric materials may include unstable conformations, the AEM and PEM are equilibrated using the annealing procedure, which accelerates the attainment of equilibrium by helping the system escape from various local minima and promote the migration of species for phase-segregation. After finishing the annealing procedure, a 100ps NVT MD simulation and a subsequent 500ps NPT MD simulation were performed at 353.15 K. Then, 100 ns NPT MD simulations were performed at the same temperature, from which the last 50 ns parts were used for the statistical analyses of properties. The equilibrated structures are presented in Figure 21.

Following the equilibration simulations, uniaxial deformation was applied up to 300 % strain at T=353.15 K for 1 ns, indicating that the strain was applied uniformly across the simulation box with the constant strain rate of 0.000186 Å/fs, and correspondingly the atomic coordinates were rescaled to the new box dimensions at each time step. This procedure was employed for the uniaxial deformation in *z*-axis direction. As the strain of 300 % was used in the initial simulations of Nafion and PSU-S, we also employed the same strain for comparison. Following the 1 ns deformation simulation, each system was allowed to equilibrate for 5 ns via NPT.

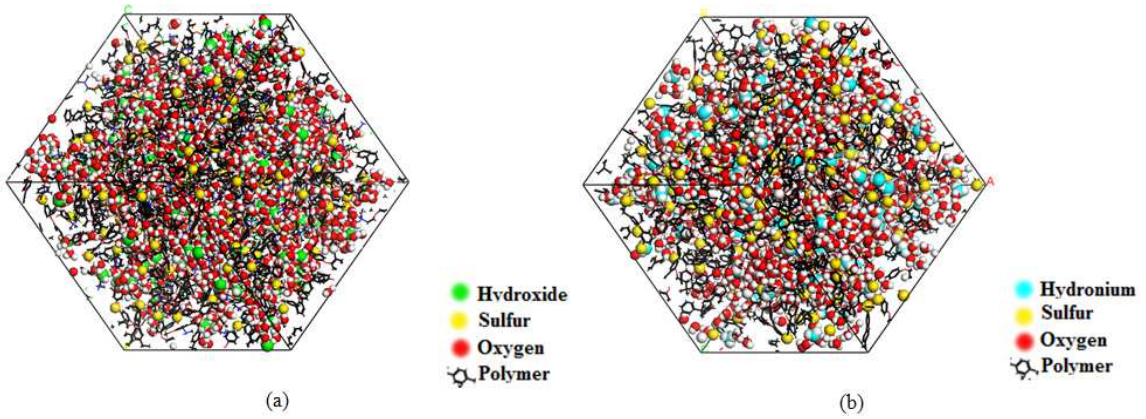

Figure 21: Nanophase-segregated structures of hydrated PSU-A (a) and PSU-S (b) membranes at 353.15 K with 20 wt % of water content. Equilibrated structures are shown before the deformation. The oxygen (red) represents the oxygen atoms belonging to water molecules.

Results and Discussion

Nanophase-Segregated Structures

Distribution of Quaternary Ammonium Groups

Water channel formation through the anion exchange membrane is a key factor for understanding the structure and properties of the AEM. In this study, we focus on the hydrophilic quaternary ammonium groups of the polymer as the main factor in determining the nanophase-segregation because the water molecules gather around such hydrophilic groups. To investigate the spatial distribution of the ammonium groups, the pair correlation function (PCF) is calculated by equation (1), representing the probability density of finding B atoms at a distance r from *A* atoms, averaged over the equilibrium trajectory:

$$g_{A-B}(r) = \left(\frac{n_B}{4\pi r^2 \Delta r}\right) / \left(\frac{N_B}{V}\right) \qquad (1)$$

where n_B is the number of atom B located at the distance r in a shell of thickness Δr from atom A, N_B is the number of B particles in the system, and V is the total volume of the system. For direct comparison, the number density (ρ_b) of atom B in a unit cell system, the number of B atoms divided by the total volume of the unit cell, is multiplied by $g_{A-B}(r)$.

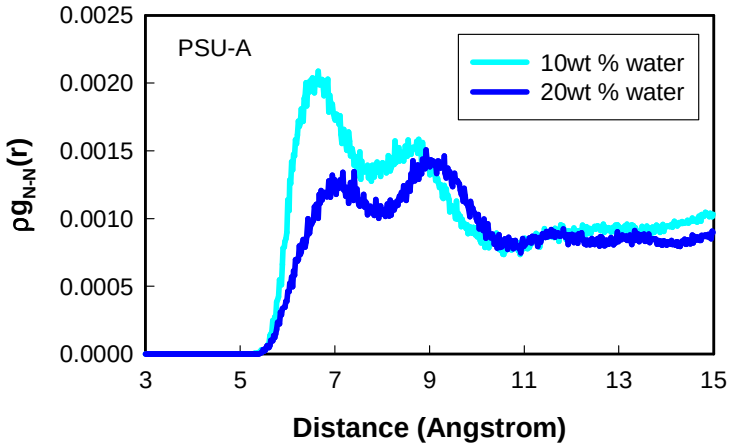

(a)

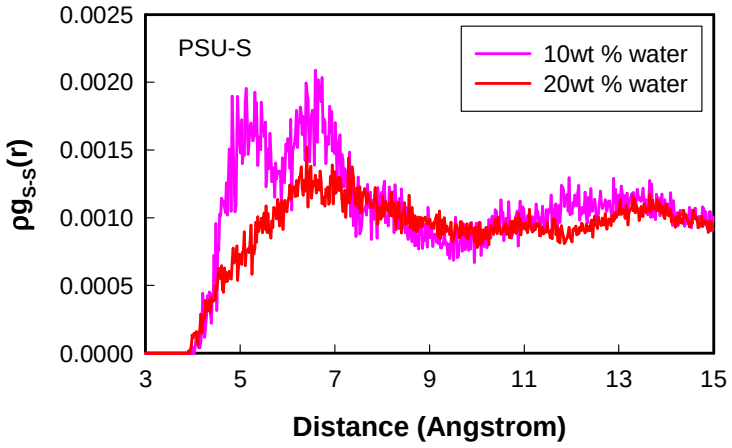

(b)

Figure 22: Pair correlation function of (a) nitrogen-nitrogen, in the hydrated anion exchange membranes and (b) sulfur-sulfur, in the hydrated proton exchange membranes.

The PCF of the quaternary ammonium pair ($g_{N-N}(r)$) for PSU-A is shown in Figure 22a. First, it is clearly observed that the PCF has two peaks for both water contents whose peak positions are shifted outwards with increasing water content: the first peak moves from 6.4 Å to 6.9 Å and the second peak increases from 8.4 Å to 9.1 Å. This shift means that the distance between ammonium groups is increased as the membrane is hydrated with more water. Such increased separation between hydrophilic ionic groups is similarly observed in the PSU-S membrane through the PCF of the sulfonate pair ($g_{S-S}(r)$): the two peaks at 5.0 Å and 6.4 Å merge into one broader peak at 6.9 Å with increasing water content, indicating that the S-S pairs at ~5.0 Å distance become farther apart as a function of water content. Thus, it is clear that the distribution of ionic groups attached on the polysulfone backbone depends on the extent of the hydration. From our previous study on the hydrated sulfonated PEEK membrane,[8, 130] this concentration-dependent distribution of the ionic group was observed. This behavior implies that the polymer electrolyte membranes adapt their structures as a function of water content. Another difference observed from Figure 22 is that the correlation distance between quaternary ammoniums (6.4 Å - 9.0 Å) is greater than that between sulfonates (5.0 Å - 6.9 Å), which would be due to the bulky size of quaternary ammonium (-$N(CH_3)^+$) compared to that of sulfonates (-SO_3^-).

Solvation of Quaternary Ammonium

To investigate how the quaternary ammonium is solvated by water, the PCF of the nitrogen-oxygen (water) pair ($\rho g_{N-O(water)}(r)$), Figure 23, is analyzed. The first solvation shell is observed at 4.6 Å commonly for both 10 wt % and 20 wt % of water content, while the second solvation shell is found at 7.0 Å and 7.2 Å for 10 wt % and 20 wt % of

water content, respectively. Compared to the PCF of the sulfur-oxygen (water) pair ($\rho g_{S-O(water)}(r)$ in Figure 23) with the first peak at 4.0 Å and the second peak at 5.4 Å, the $\rho g_{N-O(water)}(r)$ is found at a farther distance, which is also due to the bulky size of the quaternary ammonium. Accordingly, the number of water molecules surrounding such a bulky quaternary ammonium group should be larger than that surrounding the sulfonate groups. To confirm this, the water coordination number (CN) is calculated by integrating the pair correlation function (Figure 23) over the first solvation shell. As presented in Table 12, the water CN of the quaternary ammonium groups (CN (N)) in the PSU-A (6.9 and 11.5 for 10 wt % and 20 wt % of water content, respectively) are almost three times larger than that (CN (S)) of the sulfonates in the PSU-S (2.4 and 4.0 for 10 wt % and 20 wt % of water content, respectively). Thus, it is concluded that more water molecules are involved to solvate the quaternary ammonium groups in PSU-A membrane due to its bulkiness, in comparison to the sulfonate groups in PSU-A membrane.

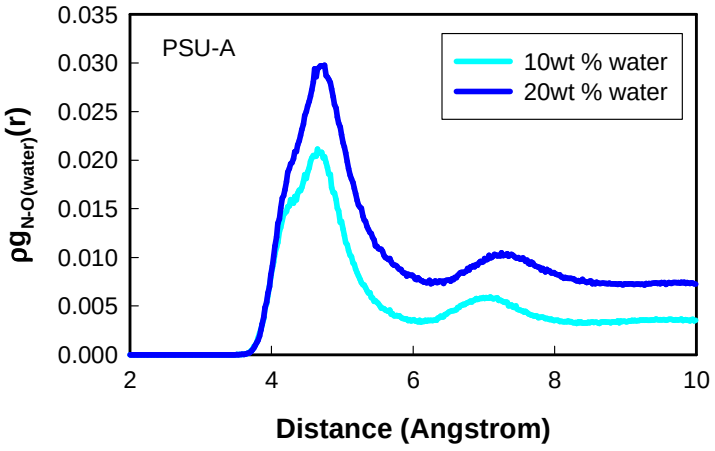

(a)

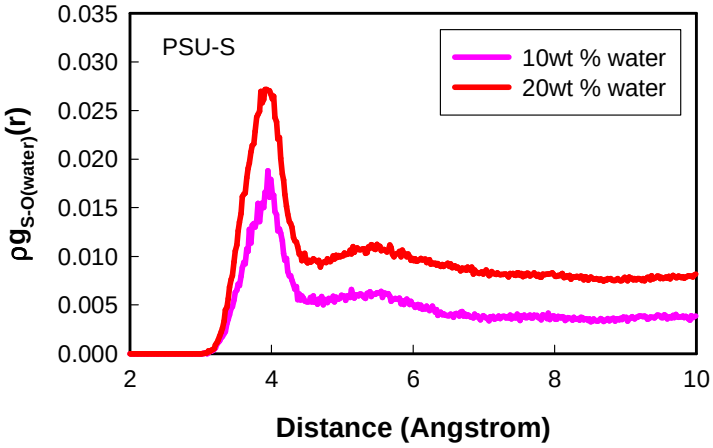

(b)

Figure 23: Pair correlation function of (a) nitrogen-oxygen (water), in the hydrated anion exchange membranes and (b) sulfur-oxygen (water), in the hydrated proton exchange membranes.

On the other hand, it is noteworthy from Table 12 that the CN (N) is larger than the average number of water molecules per ionic group (λ_N is 3.6 and 8.1 for 10 wt % and 20 wt % respectively), whereas the CN (S) is smaller than λ_S (3.7 and 8.2 for 10 wt % and 20 wt % respectively). Although the value of λ has been used to indicate the hydration level of polymer electrolyte membranes, it should be noted that λ is simply an arithmetically averaged number of water molecules without reflecting the actual local structures around the ionic groups. Hence, from the comparison between CN and λ, we can obtain more detailed information about the association of the ionic groups with the water phase in the membranes. For instance, from the observation that CN (S) is smaller than λ_S, it is inferred that the sulfonate group is solvated at the interface between the polymer phase and the water phase. In contrast, the observation that CN (N) is larger than λ_N, indicates that the quaternary ammonium group is located deeper inside of the water phase in order to be solvated by more water molecules. Considering that the PSU-A and PSU-S membranes have the same water content for comparison, this analysis means that

the water phase in the PSU-A membrane would be more perturbed by the ionic groups. Consequentially, the hydrogen-bonding network would be interrupted as well. This feature will be addressed later with the analysis of the water phase.

Table 12: Coordination Numbers (CNs) for solvation of ionic groups and ions in water

	PSU-A (AEM)		**PSU-S (PEM)**	
Water Content (wt %)	**N - O (H_2O)**		**S - O (H_2O)**	
	CN (N)	r^a (Å)	CN (S)	r^a (Å)
10	6.9	6.1	2.4	4.6
20	11.5	6.1	4.0	4.6
Water Content (wt %)	**O (OH^-) - O (H_2O)**		**O (H_3O^+) - O (H_2O)**	
	CN (OH^-)	r^a (Å)	CN (H_3O^+)	r^a (Å)
10	4.2	3.1	1.6	3.8
20	5.2	3.1	3.2	3.8

r^a represents the upper bound for integration, obtained from trough following the solvation shell

Correlation between Quaternary Ammonium and Hydroxide Anions

Next, to analyze the correlation of quaternary ammonium groups with hydroxide anions, we calculate $\rho g_{N-O(hydroxide)}(r)$. The correlations, shown in Figure 24, suggest that the electrostatic interaction holds a hydroxide ion around the quaternary ammonium at 4.6 Å and 4.7 Å for 10 wt % and 20 wt % of water content, respectively. First, it is clear that the $\rho g_{N-O(hydroxide)}(r)$ is weakened with increasing water content through solvation. By comparing to $\rho g_{S-O(hydronium)}(r)$ of PSU-S in Figure 24 showing the peak at 3.9 Å for both 10 wt % and 20 wt % of water contents, it is found that $\rho g_{N-O(hydroxide)}(r)$ is much weaker

than $\rho g_{S-O(hydronium)}(r)$ and the extent of the decrease of $\rho g_{N-O(hydroxide)}(r)$ is more significant than that of $\rho g_{S-O(hydronium)}(r)$ as a function of water content. We think this is because of the three bulky methyl groups attached on the quaternary ammonium, shielding its electrostatic interaction with hydroxide anion. Hence, the hydroxide ions can spread out more broadly from the quaternary ammonium group. In contrast, the hydronium has strong correlation with sulfonate groups since the oxygen atoms on sulfur interact with hydronium directly, such that the distance of the correlation does not depend much on the water content. These different correlations for hydroxide and hydronium are also reflected in their solvation in water.

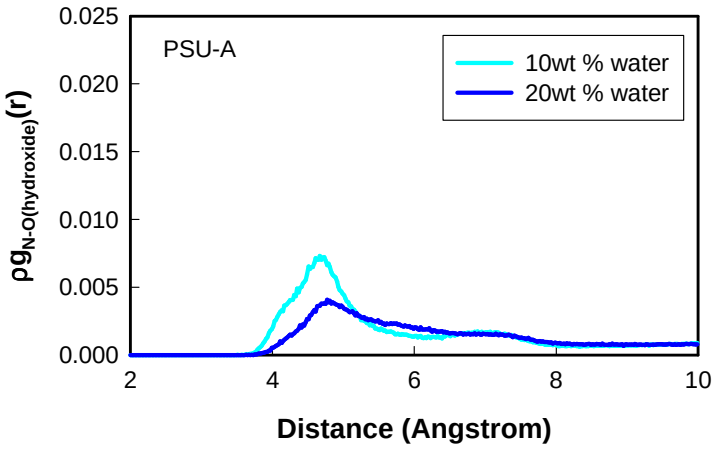

(a)

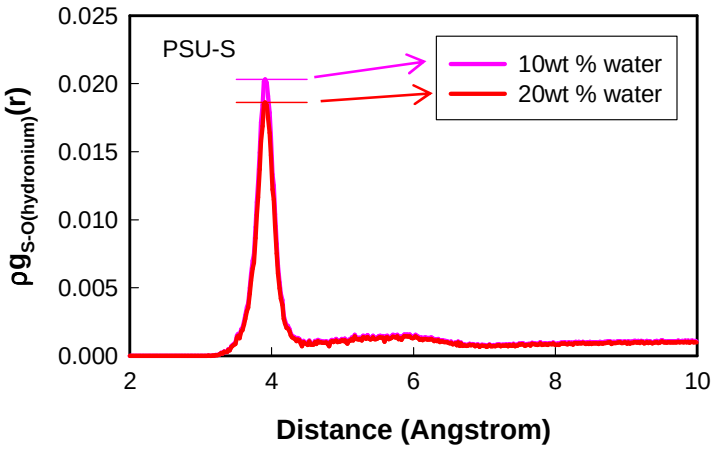

(b)

Figure 24: Pair correlation function of (a) nitrogen-oxygen (hydroxide), in the hydrated anion exchange membranes and (b) sulfur-oxygen (hydronium), in the hydrated proton exchange membranes.

Solvation of Hydroxide Anion

The relatively weak correlation between quaternary ammonium and hydroxide implies that the hydroxide would be well solvated by water. It is indeed confirmed by $\rho g_{O(hydroxide)-O(water)}(r)$ in Figure 25a. Compared to the hydronium-water correlation, $\rho g_{O(hydronium)-O(water)}(r)$, the stronger intensity of $\rho g_{O(hydroxide)-O(water)}(r)$ indicates that the hydroxide ions are better solvated in the water phase than the hydronium. For quantitative evaluation of this correlation difference, the water CNs of the hydroxide and hydronium are calculated as CN (OH^-) and CN (H_3O^+), respectively. As summarized in Table 12, CN (OH^-) is 4.2 and 5.2 for 10 wt % and 20 wt % of water content, respectively, while CN (H_3O^+) is 1.6 and 3.2 for 10 wt % and 20 wt % of water content, respectively, showing that the number of water molecules surrounding the hydroxide is larger than that surrounding the hydronium by ~260 % and ~140 % for 10 wt % and 20 wt % of water

content, respectively. These coordination numbers are consistent with reported values of 6 and 3 for hydroxide and hydronium in bulk water, respectively.[150, 151] Considering that the hydroxide and hydronium have the same amount of charge with opposite signs, however, a question would be raised about the reason for the better solvation of the hydroxide in comparison to the hydronium. We think that this would be due to the smaller size of the hydroxide with higher charge density, which leads to easier accommodation in water phase. This is also consistently confirmed by the DFT solvation energy calculation using the Poisson-Boltzmann model with B3LYP/6-31G**: -112.37 kcal/mol for OH^- and -99.08 kcal/mol for H_3O^+. Therefore, the better dissociation of the hydroxide from the ammonium group (Figure 24) can be explained by the better solvation of the hydroxide. Another point we should note is the effective size of the $OH^- - H_2O$ cluster. Since OH^- is surrounded by more water molecules than H_3O^+, the effective size of the $OH^- - H_2O$ cluster is larger than that of the $H_3O^+ - H_2O$ cluster, implying that the transport of OH^- would be less than that of H_3O^+.

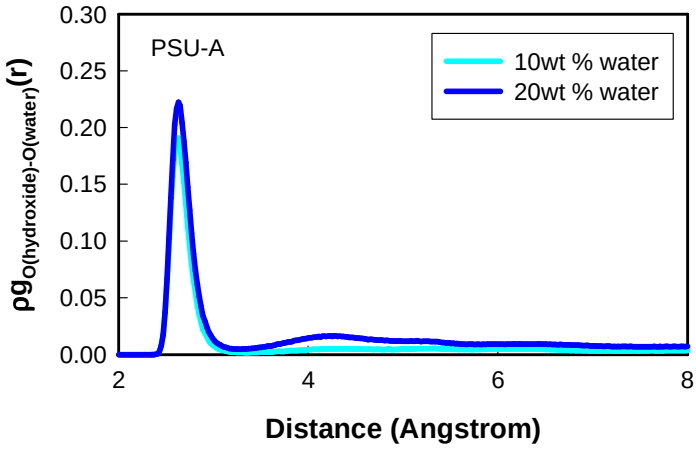

(a)

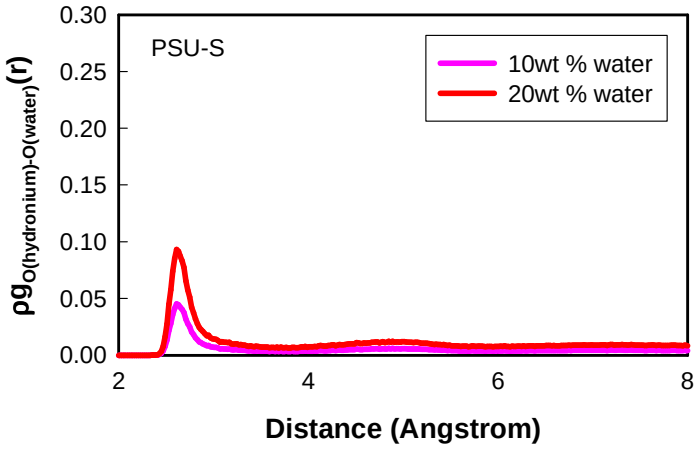

(b)

Figure 25: Pair correlation function of (a) oxygen (hydroxide)-oxygen (water), in the hydrated anion exchange membranes and (b) oxygen (hydronium)-oxygen (water), in the hydrated proton exchange membranes.

Internal Structure in Water Phase

From extensive studies on the proton transport through the water phase in polymer membranes,[152-157] a general consensus has been established, stating that the proton diffusion rate in bulk water is approximately four to eight times larger than that in the hydrated membrane. As pointed out by Kreuer,[152, 154] such an observation is attributed to the internal structure of the water phase, especially the hydrogen bonding network that aids efficient proton hopping. In contrast to the bulk water phase, the water phase in hydrated membranes has a relatively less developed hydrogen bonding network. Thus, a more developed internal water phase is essential to facilitating proton transport in the hydrated polymer membrane.

In order to analyze the internal structure in the water phase, we calculated $\rho g_{O(water)-O(water)}(r)$ for PSU-A and PSU-S membranes as shown in Figure 26. It is clearly

observed that the two $\rho g_{O(water)-O(water)}(r)$ are nearly the same for both systems at 20 wt % of water content, whereas, at 10 wt % of water content, the first solvation shell (from r = 2.6 to 4.1 Å) of the water in PSU-A is much less matured than that in PSU-S. These results indicate that the development of the internal structure of the water phase would be deterred by better solvation of OH^- at low water content conditions.

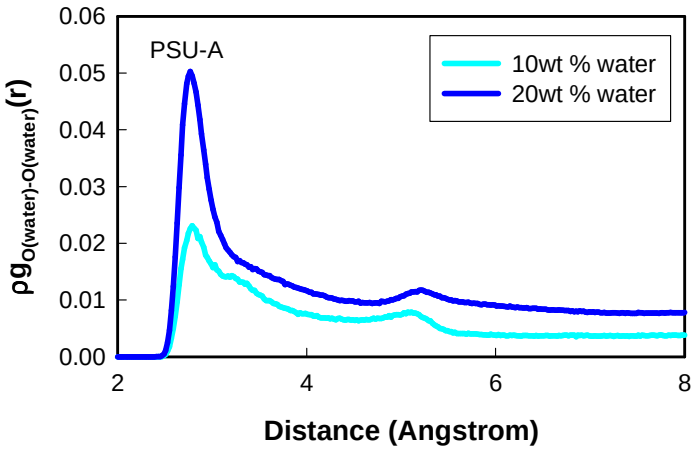

(a)

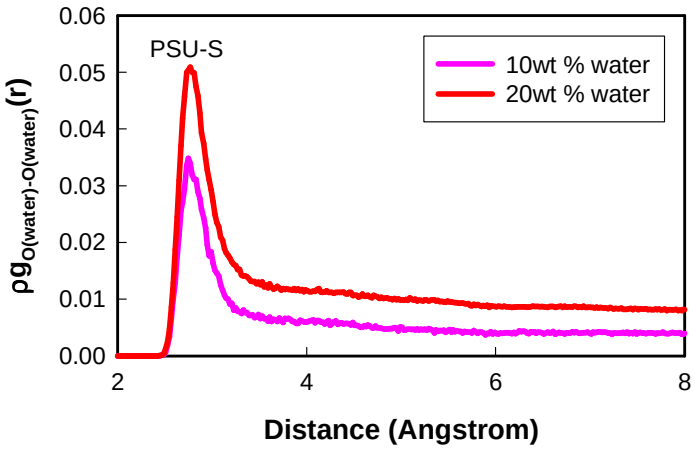

(b)

Figure 26: Pair correlation function of (a) oxygen (water)-oxygen (water), in the hydrated anion exchange membranes and (b) oxygen (water)-oxygen (water), in the hydrated proton exchange membranes.

Then, the next question would be how to attain more organized internal structures in the water phase of the PSU-A membrane. So far, we have reported that the internal structure in the water phase is determined by the nanophase-segregation in the polymer membranes with a given acidity.[8, 55, 85, 127-130] As the polymer membrane has a greater extent of nanophase-segregation between the hydrophobic polymer domain and the water phase, more water molecules can gather together, which results in a more developed hydrogen bonding network in the water phase. We have also reported that such a well-developed water phase facilitates better ionic transport. Therefore, we analyze the nanophase-segregation in PSU-A and PSU-S for comparison.

Extent of Nanophase-Segregation

Considering that the water phase is formed through nanophase-segregation between hydrophobic polymer backbones and hydrophilic pendant groups in the presence of water molecules, the difference in nanophase-segregation for PSU-A and PSU-S is the consequence of the different ionic groups (ammonium vs. sulfonate) because all other molecular variables are the same. To characterize the extent of nanophase-segregation of PSU-A and PSU-S membranes, we calculate the structure factor, $S(q)$ at each water content, which corresponds to the small angle scattering experiments (SAXS and SANS). This structure factor, $S(q)$ has been used to understand various systems such as copolymer systems[158] and polymer blend systems[42] as well as hydrated polymer membranes[8, 127-129] It is defined as follows:

$$\mathbf{S}(\mathbf{q}) = \left\langle \sum_{r_i} \sum_{r_j} exp\left(i\mathbf{q}\cdot\mathbf{r}_{ij}\right)\left(\xi^i \xi^j - \langle\xi\rangle^2\right) \right\rangle / L^3 \quad (8)$$

where the angular bracket denotes a thermal statistical average, ξ^i represents a local density contrast, $(\phi_A^j - \phi_B^j)$, $\boldsymbol{q}$ is the scattering vector and $\boldsymbol{r}_{ij}$ is the vector between the sites *i* and *j*. While SAXS and SANS experiments measure the electron-density contrast and deuterium-density contrast respectively, our structure factor is calculated from an artificial density contrast as follows. The local density variables are ϕ_A^j and ϕ_B^j: ϕ_A^j is equal to 1 if the site *j* is occupied by a hydrophilic entity such as water or a sulfonate group and equal to 0 otherwise, and ϕ_B^j is equal to 1 if the site is occupied by hydrophobic entities such as the polysulfone backbone or equal to zero otherwise. The quantity **S**(**q**) is spherically averaged as follows:

$$S(q) = \sum_{|\mathbf{q}|} \mathbf{S}(\mathbf{q}) / \sum_{|\mathbf{q}|} 1 \quad (9)$$

with $q = (2\pi / L)n$, where $n = 1, 2, 3, \cdots$ denotes that, for a given *n*, a spherical shell is taken as $n - 1/2 \le qL/2\pi \le n + 1/2$. Our previous studies for the hydrated Nafion membrane[127] led to a characteristic dimension of nanophase-segregation of 30 Å - 50 Å and similar studies for the hydrated Dendrion membrane[128, 129] and sulfonated PEEK[8] led to 20 Å - 40 Å and ~30 Å, respectively.

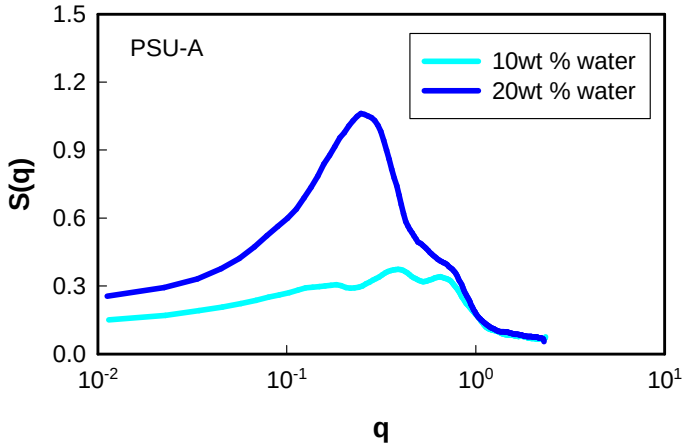

(a)

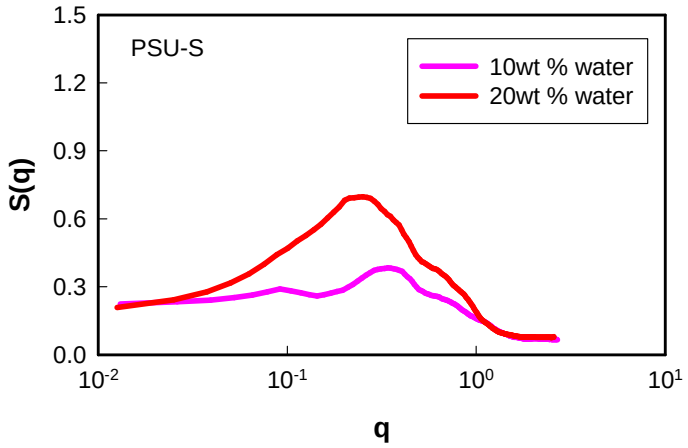

(b)

Figure 27: Structure factor profile for (a) PSU-A and (b) PSU-S

The structure factor profiles calculated from the hydrated PSU-A and PSU-S are presented in Figure 27. At 10 wt % of water content, it is commonly observed that both PSU-A and PSU-S have a peak at q = ~ 0.3 Å^{-1}, corresponding to ~ 20 Å, with nearly the same intensity of $S(q)$, meaning that the extent of nanophase-segregation is very similar. As the number of water molecules increases, this characteristic correlation length

increases accordingly: the position of the main peak is shifted to q = 0.24 $Å^{-1}$ corresponding to ~ 26 Å at 20 wt % of water content. This result indicates that the dimension of the water domain in PSU-A and PSU-S is increased to almost the same extent. It is understandable because the backbones and number of functional groups for PSU-A and PSU-S are exactly the same, so that the nanophase-segregation with respect to water molecules should be almost identical. However, it is noted from Figure 27a and Figure 27b that the intensity of $S(q)$ from PSU-A is much larger than that from PSU-S. Considering such intensity of $S(q)$ depends on the concentration contrast between the hydrophobic polymer domain and water phase, the stronger intensity in PSU-A than in PSU-S means that the water phase in PSU-A is more concentrated than that in PSU-S, which seems consistent with the results shown in Figure 23, and Figure 25. The quaternary ammonium is surrounded by more water molecules compared to the sulfonates (Figure 23), and those water molecules solvate the hydroxide ions better than the hydronium ions (Figure 25). Reports have suggested lower segregation strength from the polymer backbone to sulfonic groups.[45] However, phase segregation is largely influenced by the composition of the polymer backbone. Owing to the fact that both PSU-A and PSU-S have the same backbone, only differentiated by the sulfonate or quaternary ammonium group, and studied under the same levels of hydration, the similar phase segregation among the systems is unsurprising. Therefore, it is conclusive that the dimensions of the water phase in PSU-A and PSU-S are nearly the same, while the concentration of water in PSU-A is higher than that in PSU-S.

Transport Properties

There have been many studies on ion transport in nanostructures of ionomer membranes via experiments[154, 159, 160] and simulations.[8, 127-130] These studies have consistently proven that the diffusion of water and hydronium are enhanced in more nanophase-segregated structures. This enhancement is because the water molecules form a more bulk water-like structure in the phase-segregated morphology. In the resulting well-developed hydrogen-bonding network, moving water molecules do not undergo significant energy change during their displacement. The mean square displacement (MSD) of molecules, such as water, hydroxide and hydronium, are calculated from the final 50ns of the simulation trajectories, and the diffusion coefficients, *D*, are obtained from the linear part of the MSD by the following equation:

$$D = \lim_{t\to\infty} \frac{1}{6t} \left\langle \left(r(t) - r(0) \right)^2 \right\rangle \quad (4)$$

where $r(t)$ and $r(0)$ are the positions of a water molecule at time t and zero, respectively. The calculated diffusion coefficients only represent the vehicular diffusion of water, hydronium, and hydroxide. The classical MD simulations performed do not account for secondary mechanisms of transport, including proton hopping for hydronium or hydroxide. It is noted from Table 13 that the diffusion of water in PSU-A is ~7 % and ~40 % of that in PSU-S at 10 wt % and 20 wt % of water content, respectively, while the diffusion of hydroxide in PSU-A is ~ 6 % and ~11 % of the diffusion of hydronium in PSU-S at 10 wt % and 20 wt % of water content, respectively. We note that these values are lower than those calculated from previous simulations of Nafion. (~1.0×10^{-5} cm^2/s)[4, 43] This is consistent with the observation that polysulfone-based PEMs exhibit lower diffusivities in comparison to Nafion.[85] These values are also significantly lower than the translational diffusion coefficients in bulk water. (~6×10^{-5} cm^2/s)[20]

Table 13: Diffusion coefficients (*D*) for PSU-A and PSU-S at 353.15 K

Water Content	D ($\times 10^{-5}$ cm^2/s)			
	Water		Hydroxide[a]	Hydronium[a]
	PSU-A	PSU-S	PSU-A	PSU-S
10 wt %	0.005702	0.07771	0.0001636	0.002856
20 wt %	0.073800	0.18810	0.0037050	0.033100

a The diffusion coefficient for hydroxide and hydronium is calculated from the vehicular mechanism.

What we understand from our previous studies is that the molecular diffusion is enhanced more with increased nanophase-segregation. At first glance, therefore, our simulation results in this study seem to be contradictory to our understanding since the molecular diffusion of water and ions are lower in PSU-A in comparison to PSU-S, despite its more developed nanophase-segregation, especially at 20 wt % of water content as shown in Figure 27. We think a clue might be found in the solvation of OH^-. As discussed above, OH^- is solvated better than H_3O^+, which results in a larger solvation cluster for OH^- and, thereby the diffusion of OH^- through water phase could be deterred.

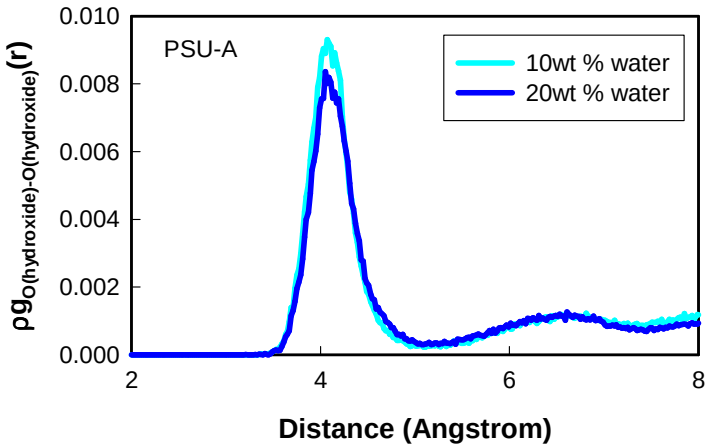

(a)

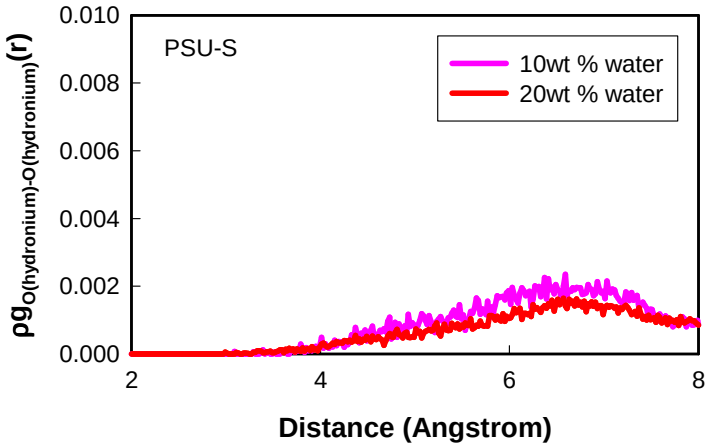

(b)

Figure 28: Pair correlation function of (a) oxygen (hydroxide)-oxygen (hydroxide), in the hydrated anion exchange membranes and (b) oxygen (hydronium)-oxygen (hydronium), in the hydrated proton exchange membranes.

Another interesting clue is the pair correlation among charge carriers: the $OH^- - OH^-$ correlation in PSU-A and the $H_3O^+ - H_3O^+$ correlation in PSU-S. Figure 28 shows a surprising comparison between $\rho g_{O(hydroxide)-O(hydroxide)}(r)$ and $\rho g_{O(hydronium)-O(hydronium)}(r)$: the hydroxide ions have a very strong first correlation peak at ~ 4 Å and the second peak

at ~ 6.6 Å whereas the hydroniums have a very broad peak at ~ 6.6 Å, but no peak at ~ 4 Å. Thus, the molecular view based on Figure 28a is that the hydroxide ions in PSU-A are distributed regularly through water phase with ~ 4 Å of distance from each other, which is not the case for the hydroniums in PSU-S (Figure 28b). From such differences in the correlation between charge carriers (Figure 28) as well as the diffusion coefficients (Table 4), it is presumed that the high correlation among hydroxide ions may restrict the mobility of OH^- through the water phase, which seems reasonable since the H_3O^+ does not show such strong correlation at ~ 4 Å and correspondingly has a larger diffusion coefficient. Here, it is also noted that the correlation between hydroxide ions could affect the water diffusion since the restricted movement of OH^- may restrain the diffusivity of water molecules. For a rationalization of why only the hydroxide ions have stronger correlation at ~ 4 Å, we may scrutinize the difference between OH^- and H_3O^+. Although both charge carriers have the same amount of net charge (-1.0 and +1.0 for OH^- and H_3O^+, respectively), there is only one hydrogen in the OH^- compared to three hydrogen in the H_3O^+. Thus, the hydroxide ion has larger charge values per atom in a more compact size, which would facilitate the solvation in water through stronger associative electrostatic interaction in addition to hydrogen bonding interaction. This would cause the hydroxide anion mobility to be suppressed by the greater number of solvating water molecules. Furthermore, the uniaxial molecular structure of the hydroxide may induce more dipole-dipole interaction with preferred orientations in comparison to the tripod shape of the hydronium, which imposes another restriction on the hydroxide ion mobility. Therefore, from this study, it is learned that the transport of the hydroxide ion would be restrained molecularly despite the greater nanophase-segregation in PSU-A

membrane. We find our lower transport results consistent with literature reported values. The diffusion coefficient of hydroxide ions is half of that of protons in bulk water as measured in experiment.[138] Additionally, the diffusion coefficient of protons in PEM is usually four times higher than for hydroxide in AEM, and in general for nearly all media.[137, 161] We believe that a more detailed elucidation is required to understand the low diffusivity of the hydroxide anion, which is left for future study.

Deformation of polysulfone-based polymer membranes

Similar to the Nafion simulations presented earlier, the local structure of polysulfone-based proton and anion exchange polymer membranes show little change as a result of deformation. Of greater interest is the effect of uniaxial stretching on the phase-segregated membrane morphology. The nanophase-segregation of the hydrated polymer membrane describes the extent to which the water and polymer phases are separated. A more developed separated structure is essential to for improving proton transport properties. To characterize the effect of stretching on nanophase-segregation, the anisotropic structure factor is calculated as described for Nafion in Chapter 3. The structure factor for the isotropic structure that is calculated from the Fourier transform of the PCF is a spherically averaged measure of particle arrangement in in real space. In this simulation study, however, the structure is uniaxially extended, which would develop anisotropic feature in the hydrated membrane. In order to evaluate the effect of such uniaxial deformation, therefore, the directional structure factor was calculated along the direction of specific reciprocal space vectors, **k**, such as (100), (010), and (001). These directions are chosen based on the deformation direction during our MD simulations.

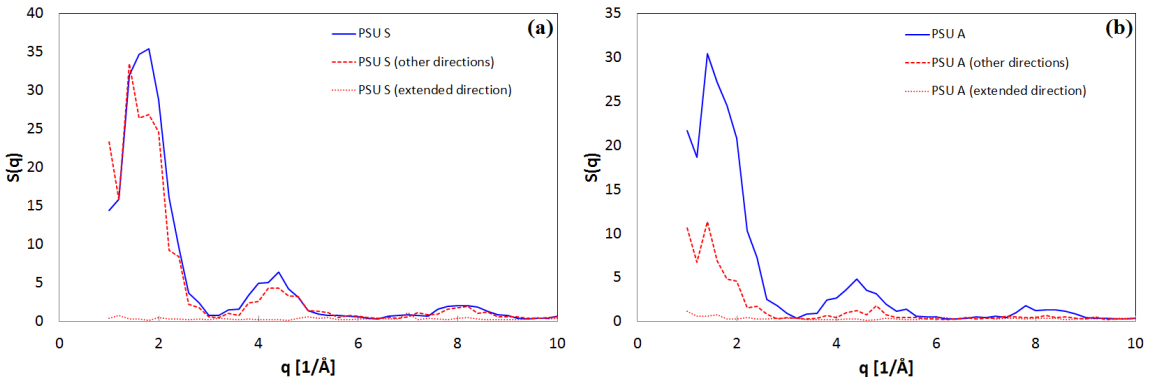

Figure 29: Structure factor profile for (a) PSU-S and (b) PSU-A. The blue profile represents the membrane before deformation. The dashed red line is the structure factor calculated perpendicular to the deformation, while the dotted red line is in the direction of stretching.

Figure 29 shows the structure factor profile calculated from hydrated PSU-S and PSU-A before and after deformation. The structure factor profiles are calculated as a function of the scattering vector, **q**. Before the deformation, the strongest peak is found at q=1.5 $[LÅ]^{-1}$ whereas its intensity is significantly decreased after the deformation, especially in the direction of extension. We believe this change in the structure factor profile indicates that the nanophase-segregated structure is significantly deformed and rearranged during the uniaxial extension, and thereby the long-range correlation along the extended direction is suppressed very much. The other directions perpendicular to the extended direction also show a small reduction in their intensities in Figure 29, meaning that the nanophase-segregated structure in the hydrated PSU membranes lose some portion of the long range correlation at q=1.5 $[LÅ]^{-1}$ during the deformation. Instead, it should be noted that the longest range correlation in our structure factor profile analysis at k=1 $[LÅ]^{-1}$ is increased more than twofold. We believe this is clear evidence that the nanophase-segregated structure develops greatly in the perpendicular direction to the extended direction, implying a more developed water phase correspondingly, since the

enhanced segregation and developed water phase are desirable for transport properties in the membrane.

Table 14: Vehicular diffusion coefficients (D) of water and hydronium ions

	D ($\times 10^{-5}$ cm^2/s)					
Simulation	**Water**			**Hydroxide/Hydronium**		
	Total	**Def Perp.**	**Def Ext.**	**Total**	**Def Perp.**	**Def Ext.**
Undeformed PSU-A	0.0051	0.0022	0.0032	0.0006	0.0003	0.0002
Deformed PSU-A	0.0071	0.0034	0.0038	0.0014	0.0007	0.0008
Undeformed PSU-S	0.0295	0.0157	0.0128	0.0004	0.0003	0.0001
Deformed PSU-S	0.7353	0.4814	0.1401	0.0017	0.0009	0.0008

Similar to deformed Nafion, the transport properties of water, protons, and hydroxide anions in PSU-based polymers give some indication of the performance in PEM and AEM environments. By far, the most significant improvement in diffusivity was observed for water in the PSU-S system following deformation. Particularly, the diffusion of water in the directions perpendicular to stretching is nearly four times larger than in the direction parallel to drawing. The diffusivities observed in the PSU-A system are significantly lower, as expected. Overall, the total diffusivities of all species are improved following deformation.

Multiblock Copolymer-based Anion Exchange Membranes

The simulations discussed earlier provide a fundamental comparison between PEM and AEM using a well-known polymer backbone. The drawbacks hindering AEM development were highlighted by the choice of a hydrocarbon-based polymer backbone relative to PEMs with similar backbones. In this section, we turn our attention to new AEMs with novel molecular architectures in polymer backbone. Recently, AEM studies have sought to design more stable, high conducting membranes by mimicking the

properties desirable in PEMs. The challenges of hydrocarbon-based AEMs, like the quaternary ammonized polysulfone-based membrane described earlier, include poor hydroxide conductivity at low levels of hydration as well as poor stability due to the chemical degradation.

To achieve improved transport properties in AEMs similar to those of PEMs, it is thought that we need to create more nanophase-segregation at moderate hydration levels. For this, increasing the hydrophobicity of the polymer backbone is considered in order to induce more developed water domains and channels via nanophase-segregation. Consequently, this should facilitate better transport of water molecules and hydroxide ions.

So far, significant progress has been made in designing multiblock anionic conducting polymer membranes.[162] Although the new membranes attained desirable levels of ionic conductivity, they exhibited undesirably high water uptake. This leads to both swelling and unstable properties as a function of operating temperatures. To address this, recent efforts have attempted 1) to regulate the hydrophobicity of the polymer by employing fluorination in multiblock copolymers and 2) to optimize the ion exchange capacity via the number of hydrophilic polar groups. We sought to model the new molecular architectures of polymers with the variables abovementioned to establish structure-property relationships.

The chemical synthesis of novel anion exchange membranes was performed by Dr. Kohl's Research Group at Georgia Tech.[163] The chemical structure of the one and two-tethered multiblock copolymers is shown in Figure 30.

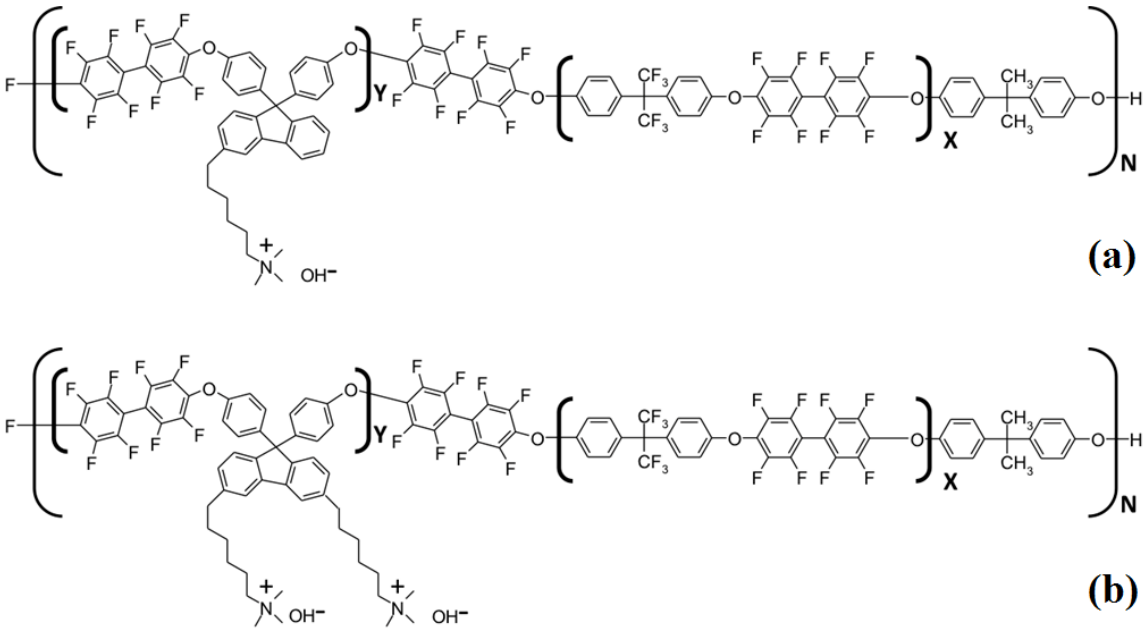

Figure 30: Chemical structures of recently synthesized multiblock copolymers for anion exchange membranes with (a) one and (b) two anion tether groups.

Modeling and Simulation Methods

The anion exchange membranes consisting of quaternary ammonized multiblock copolymers were modeled and simulated using the same protocol described earlier in this chapter. The force fields used for simulating these polymers are also the same as those used before. The block compositions and number of tethered side chains were determined to have the same conditions as their experimental counterparts. In this study, we simulated three polymer configurations: X_5Y_7-1, X_5Y_7-2, and X_3Y_8-2. In our simulations, each hydrated membrane contains four polymer chains with two repeat units (N=2 in Figure 30) and the experimentally determined water content. A summary of the simulated polymers is provided in Table 15. The analyses were implemented using the equilibrated polymer membranes. Despite similar molecular weights among the polymer

chains and densities of the hydrated membranes, the size of the simulation cell varies due to the difference in water uptake.

Table 15: Summary of simulated block copolymer anion exchange membranes

Ionomers	X_5Y_7-1	X_5Y_7-2	X_3Y_8-2
Molecular weight per chain (daltons)	18599	20590	19927
Dimension of simulation box (Å)	49.69±0.09	63.31±0.06	54.18±0.06
No. of quaternary ammonium per chain	14	28	32
Density (g/cm^3) at 353.15 K	1.11±0.006	1.12±0.003	1.16±0.004
Water content (wt %)	8.0	50.8	26.7
λ	7.5	44.1	13.9

Results

Experimental Characterization

The synthesis and experimental characterization of the polymers presented here were performed by Professor Kohl's Group at Georgia Tech.[163] Table 16 presents the basic characteristics and properties of the newly synthetized polymer membranes. From the seven noted multiblock copolymers, the following configurations were selected for simulation: $X_{5.4}Y_7$-1, $X_{5.4}Y_7$-2, and $X_{3.1}Y_8$-2. For simplicity, the block ratios of the amorphous membranes were set to X_5Y_7-1, X_5Y_7-2, and X_3Y_8-2, respectively, for simulations. From the measurements shown in Table 16, the $X_{5.4}Y_7$-2 copolymer demonstrated the highest hydroxide conductivity. However, the highest hydroxide conductivity came with the concession of high water uptake (50.77 wt %). The one-tether copolymers show lower water uptakes, but also demonstrate low conductivity and ion exchange capacities. Thus, it seems that the high conductivity of $X_{5.4}Y_7$-2 is due to the addition of a second tethered quaternary ammonium group to the block copolymer backbone. Modifying the ratios has demonstrated that high hydroxide conductivity can be

achieved while lowering the water uptake by nearly half of the initially synthesized $X_{5.4}Y_7$-2 copolymer.

Table 16: Summary of membrane properties [163]

Membrane	Channel size (nm)	Molecular Weight (GPC)	IEC (meq/g)	OH^- Conductivity (mS/cm)		Water uptake (wt %)
				R.T.	80°C	
Y_8-1	16.5 ± 3.9	18k	1.18	13.1	36.1	35.9
$X_{3.1}Y_{3.6}$-1	7.8 ± 1.2	88.6k	0.66	16.4	51.5	5.5
$X_{5.4}Y_7$-1	9.7 ± 1.6	68.2k	0.73	14.2	34.7	8.0
$X_{5.4}Y_7$-2	22.5 ± 2.9	68.2k	1.30	38.2	119.7	50.8
$X_{3.1}Y_8$-2	15.3 ± 1.3	55.9k	1.56	23.1	94.0	26.7
$X_{3.1}Y_{3.6}$-2	12.2 ± 1.4	66.0k	1.19	25.8	85.0	25.0
$X_{5.9}Y_5$-2	11.3 ± 1.9	59.0k	1.10	22.1	66.7	19.6

Understanding the structure-property relationship of these novel AEMs is important to fully characterize their performance. Limited experimental analysis is available about these block copolymers. However, nanoscale images obtained through atomic force microscopy, (AFM) shown in Figure 31, offer insight into the domain size of these membranes. These results show the domain size ordering of $X_{5.4}Y_7$-2 > $X_{3.1}Y_8$-2 > $X_{5.4}Y_7$-1, which is consistent with the conductivity trends. The conductivity and domain size characterization offer a basis for comparison and validation of simulation results.

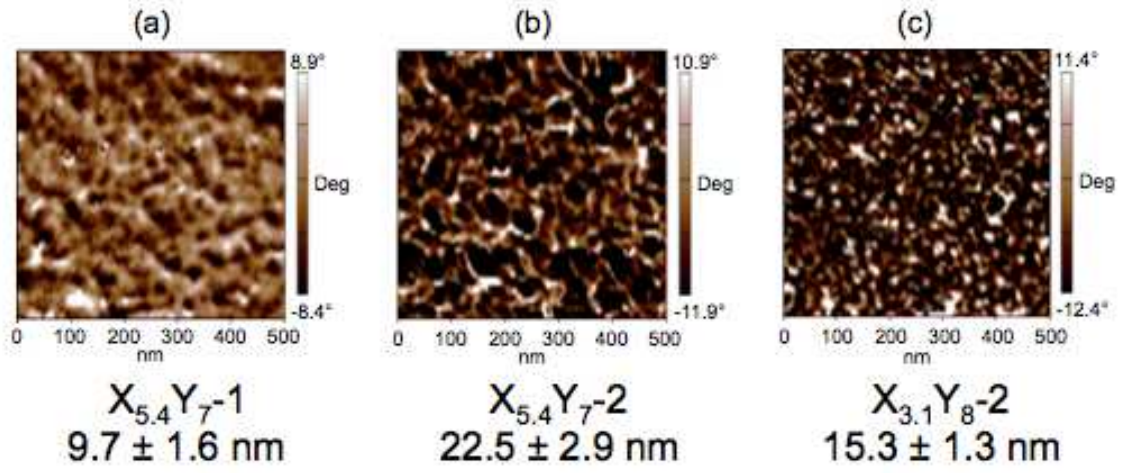

Figure 31: Atomic Force Microscopy images of mPES membranes.[163]

Computational Results

The equilibrated structures of the simulated hydrated X_5Y_7-1, X_5Y_7-2, and X_3Y_8-2 membranes are shown in Figure 32. The gray and green regions denote the carbon and fluorine in the polymer backbone, while the red regions represent the oxygen from the water molecules. These structures indicate the low level of hydration in X_5Y_7-1 and the high water content in X_5Y_7-2. The structure-property relationships were characterized using pair correlation functions for local structure, structure factor for domain sizing and correlation, and mean squared displacement for diffusivity. These analyses were performed as previously described in the chapter. The hydroxide anion transport in AEMs is expected to correlate with water channel development. The first clues about the structure of the hydrated membranes can be found in the local structure, characterized by the pair correlations of key molecular groups. Of particular interest are quaternary ammonium groups, water, and hydroxide molecules. The local distribution of these molecules is investigated in the following sections.

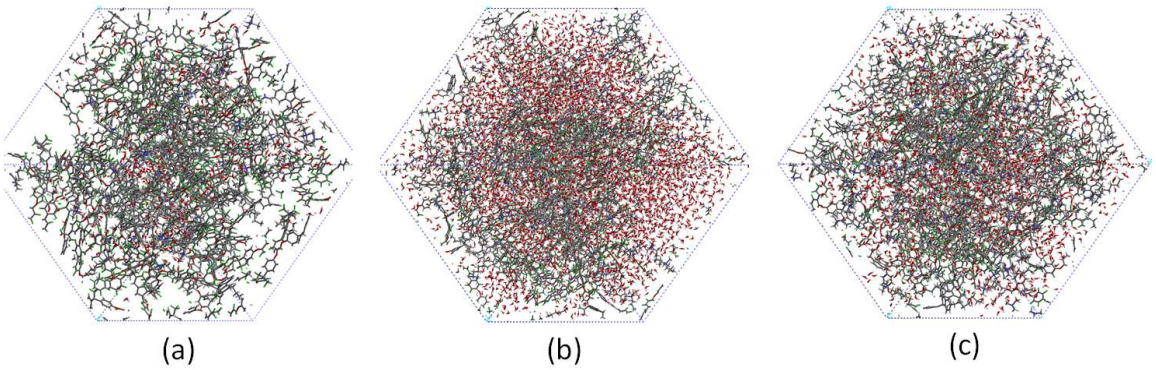

Figure 32: Equilibrated structures of (a) X_5Y_7-1, (b) X_5Y_7-2, and (c) X_3Y_8-2.

Quaternary ammonium group distribution

The PCF of the nitrogen-nitrogen pair in Figure 33 shows unique profiles for each of the polymer membranes. First, it is found that the X_5Y_7-2 profile shows the lowest nitrogen-nitrogen peak intensity compared to those of other membranes, which is likely due to the high water content (~50 wt %) in the X_5Y_7-2 membrane. Next, it is also found that both X_5Y_7-1 and X_3Y_8-2 show the first hydration peaks at ~7 Å, while X_5Y_7-2 does not show a peak at the same location. This suggests that quaternary ammonium groups in the X_5Y_7-2 membrane are unlikely to be found in close proximity to one another as observed in the other membranes. We think that this is also likely due to the high water content (~50 wt %) in the X_5Y_7-2 membrane.

A more distant second peak is found in all three membranes. X_5Y_7-1 shows a narrow second peak at ~8.8 Å while X_5Y_7-2 and X_3Y_8-2 share a common broad peak at 9.3 Å. Additionally, the X_5Y_7-1 profile notably lacks a third peak centered at ~12.5 Å, whereas this peak is only observed for the two-branch membrane systems (X_5Y_7-2 and X_3Y_8-2). It is thought that this peak at ~12.5 Å is due to the intramolecular correlation of quaternary ammonium groups. Furthermore, this may suggest the cationic groups on the same monomer are spaced farther apart, resulting in a rearrangement of the copolymer

backbone, and subsequently, increased ion exchange capacity. Conclusively, the quaternary ammonium groups are highly solvated with respect to water throughout the membrane, so that the N-N correlation is very sensitive to the water content.

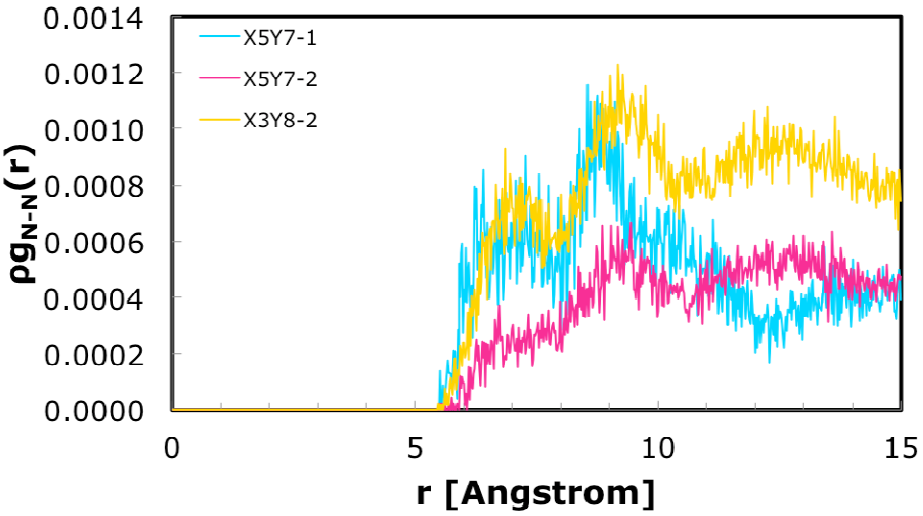

Figure 33: Pair correlation function of nitrogen-nitrogen for quaternary ammonium groups in simulated X_5Y_7-1, X_5Y_7-2, and X_3Y_8-2.

Solvation and dissociation of ionic groups

To investigate the solvation of quaternary ammonium in the hydrated membranes, the PCF for Nitrogen (quaternary ammonium)-Oxygen (water) pair is analyzed as shown in Figure 34. From the calculated profiles, it is apparent that the more hydrated membranes displayed the most intense peaks. While the first solvation peak for each membrane has the same position, the thickness of the solvation shell is clearly increased as a function of water content. Correspondingly, the second peak position is shifted out with increasing the water content. From this result, it is implied that the water channels are formed and developed in the membrane as a function of water content. In other words, the more developed water channels may allow better transport of water and ions.

To confirm this, the coordination number of water surrounding quaternary ammonium is calculated by integrating the first solvation shell in Figure 34. The results are presented in Table 17. The coordination numbers are 7.8, 20.3, and 14.1 for X_5Y_7-1, X_5Y_7-2, and X_3Y_8-2, respectively. Overall, the calculated coordination numbers confirm the solvation trend indicated in Figure 34. The quaternary ammonium groups in the X_5Y_7-2 membrane are the most solvated and surrounded by the most water molecules, while those in the X_5Y_7-1 membrane are surrounded by the least.

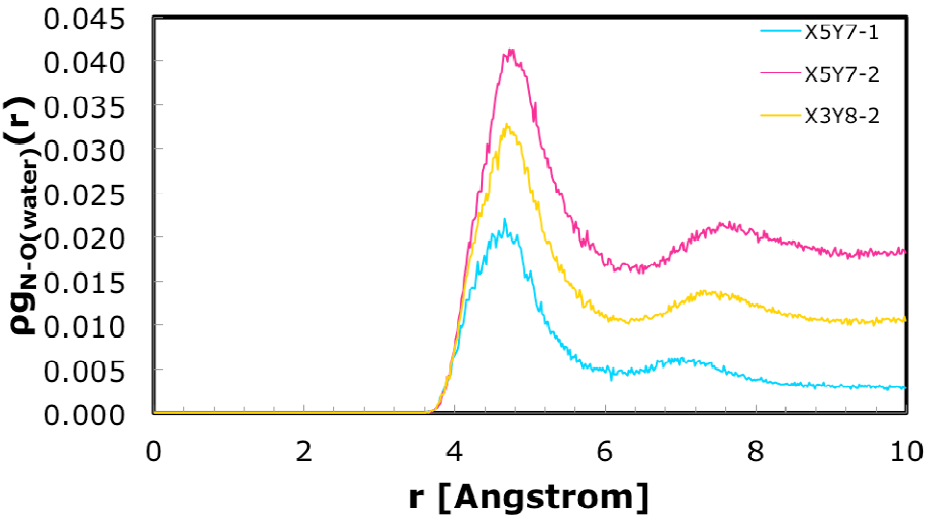

Figure 34: Pair correlation function of nitrogen-oxygen (water) for quaternary ammonium groups in simulated X_5Y_7-1, X_5Y_7-2, and X_3Y_8-2.

Another clue regarding the membrane performance can be found in the pair correlation functions between quaternary ammonium groups and hydroxide anions. These profiles are analyzed as shown in Figure 35. An inverse relationship between peak intensity and membrane conductivity is readily apparent. The poorest conducting membrane, X_5Y_7-1, shows a sharp peak at ~4.7 Å for the PCF of the N (quaternary ammonium) and O (hydroxide), while, X_5Y_7-2 shows no clearly centered peak. This indicates that the hydroxide is more closely correlated with the quaternary ammonium in

X_5Y_7-1, while almost completely dissociated in X_5Y_7-2. More indicative of the condition of hydroxide ions in the hydrated membrane is the degree of solvation. This can be quantified through the water coordination number for the hydroxide ions as presented in Table 17. The trend here is opposite of that found from the pair correlation between quaternary ammonium and hydroxide. Whereas the hydroxide ions are closely correlated with quaternary ammonium in the lower conducting membranes, the hydroxide ions are more highly solvated in high conducting membranes. X_5Y_7-2 and X_3Y_8-2 show the highest CNs of 5.9 and 5.6, respectively. X_5Y_7-1 shows the lowest CN of 4.9. Physically, the hydroxide ions surrounded by more water molecules diffuse more readily through the membrane. Furthermore, this implies that the internal membrane structure of X_5Y_7-2 and X_3Y_8-2 are better developed for hydroxide ion transport. A more clear indication of this phenomenon can be found by analyzing the extent of the nanophase-segregation of these membranes.

Table 17: Coordination Numbers (CNs) for the solvation of quaternary ammonium groups and hydroxide anions

	N-O (H_2O)		**OH-O (H_2O)**	
	CN (N)	**r^a (Å)**	**CN (OH)**	**r^a (Å)**
X_5Y_7-1	7.8	6.2	4.9	3.2
X_5Y_7-2	20.3	6.4	5.9	3.2
X_3Y_8-2	14.1	6.3	5.6	3.2

r^a represents the upper bound for integration, obtained from trough following the solvation shell

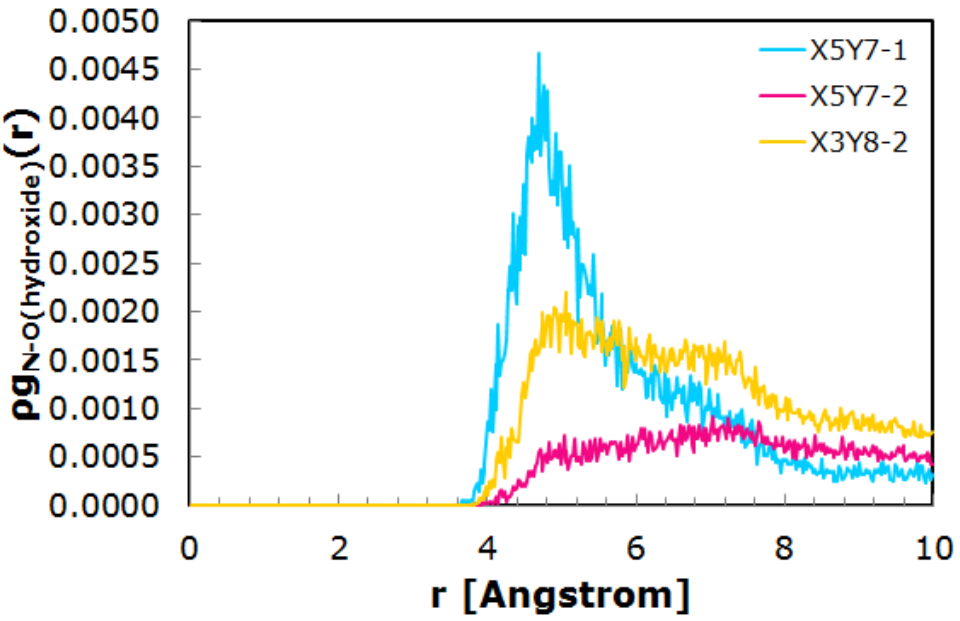

Figure 35: Pair correlation function of nitrogen-oxygen (hydroxide) for quaternary ammonium groups in simulated X5Y7-1, X5Y7-2, and X3Y8-2.

Nanophase segregation

The isotropic structure factor, described earlier, is used to characterize the extent of nanophase segregation of the three membranes. The structure factor profile can be obtained from small-angle scattering experiments such as SAXS and SANS. These measurements can be used to characterize density-density spatial correlation, providing nano-scale domain size in polymer membranes. In this section, the structure factor is calculated to discuss the effect of molecular architecture on the nanophase segregation. Figure 36 shows the structure factor profiles for the three simulated anion exchange membranes. From the profile, X_5Y_7-2 shows the greatest peak intensity and lowest value of q_{max}, indicating the largest water domain size among the membranes in this study. X_5Y_7-2 also shows two distinct peaks. For analysis, the second peak, located at q = 2.3 is used. X_3Y_8-2 shows a peak centered at q = 2.8. Last, X_5Y_7-1 does not show a distinct peak, and therefore, no significant nanophase-segregation can be claimed to occur. An

approximate domain size of 1.8 nm is estimated for X_5Y_7-1. Similarly, the domain sizes for X_5Y_7-2 and X_3Y_8-2 are 2.7 and 2.2 nm, respectively. These results show strong agreement with the experimentally measured domain size ordering of 22.5 nm (X_5Y_7-2) > 15.3 nm (X_3Y_8-2) > 9.7 nm (X_5Y_7-1) indicated in Figure 31.

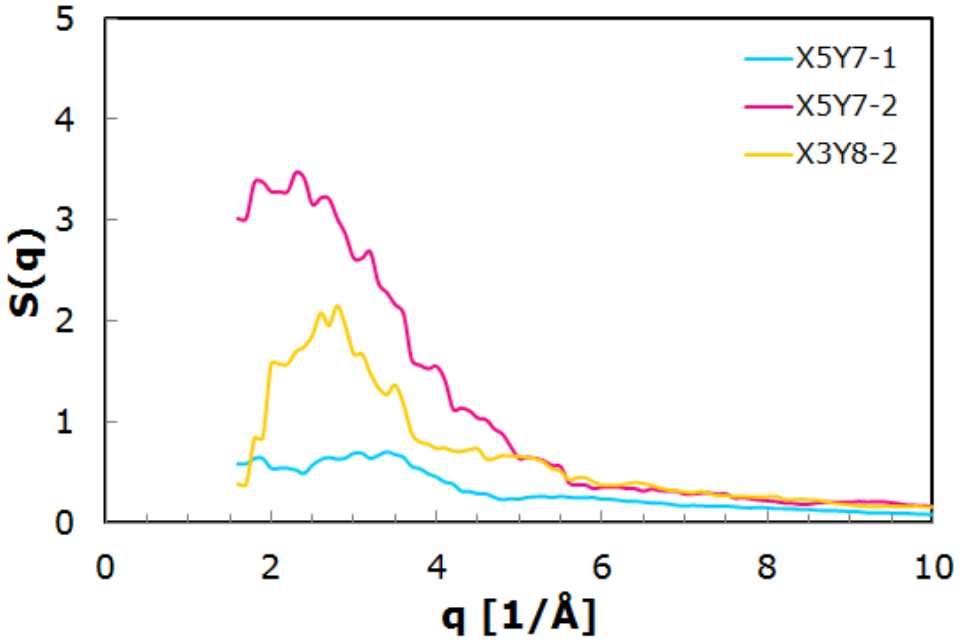

Figure 36: Structure factor profiles calculated from X5Y7-1 (blue), X5Y7-2 (pink), and X3Y8-2 (yellow). The interdomain spacing calculated from qmax are 1.8, 2.7, and 2.2 nm for X5Y7-1, X5Y7-2, and X3Y8-2 respectively.

Transport Property Analysis

A final indication of the AEM performance is determined from the transport properties. The mean squared displacement provides information regarding the mobility of water and hydroxide in the hydrated membrane. The MSD for water and hydroxide are shown in Figure 37 and Figure 38, respectively. The overall displacement of both water and hydroxide indicate that the respective molecules exhibit the highest mobility in the X_5Y_7-2 membrane and the lowest in X_5Y_7-1. In particular, the displacement of water and hydroxide in X_5Y_7-2 are much higher than the other membranes, which is mainly due to

the abnormally high water content (~50 wt %) in the membrane, compared to other polymer electrolyte membranes. A more quantitative indicator of the transport properties is the vehicular diffusivity of water and hydroxide.

Table 18: Vehicular diffusion coefficients for X_5Y_7-1, X_5Y_7-2, and X_3Y_8-2 at 353.15 K

	D ($\times 10^{-5}$ cm^2/s)	
Simulation	**Water**	**Hydroxide**
X_5Y_7-1	0.0305	0.0031
X_5Y_7-2	0.5051	0.2078
X_3Y_8-2	0.1099	0.0238

Table 18The diffusivities of the simulated membranes (Table 18) are calculated from the slope of the MSD as described earlier in the chapter. The diffusion coefficients of water and hydroxide show the same trend as those found in the simulated nanophase-segregation. The mobility of hydroxide ions is significant as it relates directly to the conductivity of ions in the membrane. As described in equation 7, the conductivity increases as diffusivity of the hydroxide ion increases. However, the diffusivities calculated diffusivities in Table 18 only represent the vehicular diffusion and do not take into account any secondary diffusion mechanism, such as ion hopping. Still, the trends found in the vehicular diffusivity of the hydroxide ions agree with the trends shown in the experimentally measured conductivities. This trend is also likely to be found for the ion hopping contribution of the hydroxide diffusivity. For verification, the structural or Grotthuss diffusion of hydroxide ions is necessary to accurately determine the total diffusivity and calculate the conductivity of a simulated membrane. However, this estimation of ion hopping in anion exchange membranes is unique to that in proton exchange membranes and requires a different treatment. Some examples of

computational calculations of hydroxide hopping have been performed, but rely on reactive force fields, which are not used in this work.[43] For future study, we plan to develop a computational approach to approximating ion hopping in anion exchange membranes using a transition state-theory approach, similar to that performed for proton exchange membranes as described earlier.

One last discussion should be made regarding the calculated diffusivities in the simulated anion exchange membranes. The diffusivities, similar to the calculated mean squared displacement, show X_5Y_7-2 to have a significantly larger value than the other membranes in this study. The diffusivities of both water and hydroxide in X_5Y_7-2 are an order of magnitude larger than those in other membranes. A potential explanation of this is likely due to the relatively high water content in the X_5Y_7-2 model. Initially, this discrepancy is alarming as the differences in conductivity from the experimental membranes are not as dissimilar. However, the simulated membranes are much smaller in scale, and local differences are likely amplified. The ~50 wt % water level in X_5Y_7-2 results in much larger phase segregation than observed in the other membranes. In a simulated system, this could result in a much higher calculated MSD and diffusivity. Conversely, the 8 % water uptake in X_5Y_7-1 is also unexpectedly low. The small-scale of the MD simulation, combined with the low water content, may result in calculated diffusivity lower than that measured experimentally. Still, the ordering results and magnitude of the diffusivities calculated provide valuable guidance for future study and design of AEMs. Thus, we think that our molecular dynamics simulations in this study provide a qualitative understanding of diffusivity trends. In order to investigate the transport properties of these membranes more quantitatively, we plan to develop a larger-

scale coarse-grained simulation approach. We also plan to implement a transition state theory based method for the hopping mechanism of hydroxide in the water phase.

To confirm whether the calculated transport properties are affected by longer time-scale simulations, an additional 30 ns equilibrium NPT simulation was completed for the three polymers. The trajectories of the 30 ns simulations were used to calculate the mean squared displacement of water and hydroxide ions, and subsequently, their respective diffusivities in the polymer membranes. These diffusivities show agreement with the initial 5 ns simulation study. Thus, it can be concluded that the diffusivity results presented in Table 18 reflect the equilibrium transport properties for the respective polymer membranes.

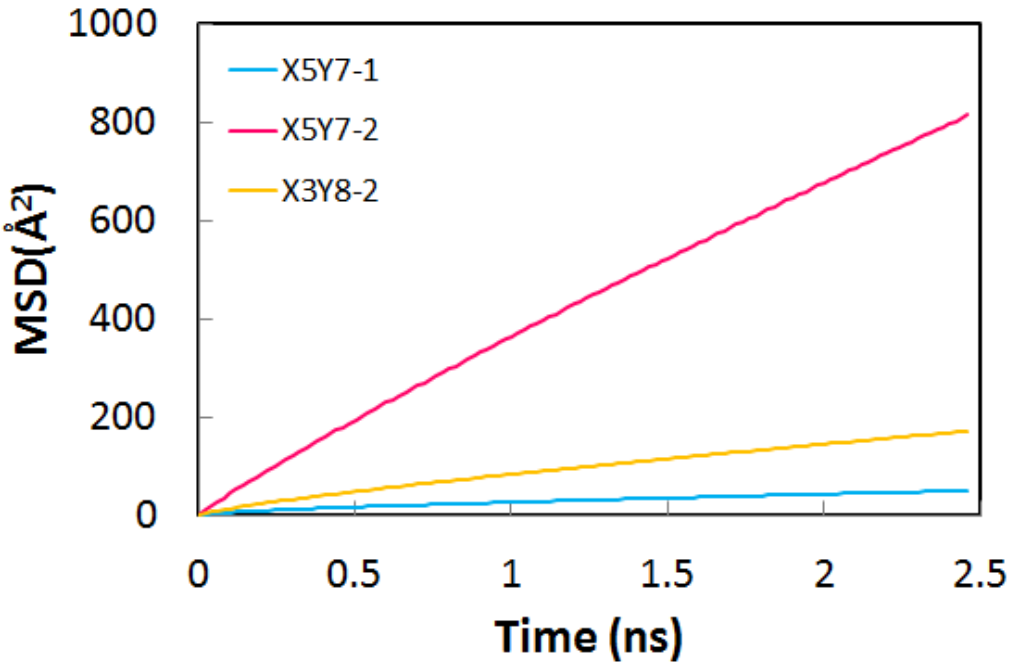

Figure 37: Mean squared displacement of water ions in block copolymer anion exchange membranes

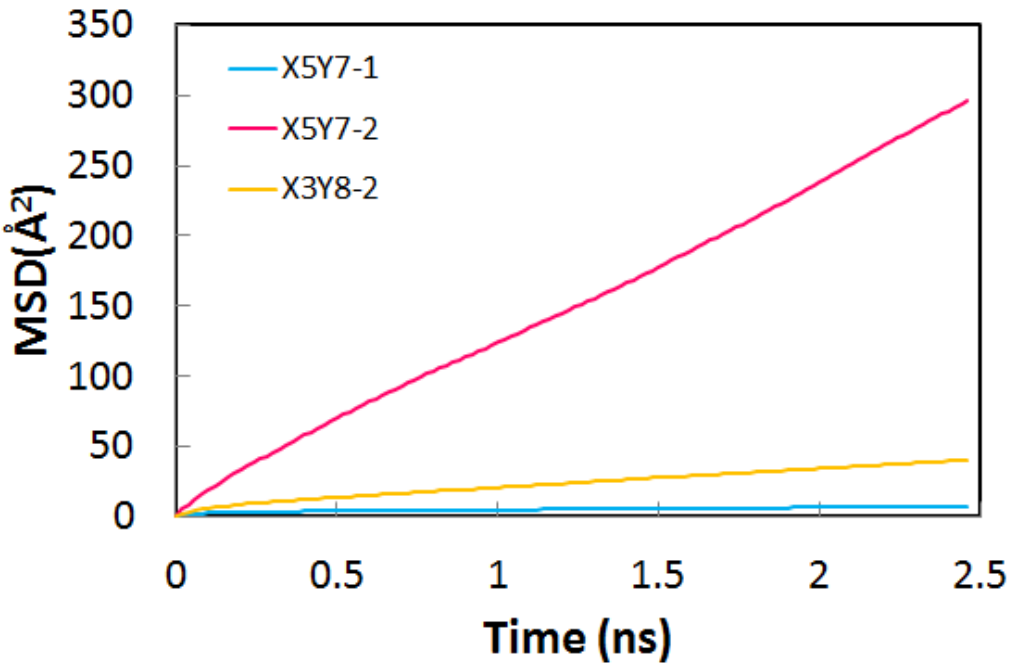

Figure 38: Mean squared displacement of hydroxide ions in block copolymer anion exchange membranes

Summary

First, we performed molecular dynamics simulations of a hydrocarbon-based anion exchange membrane (PSU-A) and proton exchange membrane (PSU-S) to compare their nanophase-segregated structures and transport properties. For this purpose, we prepare the same molecular structures for both membranes except for the ionic groups and corresponding counterions: the quaternary ammonium and hydroxide for PSU-A and the sulfonate and hydronium for PSU-S.

The distribution of quaternary ammonium is investigated using the pair correlation function (PCF) of the nitrogen-nitrogen pair, showing that the distance between ammonium groups is increased with increasing water content. This is similarly observed in the PCF of the sulfur-sulfur pair in PSU-S. Such solvation of quaternary

ammonium and sulfonate by water molecules are also analyzed through the PCF of the nitrogen-oxygen (water) pair and the sulfur-oxygen (water) pair, respectively. It is observed that the solvation shell of the ammonium group is larger than that of the sulfonate group, meaning that the number of water molecules in the first solvation shell of the ammonium is more than that of the sulfonate. This is mainly due to the bulkier size of the ammonium group.

The consequence of such solvation of ionic groups is found consistently in the correlation between the ionic groups and their counterions. As the ionic groups are solvated more, the correlation of the ionic group with its counterion is weakened. It should be noted that the PCF of the ammonium-hydroxide pair is much weaker than that of the sulfonate-hydronium pair. We think that this is due to the bulky three methyl groups surrounding nitrogen that screens the electrostatic interaction with hydroxide, in addition to the better solvation of the hydroxide compared to the hydronium. Consequently, such better solvation of the hydroxide anion affects the hydrogen-bonding network of the water phase, especially at low water content condition.

The extent of nanophase-segregation is characterized using structure factor analysis. While the characteristic correlation length in PSU-A membrane has similar value with that in PSU-S membrane, the intensity of the structure factor of PSU-A is larger than that of PSU-S at 20 wt % of water content due to the larger concentration contrast between the water phase and the polymer backbone phase in the PSU-A membrane compared to the PSU-S membrane. This means that the PSU-A membrane attains more nanophase-segregation, which is mainly due to better solvation of the quaternary ammonium and hydroxide.

Within such nanophase-segregated structures, the diffusion of the hydroxide anion in PSU-A is observed to be ~ 6 % and ~ 11 % of that of the hydronium in PSU-S at 10 wt % and 20 wt % of water content, respectively, although the PSU-A has a more enhanced nanophase-segregated structure. It is thought that such lower diffusion of hydroxide might be due to the larger effective size of the $OH^- - H_2O$ cluster, and the distinctively strong $OH^- - OH^-$ correlation at ~ 4 Å in PSU-A, which is not observed from the $H_3O^+ - H_3O^+$ correlation in PSU-S.

In deformed PSU-based structures, a significant improvement in diffusivity was only observed for water in the proton-conducting version of the membrane. This is likely due to the higher extent of the nanophase segregation for PSU-S particularly in the directions perpendicular to the stretching direction. The extent of segregation is nearly identical to the undeformed membrane. The PSU-A structure shows a lower extent of phase segregation, and similarly, a smaller relative improvement in water diffusivity following deformation.

Following these simulations, we then performed MD simulation of three newly synthesized hydrated anion exchange polymer membranes. We found strong agreement between the structure and transport properties observed in our simulations with experimental measurements. Notably, the presence of a third peak of the quaternary ammonium-quaternary ammonium pair correlation in the two-branch polymer membrane suggests a new understanding of the membrane structure. This could indicate that intra-molecular quaternary ammonium groups are far apart from each other, forcing a rearrangement of the polymer backbone. Instead, the addition of tether groups may cause a reorientation of the polymer backbone, resulting in a more conductive membrane.

Additionally, the vehicular diffusion trends show strong agreement with the measured conductivities. We suggest incorporating the full hydroxide transport mechanism in future studies to better model ionic conductivity.

CHAPTER 6

SUMMARY

From the deformation simulations of Nafion, PSU-S, and PSU-A, it can be definitively concluded that the transport of water is enhanced following deformation. The overall phase segregation is shown to be more intense in the directions perpendicular to draw, while greatly reduced along the stretching axis. This suggests that water channels are better-developed through-plane. In the context of fuel-cell applications, this implies that transport properties are more enhanced in through the MEA. While a relationship between deformation and membrane performance has been established, we recommend that future simulation work focus investigating other aspects of fuel-cell membrane performance.

For hydrocarbon-based polymer membranes, a number of superacidic polymers containing different fluoroalkyl sulfonate groups were studied. The membrane containing short –OCF2SO3H pendant showed smaller hydrophilic domain size and lower proton conductivity than the membrane containing –OCF2CF2SO3H because of its less favorable aggregation of sulfonate groups and lower acidity. Also, polymer with branched sulfonate sidechain structure (PSU-S_6) produced larger interdomain size and more distinct phase separation behavior compared to other linear fluoroalkyl sulfonated polymers. We recommend future work in this area to investigate the addition of more sulfonate group tethers to the side chain structures. This is due to the improved performance in the two-tethered PSU-S_6 membrane when compared to the other single-

tether polymer membranes. This modification should increase IEC and drive greater phase segregation, ultimately resulting in more facile transport and higher conductivity.

For our study of anion exchange membranes, strong agreement was found between the structure and transport properties observed in our simulations with experimental measurements of newly synthesized AEMs. Our simulations focused on a number of block copolymers with multiple quaternary ammonium tethers per monomer unit. These structures are necessary to address the inherent transport deficiencies of AEMs when compared to PEMs of the same backbone. Thus, we suggest seeking AEMs with higher IEC while restricting water uptake. Notably, the presence of a third peak in the two-tether polymer quaternary ammonium-quaternary ammonium pair correlation profile suggests a new understanding of the membrane structure. This could indicate that intra-monomer quaternary ammonium groups are oriented far apart, forcing a rearrangement of the polymer backbone. Additionally, the vehicular diffusion trends show strong agreement with the measured conductivities.

For the newly synthesized anion exchange membranes, we suspect increasing the number of ionic groups may not directly contribute to the increase in IEC. Instead, the addition of tether groups may cause a reorientation of the polymer backbone, resulting in a more conductive membrane. To better understand these systems, we suggest the incorporation of full hydroxide diffusivity in future studies. We also recommend pursuing larger-scale, coarse grained molecular dynamics simulations of these new membranes.

APPENDIX A

SUPPORTING INFORMATION FOR PSU SIMULATIONS

This section includes relevant sections of the supporting information for the work presented in Chapter 4. It is included for completeness and was previously published in a paper published with our collaborators.[90]

Spectroscopic Characterization

^{1}H, ^{19}F and ^{13}C NMR spectra were obtained using a Varian NMR spectrometer (400 MHz for ^{1}H, 376 MHz for ^{19}F, and 100 MHz for ^{13}C) at room temperature and chemical shifts were referenced to TMS (^{1}H and ^{13}C) and $CFCl_3$ (^{19}F). GC/MS analysis was conducted using a Shimadzu QP2010S equipped with a 30 m × 0.25 mm SHR-XLB GC column and an EI ionization MS detector.

Analysis of O-D stretching band by Fourier transform infrared spectroscopy

Thin films of sulfonated polysulfone in sodium form were cast from dimethyl sulfoxide onto CaF_2 windows, dried at 50°C for 4 h, then at 80°C for 6 h and placed in an FTIR transmission flow cell (Model 64100-F, New Era Enterprises, Vineland, NJ). Humid air containing 5 mol % D_2O was flowed (20 std. cm^3 s^{-1}) through the cell while spectra were recorded using a Bruker (Billerica, MA) VERTEX 70 spectrometer with a nitrogen-cooled mercury-cadmium-telluride (MCT) detector. Humidification of the flowing air through the FTIR cell was achieved by dew-point mixing of fully-humidified and dry air streams. Air at dewpoint was produced by a water sparging system, and was then mixed with a dry air stream at controlled mass flow ratios to yield a range of relative

humidities. The relative humidity (RH) of the mixed stream was measured using an RH probe (Omega HX15-W, Omega Engineering, Inc., Stamford, CT) before being introduced to the measurement cell at the same temperature as the system. Each RH corresponded to a different hydration number (λ = mole of water/mole of sulfonate group) depending on the polymer sample. Hydration numbers were measured using a TA Instruments Q5000SA water vapor sorption analyzer and reported as a function of RH. Each spectrum was recorded at 2 cm^{-1} resolution and 100 scans. The hydrated spectra were obtained by using the dry polymer as a reference. Spectra were extracted from 2700 cm^{-1} and 2400 cm^{-1} and baselined by setting the absorbance equal to 0 at those two points. Peak fitting was performed using Origin 8.0 (OriginLabs, Northhampton, MA) data analysis software. Three Gaussian peaks were used to fit the OD region from 2700 cm^{-1} to 2400 cm^{-1}. One peak corresponding to bulk-like water, was held constant for all samples and was centered at 2509 cm^{-1} with a constrained FWHM of 170 (signature of HOD in bulk water), while the headgroup-associated and intermediate water peaks varied by sample. The peak positions and FWHM for headgroup-associated and intermediate water were determined by fitting the lowest RH samples with three peaks, the third peak being bulk water with peak position of 2509 cm^{-1} and FWHM of 170. The peak shape (peak position and FWHM) of the head-group associated water was held constant throughout the remainder of the fitting at each RH. The intermediate peak position was held constant but the FWHM was allowed to vary. Once fit, the areas are corrected for non-Condon effects.[164]

Supporting Figures

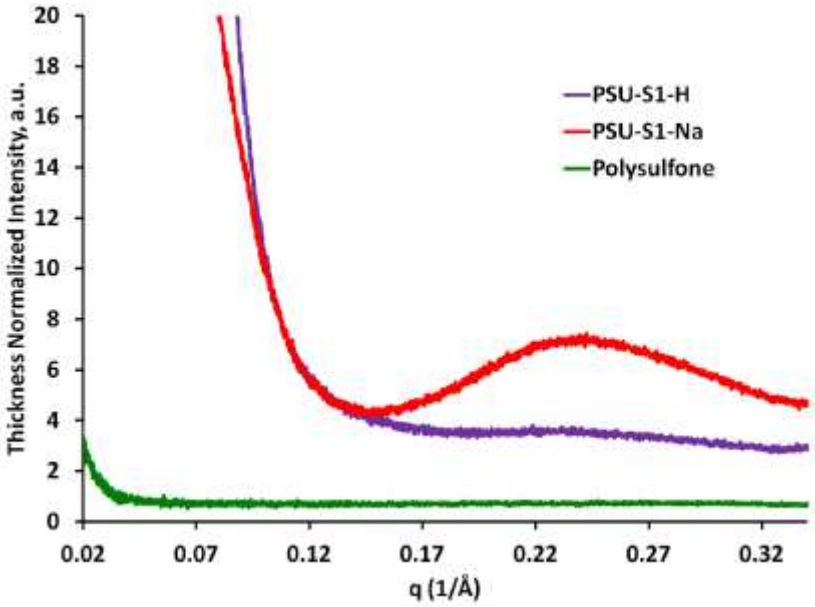

Figure 39: SAXS profiles of polysulfone (green line) and PSU-S_1 in acid (purple) and sodium salt (red) forms.

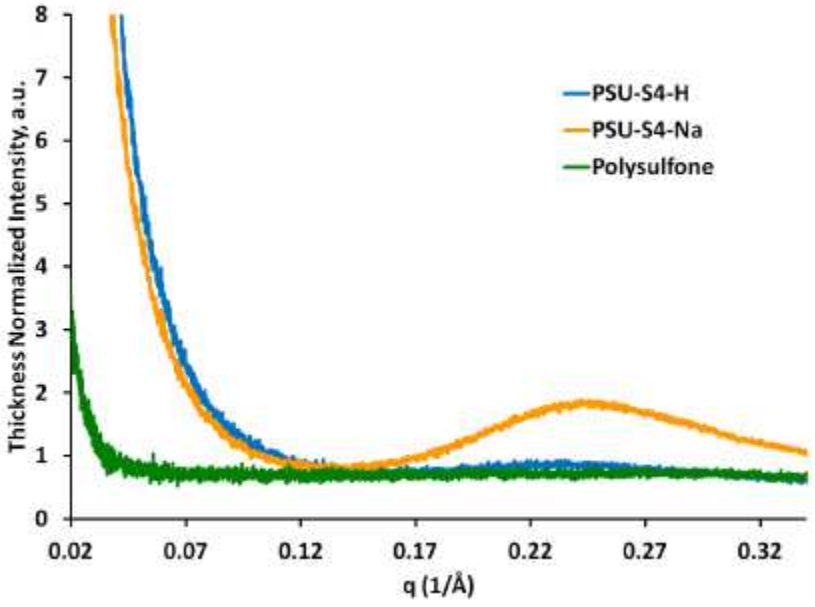

Figure 40: SAXS profiles of polysulfone (green line) and PSU-S_4 in acid (blue) and sodium salt (orange) forms.

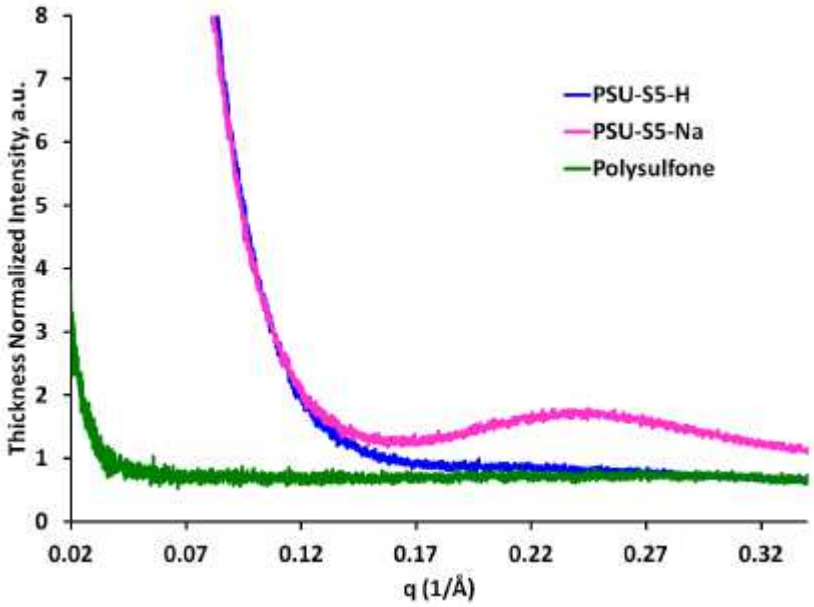

Figure 41: SAXS profiles of polysulfone (green line) and PSU-S_5 in acid (blue) and sodium salt (pink) forms.

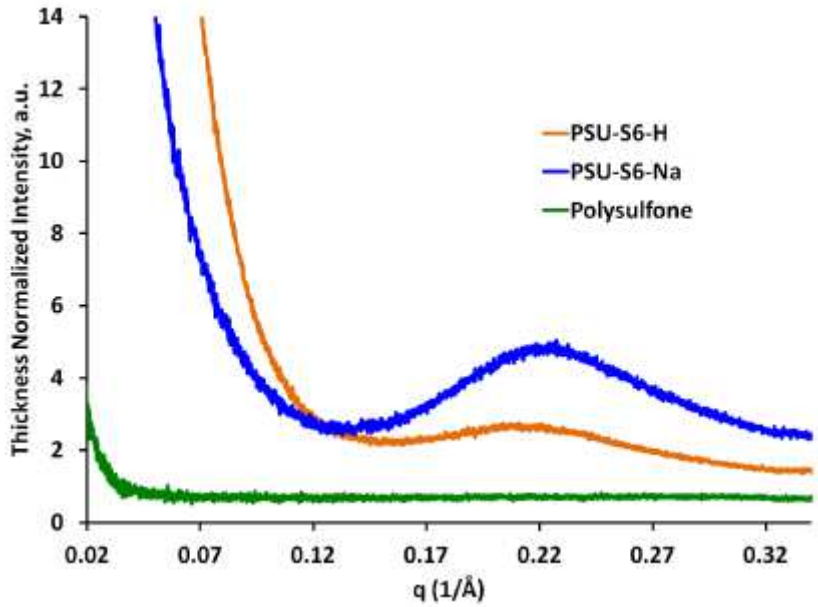

Figure 42: SAXS profiles of polysulfone (green line) and PSU-S_6 in acid (orange) and sodium salt (blue) forms.

APPENDIX B

SOURCE CODE FOR STRUCTURE FACTOR CALCULATION

This section contains the source code for calculating the structure factor of hydrated polymer membranes. The calculation first requires converting the structure into a lattice of hydrophilic and hydrophobic elements, denoted by the coordinates and assigned values of 1 or -1, respectively. Two scripts are used to complete the calculation.

Lattice Processing Code

```
#include <stdlib.h>
#include <string.h>
#include <math.h>
#include <stdio.h>
#include "information.h"
//#include "util.c"
#include "readbgf.c"


int main(int argc, char *argv[])
{
        char lattice_file_name[512];
        FILE *lattice_F;
        char line[MAX_LINE_LENGTH];
        int i,j,k,k2, lattice_size;
        int id,x,y,z;
//        char hydrophobic_file_name[512] = "hydrophobic_";
 //       char hydrophilic_file_name[512] = "hydrophilic_";

  if (argc <3) {
     printf("Usage: %s structure.bgf(input) structure.lat(output)\n",argv[0]);
     exit(1);
  }

//        strcpy(connolly_file_name,argv[1]);
        strcpy(bgffilename,argv[1]);
        strcpy(lattice_file_name,argv[2]);
//        range = (double)(atoi(argv[3]));
    printf (" structure file=%s\n lattice file=%s\n", bgffilename,lattice_file_name);
readbgf();

lattice_F=fopen(lattice_file_name,"wt");
printf ("pbc : %lf %lf %lf\n",pbc_x,pbc_y,pbc_z);
lattice_size=((int)pbc_x)+1;
lattice_size=lattice_size*lattice_size*lattice_size;
//fprintf(lattice_F,"%d\n",lattice_size);
printf("lattice_dimension (l2) =%d\n total lattice number=%d\n",((int)pbc_x)+2,lattice_size);
k=0;k2=0;
```

```
for (i=0;i<total_no_atoms;i++) {
id=0;
if (strcmp(atoms[i].potential,"O_F3C")==0) id=1;
if (strcmp(atoms[i].potential,"H_F3C")==0) id=1;
if (strcmp(atoms[i].potential,"O_OH")==0) id=1;
if (strcmp(atoms[i].potential,"H_OH")==0) id=1;
if (strcmp(atoms[i].potential,"O_H3O")==0) id=1;
if (strcmp(atoms[i].potential,"H_H3O")==0) id=1;
if (strcmp(atoms[i].potential,"O_2")==0) id=-1;
if (strcmp(atoms[i].potential,"O_2a")==0) id=1;
if (strcmp(atoms[i].potential,"O_3")==0) id=-1;
if (strcmp(atoms[i].potential,"S_3")==0) id=1;
if (strcmp(atoms[i].potential,"C_3T")==0) id=-1;
if (strcmp(atoms[i].potential,"O_R")==0) id=-1;
if (strcmp(atoms[i].potential,"C_3")==0) id=-1;
if (strcmp(atoms[i].potential,"C_")==0) id=-1;
if (strcmp(atoms[i].potential,"F_")==0) id=-1;
if (strcmp(atoms[i].potential,"F_3")==0) id=-1;
if (strcmp(atoms[i].potential,"N_3")==0) id=1;
if (strcmp(atoms[i].potential,"C_R")==0) id=-1;
if (strcmp(atoms[i].potential,"H_")==0) id=-1;

x=(int)(atoms[i].x[0])+1;
y=(int)(atoms[i].x[1])+1;
z=(int)(atoms[i].x[2])+1;
if (id==1) k++;
if (id==-1) k2++;
      fprintf(lattice_F,"%d %d %d %d\n",x,y,z,id);
}


printf("No. of hydrophilic lattice=%d\n",k);
printf("No. of hydrophobic lattice=%d\n",k2);
printf("Done.\n");

fclose(lattice_F);
}
```

Structure Factor Calculation Code

```c
/* ------------------------------------------------------

   Program for the calculation of the structure factor

------------------------------------------------------ */
#include <stdio.h>
#include <stdlib.h>
#include <math.h>
#include <string.h>
#define ls 55
#define l2 56
//#define element 4
//int LAT[l2][l2][l2][element];
int LAT[l2][l2][l2];
//#define lat(a,b,c,e) LAT[a][b][c][e]
#define lat(a,b,c) LAT[a][b][c]
#define PI 3.141592654
#define dr 1
#define maxr 20
#define maxs 10000
#define total_lattice ls*ls*ls
#define na 5343  /* no. of A segment hydrophilic */
#define nb 9384 /* no. of B segment hydrophobic */
double sval[dr*10*maxr*2][2];
double scs[maxs][2];

int main(int argc, char *argv[])
{

    int x,y,z,lat1,lat2,lat3,id;
    char name1[50],name2[50];
    FILE *fp1,*fp2;
    double piavg, piavg2;
    int i,j,k;
    int rx,ry,rz,xx,yy,zz,xx2,yy2,zz2;
    double corr,corr0,con1,con2,dist;
    int count, nx,ny,nz;
    double ll1,ll2,zero,st, fir, sec;

    if (argc <3)
    {
        printf("Usage: %s structure.lat(input) structure.sf(output)\n",argv[0]);
       exit(1);
    }

    strcpy(name1,argv[1]);
    strcpy(name2,argv[2]);

    fp1=fopen(name1,"rt");
```

```
50
51  printf("\n In loading file.....\n") ;
52
53      //fscanf(fp1,"%*d\n");
54      for (i=0;i<total_lattice;i++)
55      {
56        fscanf(fp1,"%d %d %d %d\n",&lat1,&lat2,&lat3,&id);
57        lat(lat1,lat2,lat3)=id;
58     }
59      fclose(fp1);
60
61      for (i=0;i<(dr*10*maxr*2);i++)
62      {
63          for (j=0;j<2;j++)
64          {
65              sval[i][j]=0.0;
66          }
67      }
68
69      for (i=0;i<maxs;i++)
70      {
71      for (j=0;j<2;j++)
72          {
73          scs[i][j]=0.0;
74          }
75      }
76
77
78       printf("\n Calculating the structure factor.\n");
79
80      piavg=((double)(nb-na))/((double)(ls*ls*ls));
81      piavg2=piavg*piavg;
82
83
84
85
86      for (rx=0;rx<(ls/2);rx++)
87      {
88          printf("%d \n",rx);
89          for (ry=(-1)*(ls/2);ry<(ls/2);ry++)
90          {
91              for (rz=(-1)*(ls/2);rz<(ls/2);rz++)
92              {
93
94                  /* printf("(%d %d %d)\n",rx,ry,rz); */
95
96                  if (rx==0)
97                  {
98                      if (ry<0) continue;
```

```
99                  if (ry==0)
100                 {
101                 if (rz<0) continue;
102             }
103             }
104
105             corr=0.0;
106
107             for (xx=1;xx<=ls;xx++)
108             {
109                 for (yy=1;yy<=ls;yy++)
110                 {
111                     for (zz=1;zz<=ls;zz++)
112                     {
113                     if (lat(xx,yy,zz)==-1){ con1=-1.0;}
114                         else if (lat(xx,yy,zz)==1) { con1=1.0;}
115                         else
116                         {
117                         corr=corr-piavg2;
118                         continue;
119                     }
120                         xx2=xx+rx;
121                         yy2=yy+ry;
122                         zz2=zz+rz;
123                         if (xx2>ls) xx2=xx2-ls;
124                         if (yy2>ls) yy2=yy2-ls;
125                         if (zz2>ls) zz2=zz2-ls;
126                         if (xx2<1) xx2=xx2+ls;
127                         if (yy2<1) yy2=yy2+ls;
128                         if (zz2<1) zz2=zz2+ls;
129                         if (lat(xx2,yy2,zz2)==-1){con2=-1.0;}
130                         else if (lat(xx2,yy2,zz2)==1) { con2=1.0;}
131                         else { con2=0.0;}
132
133                         corr=corr+con1*con2-piavg2;
134
135                     }
136                 }
137             }
138
139             if ((rx==0)&&(ry==0)&&(rz==0))
140             {
141             corr0=corr/((double)(ls*ls*ls));
142             continue;
143             }
144
145             count=0;
146             for (nx=0;nx<maxr;nx++)
147             {
```

```
                    for (ny=0;ny<maxr;ny++)
                    {
                        for (nz=0;nz<maxr;nz++)
                        {
                            dist=sqrt((double)(nx*nx+ny*ny+nz*nz));
                            if (dist>((double)(maxr))) continue;
                            scs[count][0]=dist;
                            scs[count][1]+=cos(2*PI*(nx*rx+ny*ry+nz*rz)/((double)(ls*dr)))*corr/((double)(ls*ls*ls));
                            count=count+1;
                    }
                    }
                }

            }
        }
    }

    for (i=0;i<=maxs;i++)
    {
        scs[i][1]=scs[i][1]*2+corr0;
    }

    for (i=0;i<maxs;i++)
    {
        for (j=0;j<2*maxr;j++)
        {
            for (k=0;k<10;k++)
            {
                ll1=(double)(j-0.5+k/10.0);
            ll2=(double)(j+0.5+k/10.0);

            if ((scs[i][0]>=ll1)&&(scs[i][0]<=ll2))
            {
                sval[(int)(10*(j+k/10.0))][0]+=scs[i][1];
                sval[(int)(10*(j+k/10.0))][1]+=1.0;
            }

            }
        }
    }
```

```
    zero=fir=sec=0.0;
    fp2=fopen(name2,"wt");
    for (i=0;i<(10*maxr*2*dr);i++)
    {
        if (sval[i][1]==0) continue;
        st=sval[i][0]/sval[i][1];

        fprintf(fp2,"%.2f    %f\n",((double)i)/(10.0*((double)dr)),st);
        if ((((double)i)/(10.0*dr) >=1.0)&&(((double)i)/(10.0*dr) <=(double)(maxr/dr-2.0)))
        {
            zero+=st;
            fir+=st*2*PI*(double)i/(10.0*dr*ls);
            sec+=st*(2*PI*(double)i/(10.0*dr*ls))*(2*PI*(double)i/(10.0*dr*ls));
        }
    }
    fprintf(fp2,"%f    %f\n",fir/zero,sqrt(sec/zero));
    fclose(fp2);

    printf("\n The Calculation is over.\n");

}
```

APPENDIX C

TCL SCRIPT FOR RDF, MSD, AND PROPERTY ANALYSIS

The script below is an example used to analyze the results of molecular dynamics simulation trajectories. Statistical properties, mean squared displacement, and radial distribution function profiles were obtained using modified versions of the script below for each simulated membrane.

```
#################################################################
# # Script to plot RDF & Volume for a MD trajectory
# # Cerius2: Version 4.10
#################################################################

# Initialize
CRYSTAL/ENABLE_DISPLAY_STYLE_MAINTENANCE  YES
CRYSTAL/AUTO_CRYS_BONDS  NO
##
# Load Structure and Trajectory
FILES/LOAD  "./X3Y8_2_2_4Chains_128_OH_1653_H2O_050.msi"
MD_ANALYSIS/TRAJECTORY  "./X3Y8_2_2_4Chains_128_OH_1653_H2O_NPT_353K_5ns_4_c2.trj"
##
# Specify RDF parameters
MD_ANALYSIS/RDF_CUTOFF  15
MD_ANALYSIS/RDF_INTERVAL  0.02000
MD_ANALYSIS/RDF_BETWEEN  "FF TYPES"
# Create Graphs
# Nitrogen-Nitrogen pair
MD_ANALYSIS/FIRST_FRAME_NO 1
MD_ANALYSIS/LAST_FRAME_NO 251
MD_ANALYSIS/RDF_TYPE  "N_3" "N_3"
MD_ANALYSIS/RDF
GRAPHS/SAVE-GALLERY  "./analysis/RDF_NN_5ns.grf"
# Shorter cutoff for other pairs
# Specify RDF parameters
MD_ANALYSIS/RDF_CUTOFF  10
MD_ANALYSIS/RDF_INTERVAL  0.02000
MD_ANALYSIS/RDF_BETWEEN  "FF TYPES"
```

```
# Create Graphs
MD_ANALYSIS/FIRST_FRAME_NO 1
MD_ANALYSIS/LAST_FRAME_NO 251
MD_ANALYSIS/RDF_TYPE  "N_3" "O_F3C"
MD_ANALYSIS/RDF
GRAPHS/SAVE-GALLERY  "./analysis/RDF_NH2O_5ns.grf"
MD_ANALYSIS/RDF_TYPE  "N_3" "O_OH"
MD_ANALYSIS/RDF
GRAPHS/SAVE-GALLERY  "./analysis/RDF_NOH_5ns.grf"
MD_ANALYSIS/RDF_TYPE  "O_OH" "O_F3C"
MD_ANALYSIS/RDF
GRAPHS/SAVE-GALLERY  "./analysis/RDF_OHH2O_5ns.grf"
MD_ANALYSIS/RDF_TYPE  "O_F3C" "O_F3C"
MD_ANALYSIS/RDF
GRAPHS/SAVE-GALLERY  "./analysis/RDF_H2OH2O_5ns.grf"
MD_ANALYSIS/RDF_TYPE  "O_OH" "O_OH"
MD_ANALYSIS/RDF
GRAPHS/SAVE-GALLERY  "./analysis/RDF_OHOH_5ns.grf"
##
## PROPERTIES
# Volume
MD_ANALYSIS/SELECT_PROPERTIES  "     Volume"
MD_ANALYSIS/FIRST_FRAME_NO 1
MD_ANALYSIS/LAST_FRAME_NO 251
MD_ANALYSIS/PROFILE
GRAPHS/SAVE-GALLERY  "./analysis/volume_5ns.grf"
#
# Density
MD_ANALYSIS/SELECT_PROPERTIES  "     Density"
MD_ANALYSIS/FIRST_FRAME_NO 1
MD_ANALYSIS/LAST_FRAME_NO 251
MD_ANALYSIS/PROFILE
GRAPHS/SAVE-GALLERY  "./analysis/density_5ns.grf"
#
# POTENTIAL ENERGY
MD_ANALYSIS/SELECT_PROPERTIES  "     Potential Energy"
MD_ANALYSIS/FIRST_FRAME_NO 1
MD_ANALYSIS/LAST_FRAME_NO 251
MD_ANALYSIS/PROFILE
GRAPHS/SAVE-GALLERY  "./analysis/PotEng_5ns.grf"
#
# CELL PARAMETERS
MD_ANALYSIS/SELECT_PROPERTIES  "     Cell Parameters"
MD_ANALYSIS/FIRST_FRAME_NO 1
MD_ANALYSIS/LAST_FRAME_NO 251
MD_ANALYSIS/PROFILE
GRAPHS/SAVE-GALLERY  "./analysis/CellParams_5ns.grf"
```

```
## MSD
# Full 5 ns
MD_ANALYSIS/FIRST_FRAME_NO 1
MD_ANALYSIS/LAST_FRAME_NO 251
# OH
SELECT/FFTYPE RESTART O_OH -SCOPE Model(.)
MD_ANALYSIS/MSD_ATOMS SELECTED
MD_ANALYSIS/MSD
GRAPHS/SAVE-GALLERY  "./analysis/MSD_OH_5ns.grf"
# H2O
SELECT/DESELECT_ALL -SCOPE "ALL MODELS"
SELECT/FFTYPE RESTART O_F3C -SCOPE Model(.)
MD_ANALYSIS/MSD_ATOMS SELECTED
MD_ANALYSIS/MSD
GRAPHS/SAVE-GALLERY  "./analysis/MSD_H2O_5ns.grf"

#################################################################
# END
#################################################################
```

REFERENCES

1. Vishnyakov, A. and A.V. Neimark, *Molecular simulation study of Nafion membrane solvation in water and methanol.* Journal of Physical Chemistry B, 2000. **104**(18): p. 4471-4478.
2. Vishnyakov, A. and A.V. Neimark, *Molecular dynamics simulation of microstructure and molecular mobilities in swollen Nafion membranes.* Journal of Physical Chemistry B, 2001. **105**(39): p. 9586-9594.
3. Jinnouchi, R. and K. Okazaki, *Molecular dynamics study of transport phenomena in perfluorosulfonate ionomer membrane for polymer electrolyte fuel cells.* Journal of the Electrochemical Society, 2003. **150**: p. E66-E73.
4. Jang, S.S., et al., *Nanophase-segregation and transport in Nafion 117 from molecular dynamics simulations: Effect of monomeric sequence.* Journal of Physical Chemistry B, 2004. **108**(10): p. 3149-3157.
5. Savage, J., Y.-L.S. Tse, and G.A. Voth, *Proton Transport Mechanism of Perfluorosulfonic Acid Membranes.* The Journal of Physical Chemistry C, 2014.
6. Han, K.W., et al., *Molecular Dynamics Simulation Study of a Polysulfone-Based Anion Exchange Membrane in Comparison with the Proton Exchange Membrane.* The Journal of Physical Chemistry C, 2014. **118**(24): p. 12577-12587.
7. Lucid, J., et al., *Probing the Structures of Hydrated Nafion in Different Morphologies Using Temperature-Accelerated Molecular Dynamics Simulations.* The Journal of Physical Chemistry C, 2012. **117**(2): p. 774-782.
8. Brunello, G.F., et al., *Effect of temperature on structure and water transport of hydrated sulfonated poly(ether ether ketone): A molecular dynamics simulation approach.* Journal of Renewable and Sustainable Energy, 2011. **3**(4).
9. Liu, J., et al., *On the Relationship between Polymer Electrolyte Structure and Hydrated Morphology of Perfluorosulfonic Acid Membranes.* Journal of Physical Chemistry C, 2010. **114**(25): p. 11279-11292.
10. Knox, C.K. and G.A. Voth, *Probing Selected Morphological Models of Hydrated Nafion Using Large-Scale Molecular Dynamics Simulations.* The Journal of Physical Chemistry B, 2010. **114**(9): p. 3205-3218.
11. Brunello, G.F., et al., *Molecular dynamics simulation study of hydrated sulfonated poly (ether ether ketone) for application to polymer electrolyte membrane fuel cells in comparison with sulfonated polystyrene.* Abstracts of Papers of the American Chemical Society, 2010. **240**.
12. Brunello, G., et al., *A molecular dynamics simulation study of hydrated sulfonated poly(ether ether ketone) for application to polymer electrolyte membrane fuel cells: Effect of water content.* Journal of Renewable and Sustainable Energy, 2009. **1**(3).
13. Selvan, M.E., et al., *Molecular dynamics study of structure and transport of water and hydronium ions at the membrane/vapor interface of Nafion.* Journal of Physical Chemistry C, 2008. **112**(6): p. 1975-1984.

14. Petersen, M.K., A.J. Hatt, and G.A. Voth, *Orientational dynamics of water in the Nafion polymer electrolyte membrane and its relationship to proton transport.* Journal of Physical Chemistry B, 2008. **112**(26): p. 7754-7761.
15. Cui, S., et al., *Comparison of the Hydration and Diffusion of Protons in Perfluorosulfonic Acid Membranes with Molecular Dynamics Simulations.* Journal of Physical Chemistry B, 2008. **112**(42): p. 13273-13284.
16. Jang, S.S. and W.A. Goddard, III, *Structures and transport properties of hydrated water-soluble dendrimer-grafted polymer membranes for application to polymer electrolyte membrane fuel cells: Classical molecular dynamics approach.* Journal of Physical Chemistry C, 2007. **111**(6): p. 2759-2769.
17. Devanathan, R., A. Venkatnathan, and M. Dupuis, *Atomistic simulation of nafion membrane. 2. Dynamics of water molecules and hydronium ions.* Journal of Physical Chemistry B, 2007. **111**(45): p. 13006-13013.
18. Cui, S., et al., *A molecular dynamics study of a nafion polyelectrolyte membrane and the aqueous phase structure for proton transport.* Journal of Physical Chemistry B, 2007. **111**(9): p. 2208-2218.
19. Brandell, D., et al., *Molecular dynamics studies of the Nafion (R), Dow (R) and Aciplex (R) fuel-cell polymer membrane systems.* Journal of Molecular Modeling, 2007. **13**(10): p. 1039-1046.
20. Jang, S.S., et al., *Nanophase segregation and water dynamics in the dendrion diblock copolymer formed from the Frechet polyaryl ethereal dendrimer and linear PTFE.* Journal of Physical Chemistry B, 2005. **109**(20): p. 10154-10167.
21. Plimpton, S.J., R. Pollock, and M. Stevens. *Particle-Mesh Ewald and rRESPA for Parallel Molecular Dynamics Simulations*. in *the Eighth SIAM Conference on Parallel Processing for Scientific Computing*. 1997. Minneapolis.
22. Plimpton, S., *FAST PARALLEL ALGORITHMS FOR SHORT-RANGE MOLECULAR-DYNAMICS.* Journal of Computational Physics, 1995. **117**(1): p. 1-19.
23. Mayo, S.L., B.D. Olafson, and W.A. Goddard, *DREIDING - A GENERIC FORCE-FIELD FOR MOLECULAR SIMULATIONS.* Journal of Physical Chemistry, 1990. **94**(26): p. 8897-8909.
24. Tuckerman, M.E., D. Marx, and M. Parrinello, *The nature and transport mechanism of hydrated hydroxide ions in aqueous solution.* Nature, 2002. **417**(6892): p. 925-929.
25. Agmon, N., *Mechanism of hydroxide mobility.* Chemical Physics Letters, 2000. **319**(3-4): p. 247-252.
26. Merle, G., M. Wessling, and K. Nijmeijer, *Anion exchange membranes for alkaline fuel cells: A review.* Journal of Membrane Science, 2011. **377**(1-2): p. 1-35.
27. Tuckerman, M., et al., *AB-INITIO MOLECULAR-DYNAMICS SIMULATION OF THE SOLVATION AND TRANSPORT OF HYDRONIUM AND HYDROXYL IONS IN WATER.* Journal of Chemical Physics, 1995. **103**(1): p. 150-161.
28. Tuckerman, M., et al., *AB-INITIO MOLECULAR-DYNAMICS SIMULATION OF THE SOLVATION AND TRANSPORT OF H3O+ AND OH- IONS IN WATER.* Journal of Physical Chemistry, 1995. **99**(16): p. 5749-5752.

29. van Duin, A.C.T., et al., *ReaxFF reactive force field for solid oxide fuel cell systems with application to oxygen ion transport in yttria-stabilized zirconia.* Journal of Physical Chemistry A, 2008. **112**(14): p. 3133-3140.
30. van Duin, A.C.T., et al., *ReaxFF: A reactive force field for hydrocarbons.* Journal of Physical Chemistry A, 2001. **105**(41): p. 9396-9409.
31. Schmitt, U.W. and G.A. Voth, *Multistate empirical valence bond model for proton transport in water.* Journal of Physical Chemistry B, 1998. **102**(29): p. 5547-5551.
32. Petersen, M.K., et al., *Excess Proton Solvation and Delocalization in a Hydrophilic Pocket of the Proton Conducting Polymer Membrane Nafion.* J. Phys. Chem. B, 2005. **109**: p. 3727-3730.
33. Schmitt, U.W. and G.A. Voth, *The computer simulation of proton transport in water.* Journal of Chemical Physics, 1999. **111**(20): p. 9361-9381.
34. Paddison, S.J., R. Paul, and K.-D. Kreuer, *Theroetically computed proton diffusion coefficients in hydrated PEEKK membranes.* Phys. Chem. Chem. Phys., 2002. **4**: p. 1151-1157.
35. Paddison, S.J. and R. Paul, *The nature of proton transport in fully hydrated Nafion (R).* Physical Chemistry Chemical Physics, 2002. **4**(7): p. 1158-1163.
36. Paddison, S.J., R. Paul, and T.A. Zawodzinski, *A statistical mechanical model of proton and water transport in a proton exchange membrane.* Journal of the Electrochemical Society, 2000. **147**(2): p. 617-626.
37. Lill, M.A. and V. Helms, *Reaction rates for proton transfer over small barriers and connection to transition state theory.* Journal of Chemical Physics, 2001. **115**(17): p. 7985-7992.
38. Lill, M.A. and V. Helms, *Compact parameter set for fast estimation of proton transfer rates.* Journal of Chemical Physics, 2001. **114**(3): p. 1125-1132.
39. Greeley, B.H., et al., *New Pseudospectral Algorithms for Electronic-Structure Calculations - Length Scale Separation and Analytical 2-Electron Integral Corrections.* Journal of Chemical Physics, 1994. **101**(5): p. 4028-4041.
40. Marten, B., et al., *New model for calculation of solvation free energies: Correction of self-consistent reaction field continuum dielectric theory for short-range hydrogen-bonding effects.* Journal of Physical Chemistry, 1996. **100**(28): p. 11775-11788.
41. Jo, W.H. and S.S. Jang, *Monte Carlo simulation of the order-disorder transition of a symmetric cyclic diblock copolymer system.* Journal of Chemical Physics, 1999. **111**(4): p. 1712-1720.
42. Jo, W.H., et al., *Effects of Ester Interchange Reactions on the Phase Behavior of an Immiscible polyester Blend: Monte Carlo Simulation.* Macromolecules, 1999. **32**(5): p. 1679-1685.
43. Chen, C., et al., *Hydroxide Solvation and Transport in Anion Exchange Membranes.* Journal of the American Chemical Society, 2016. **138**(3): p. 991-1000.
44. Arico, A.S., et al., *Nanostructured materials for advanced energy conversion and storage devices.* Nature Materials, 2005. **4**(5): p. 366-377.
45. Hickner, M.A., et al., *Alternative polymer systems for proton exchange membranes (PEMs).* Chemical Reviews, 2004. **104**(10): p. 4587-4611.

46. Li, Q.F., et al., *Approaches and recent development of polymer electrolyte membranes for fuel cells operating above 100 degrees C.* Chemistry of Materials, 2003. **15**(26): p. 4896-4915.
47. Rikukawa, M. and K. Sanui, *Proton-conducting polymer electrolyte membranes based on hydrocarbon polymers.* Progress in Polymer Science, 2000. **25**(10): p. 1463-1502.
48. Roziere, J. and D.J. Jones, *Non-fluorinated polymer materials for proton exchange membrane fuel cells.* Annual Review of Materials Research, 2003. **33**: p. 503-555.
49. Ulbricht, M., *Advanced functional polymer membranes.* Polymer, 2006. **47**(7): p. 2217-2262.
50. Zhang, H. and P.K. Shen, *Recent Development of Polymer Electrolyte Membranes for Fuel Cells.* Chemical Reviews, 2012. **112**(5): p. 2780-2832.
51. Lin, J., et al., *Direct methanol fuel cell operation with pre-stretched recast Nafion (R).* Journal of Power Sources, 2008. **183**(2): p. 491-497.
52. Venkatnathan, A., R. Devanathan, and M. Dupuis, *Atomistic simulations of hydrated Nafion and temperature effects on hydronium ion mobility.* Journal of Physical Chemistry B, 2007. **111**(25): p. 7234-7244.
53. Devanathan, R., A. Venkatnathan, and M. Dupuis, *Atomistic simulation of nafion membrane: I. Effect of hydration on membrane nanostructure.* Journal of Physical Chemistry B, 2007. **111**(28): p. 8069-8079.
54. Chang, Y., et al., *Aromatic Ionomers with Highly Acidic Sulfonate Groups: Acidity, Hydration, and Proton Conductivity.* Macromolecules, 2011. **44**(21): p. 8458-8469.
55. Chang, Y., et al., *Polymer electrolyte membranes based on poly(arylene ether sulfone) with pendant perfluorosulfonic acid.* Polymer Chemistry, 2013. **4**(2): p. 272-281.
56. Allahyarov, E. and P.L. Taylor, *Simulation Study of the Correlation between Structure and Conductivity in Stretched Nafion.* Journal of Physical Chemistry B, 2009. **113**(3): p. 610-617.
57. Jang, S.S., W.A. Goddard, III, and M.Y.S. Kalani, *Mechanical and transport properties of the poly(ethylene oxide)-poly(acrylic acid) double network hydrogel from molecular dynamic simulations.* Journal of Physical Chemistry B, 2007. **111**(7): p. 1729-1737.
58. Jang, S.S., et al., *Molecular dynamics study of a surfactant-mediated decane-water interface: Effect of molecular architecture of alkyl benzene sulfonate.* Journal of Physical Chemistry B, 2004. **108**(32): p. 12130-12140.
59. Levitt, M., et al., *Calibration and testing of a water model for simulation of the molecular dynamics of proteins and nucleic acids in solution.* Journal of Physical Chemistry B, 1997. **101**(25): p. 5051-5061.
60. Jang, S.S., et al., *The source of helicity in perfluorinated N-alkanes.* Macromolecules, 2003. **36**(14): p. 5331-5341.
61. *Jaguar*. 2008, Schrödinger, LLC: New York, NY.
62. *Cerius*^{2}, in *V.4.11*. 2014, Accelrys, Inc.: San Diego.
63. Swope, W.C., et al., *A COMPUTER-SIMULATION METHOD FOR THE CALCULATION OF EQUILIBRIUM-CONSTANTS FOR THE FORMATION OF*

PHYSICAL CLUSTERS OF MOLECULES - APPLICATION TO SMALL WATER CLUSTERS. Journal of Chemical Physics, 1982. **76**(1): p. 637-649.
64. Hoover, W.G., *CANONICAL DYNAMICS - EQUILIBRIUM PHASE-SPACE DISTRIBUTIONS.* Physical Review A, 1985. **31**(3): p. 1695-1697.
65. Nose, S., *A UNIFIED FORMULATION OF THE CONSTANT TEMPERATURE MOLECULAR-DYNAMICS METHODS.* Journal of Chemical Physics, 1984. **81**(1): p. 511-519.
66. Lin, J., et al., *PEM Fuel Cell Properties of Pre-Stretched Recast Nafion (R)*, in *Proton Exchange Membrane Fuel Cells 8, Pts 1 and 2*, T. Fuller, et al., Editors. 2008. p. 1195-1204.
67. Kreuer, K.D., *Proton conductivity: Materials and applications.* Chemistry of Materials, 1996. **8**(3): p. 610-641.
68. Kreuer, K.D., *Fast proton conductivity: A phenomenon between the solid and the liquid state?* Solid State Ionics, 1997. **94**(1-4): p. 55-62.
69. Kreuer, K.D., *On the complexity of proton conduction phenomena.* Solid State Ionics, 2000. **136**: p. 149-160.
70. Verbrugge, M.W. and R.F. Hill, *ANALYSIS OF PROMISING PERFLUOROSULFONIC ACID MEMBRANES FOR FUEL-CELL ELECTROLYTES.* Journal of the Electrochemical Society, 1990. **137**(12): p. 3770-3777.
71. Verbrugge, M.W. and R.F. Hill, *ION AND SOLVENT TRANSPORT IN ION-EXCHANGE MEMBRANES .1. A MACROHOMOGENEOUS MATHEMATICAL-MODEL.* Journal of the Electrochemical Society, 1990. **137**(3): p. 886-893.
72. Zawodzinski, T.A., et al., *DETERMINATION OF WATER DIFFUSION-COEFFICIENTS IN PERFLUOROSULFONATE IONOMERIC MEMBRANES.* Journal of Physical Chemistry, 1991. **95**(15): p. 6040-6044.
73. J. P. HANSEN, I.R.M., *Theory of Simple Liquids*. 1976: Academic Press.
74. Tuckerman, M.E., *Statistical Mechanics: Theory and Molecular Simulation*. 2010: Oxford University Press.
75. Kreuer, K.D., *On the development of proton conducting polymer membranes for hydrogen and methanol fuel cells.* Journal of Membrane Science, 2001. **185**(1): p. 29-39.
76. Kopitzke, R.W., et al., *Conductivity and water uptake of aromatic-based proton exchange membrane electrolytes.* Journal of the Electrochemical Society, 2000. **147**(5): p. 1677-1681.
77. Zaidi, S.M.J., et al., *Proton conducting composite membranes from polyether ether ketone and heteropolyacids for fuel cell applications.* Journal of Membrane Science, 2000. **173**(1): p. 17-34.
78. Xing, P.X., et al., *Synthesis and characterization of sulfonated poly(ether ether ketone) for proton exchange membranes.* Journal of Membrane Science, 2004. **229**(1-2): p. 95-106.
79. Liu, B.J., et al., *Aromatic poly(ether ketone)s with pendant sulfonic acid phenyl groups prepared by a mild sulfonation method for proton exchange membranes.* Macromolecules, 2007. **40**(6): p. 1934-1944.
80. Kaliaguine, S., et al., *Properties of SPEEK based PEMs for fuel cell application.* Catalysis Today, 2003. **82**(1-4): p. 213-222.

81. Wang, F., et al., *Direct polymerization of sulfonated poly(arylene ether sulfone) random (statistical) copolymers: candidates for new proton exchange membranes.* Journal of Membrane Science, 2002. **197**: p. 231-242.
82. Kim, Y.S., et al., *Effect of Acidification Treatment and Morphological Stability of Sulfonated Poly(Arylene Ether Sulfone)s for Proton Exchange Membranes at Elevated Temperature Operation of Fuel Cell.* Journal of Polymer Science, Part B: Polymer Physics, 2003. **41**: p. 2816-2828.
83. Kim, Y.S., et al., *State of Water of Sulfonated Poly(arylene ether sulfone)s and Nafion and its Effect on Physico-Electrochemical Properties.* Macromolecules, 2003. **36**: p. 6281-6285.
84. Harrison, W.L., et al., *Poly(arylene ether sulfone) copolymers and related systems from disulfonated monomer building blocks: Synthesis, characterization, and performance - A topical review.* Fuel Cells, 2005. **5**(2): p. 201-212.
85. Chang, Y., et al., *Aromatic Ionomers with Highly Acidic Sulfonate Groups: Acidity, Hydration, and Proton Conductivity.* Macromolecules, 2011. **44**(21): p. 8458-8469.
86. Li, N.W., et al., *Polymer Electrolyte Membranes Derived from New Sulfone Monomers with Pendent Sulfonic Acid Groups.* Macromolecules, 2010. **43**(23): p. 9810-9820.
87. Genies, C., et al., *Stability study of sulfonated phthalic and naphthalenic polyimide structures in aqueous medium.* Polymer, 2001. **42**(12): p. 5097-5105.
88. Genies, C., et al., *Soluble sulfonated naphthalenic polyimides as materials for proton exchange membranes.* Polymer, 2001. **42**(2): p. 359-373.
89. Chen, X.B., et al., *Effects of Tetracarboxylic Dianhydrides on the Properties of Sulfonated Polyimides.* Journal of Polymer Science Part a-Polymer Chemistry, 2010. **48**(4): p. 905-915.
90. Suresh, G., et al., *Self-diffusion coefficient of water in Nafion-117 membrane with different monovalent counterions: a radiotracer study.* Journal of Membrane Science, 2005. **250**(1–2): p. 39-45.
91. Hickner, M.A., et al., *Alternative polymer systems for proton exchange membranes (PEMs).* Chem. Rev., 2004. **104**(10): p. 4587-4611.
92. Kreuer, K.D., *Proton conductivity: Materials and applications.* Chem. Mater., 1996. **8**(3): p. 610-641.
93. Kreuer, K.D., et al., *Transport in proton conductors for fuel-cell applications: Simulations, elementary reactions, and phenomenology.* Chem. Rev., 2004. **104**(10): p. 4637-4678.
94. Winter, M. and R.J. Brodd, *What are batteries, fuel cells, and supercapacitors?* Chem. Rev., 2004. **104**(10): p. 4245-4269.
95. Carrette, L., K.A. Friedrich, and U. Stimming, *Fuel Cells - Fundamentals and Applications.* Fuel Cells, 2001. **1**(1): p. 5-39.
96. Mauritz, K.A. and R.B. Moore, *State of understanding of Nafion.* Chem. Rev., 2004. **104**(10): p. 4535-4585.
97. Kim, Y.S., et al., *State of water in disulfonated poly(arylene ether sulfone) copolymers and a perfluorosulfonic acid copolymer (nafion) and its effect on physical and electrochemical properties.* Macromolecules, 2003. **36**(17): p. 6281-6285.

98. Osborn, S.J., et al., *Glass transition temperature of perfluorosulfonic acid ionomers.* Macromolecules, 2007. **40**(10): p. 3886-3890.
99. Alberti, G., et al., *Polymeric proton conducting membranes for medium temperature fuel cells (110-160 degrees C).* J. Membr. Sci., 2001. **185**(1): p. 73-81.
100. Takamuku, S. and P. Jannasch, *Fully Aromatic Block Copolymers for Fuel Cell Membranes with Densely Sulfonated Nanophase Domains.* Macromol. Rapid Comm., 2011. **32**(5): p. 474-480.
101. Xing, P.X., et al., *Sulfonated poly(aryl ether ketone)s containing the hexafluoroisopropylidene diphenyl moiety prepared by direct copolymerization, as proton exchange membranes for fuel cell application.* Macromolecules, 2004. **37**(21): p. 7960-7967.
102. Tian, S.H., Y.Z. Meng, and A.S. Hay, *Membranes from Poly(aryl ether)-Based Ionomers Containing Randomly Distributed Nanoclusters of 6 or 1.2 Sulfonic Acid Groups.* Macromolecules, 2009. **42**(4): p. 1153-1160.
103. Miyatake, K. and M. Watanabe, *Emerging membrane materials for high temperature polymer electrolyte fuel cells: durable hydrocarbon ionomers.* J. Mat. Chem., 2006. **16**(46): p. 4465-4467.
104. Schuster, M., et al., *Sulfonated poly(phenylene sulfone) polymers as hydrolytically and thermooxidatively stable proton conducting ionomers.* Macromolecules, 2007. **40**(3): p. 598-607.
105. Kim, D.S., G.P. Robertson, and M.D. Guiver, *Comb-shaped poly(arylene ether sulfone)s as proton exchange membranes.* Macromolecules, 2008. **41**(6): p. 2126-2134.
106. Bae, B., et al., *Proton-Conductive Aromatic Ionomers Containing Highly Sulfonated Blocks for High-Temperature-Operable Fuel Cells.* Angew. Chem. Int. Ed., 2010. **49**(2): p. 317-320.
107. Zhang, J.L., et al., *High temperature PEM fuel cells.* J. Power Sources, 2006. **160**(2): p. 872-891.
108. Li, Q.F., et al., *Approaches and recent development of polymer electrolyte membranes for fuel cells operating above 100 degrees C.* Chem. Mater., 2003. **15**(26): p. 4896-4915.
109. Einsla, M.L., et al., *Toward improved conductivity of sulfonated aromatic proton exchange membranes at low relative humidity.* Chem. Mater., 2008. **20**(17): p. 5636-5642.
110. Roy, A., et al., *Influence of chemical composition and sequence length on the transport properties of proton exchange membranes.* J. Polym. Sci., Part B: Polym. Phys., 2006. **44**(16): p. 2226-2239.
111. Lee, H.S., et al., *Hydrophilic-hydrophobic multiblock copolymers based on poly(arylene ether sulfone) via low-temperature coupling reactions for proton exchange membrane fuel cells.* Polymer, 2008. **49**(3): p. 715-723.
112. Bae, B., K. Miyatake, and M. Watanabe, *Synthesis and Properties of Sulfonated Block Copolymers Having Fluorenyl Groups for Fuel-Cell Applications.* ACS Appl. Mater. Interfaces, 2009. **1**(6): p. 1279-1286.

113. Tsang, E.M.W., et al., *Considerations of Macromolecular Structure in the Design of Proton Conducting Polymer Membranes: Graft versus Diblock Polyelectrolytes.* J. Am. Chem. Soc., 2007. **129**(49): p. 15106-15107.
114. Matsumura, S., et al., *Ionomers for proton exchange membrane fuel cells with sulfonic acid groups on the end groups: Novel branched poly(ether-ketone)s.* Macromolecules, 2008. **41**(2): p. 281-284.
115. Yang, Y. and S. Holdcroft, *Synthetic strategies for controlling the morphology of proton conducting polymer membranes.* Fuel Cells, 2005. **5**(2): p. 171-186.
116. Ding, J.F., C. Chuy, and S. Holdcroft, *Enhanced conductivity in morphologically controlled proton exchange membranes: Synthesis of macromonomers by SFRP and their incorporation into graft polymers.* Macromolecules, 2002. **35**(4): p. 1348-1355.
117. Mikami, T., K. Miyatake, and M. Watanabe, *Synthesis and Properties of Multiblock Copoly(arylene ether)s Containing Superacid Groups for Fuel Cell Membranes.* J. Polym. Sci., Part A: Polym. Chem., 2011. **49**(2): p. 452-464.
118. Li, H.B., et al., *Poly(arylene ether sulfone) Statistical Copolymers Bearing Perfluoroalkylsulfonic Acid Moieties.* Macromolecules, 2011. **44**(4): p. 694-702.
119. Xu, K., et al., *Highly Conductive Aromatic Ionomers with Perfluorosulfonic Acid Side Chains for Elevated Temperature Fuel Cells.* Macromolecules, 2011. **44**(12): p. 4605-4609.
120. Ghassemi, H., et al., *Poly(arylene ether)s with Pendant Perfluoroalkyl Sulfonic Acid Groups as Proton-Exchange Membrane Materials.* Macromol. Chem. Phys., 2011. **212**(7): p. 673-678.
121. Nakagawa, T., et al., *Polymer Electrolyte Membrane Based on Poly(ether sulfone) Containing Binaphthyl Units with Pendant Perfluoroalkyl Sulfonic Acids.* J. Polym. Sci., Part A: Polym. Chem., 2011. **49**(14): p. 2997-3003.
122. Miyatake, K., et al., *Aromatic ionomers with superacid groups.* Chem. Commun., 2009(42): p. 6403-6405.
123. Plimpton, S.J., *Fast Parallel Algorithms for Short-Range Molecular Dynamics.* J. Comp. Phys., 1995. **117**: p. 1-19.
124. *Cerius2 Modeling Environment, Release 4.0*. 1999, Accelrys Inc.: San Diego.
125. Yeh, K.-Y., et al., *The adsorption of bisulfate and sulfate anions over a Pt(1 1 1) electrode: A first principle study of adsorption configurations, vibrational frequencies and linear sweep voltammogram simulations.* Catalysis Today, 2013. **202**: p. 20-35.
126. Ding, J., C. Chuy, and S. Holdcroft, *A Self-organized Network of Nanochannels Enhances Ion Conductivity through Polymer Films.* Chemistry of Materials, 2001. **13**(7): p. 2231-2233.
127. Jang, S.S., et al., *Nanophse-segregation and transport in Nafion 117 from molecular dynamics simulations: Effect of monomeric sequence.* J. Phys. Chem. B, 2004. **108**: p. 3149-3157.
128. Jang, S.S., et al., *Nanophase-segregation and water dynamics in the dendrion diblock copolymer formed from the Frechet polyaryl ethereal dendrimer and linear PTFE.* J. Phys. Chem. B, 2005. **109**: p. 10154-10167.
129. Jang, S.S. and W.A. Goddard, III, *Structures and Transport Properties of Hydrated Water-Soluble Dendrimer-Grafted Polymer Membranes for Application*

to Polymer Electrolyte Membrane Fuel Cells: Classical Molecular Dynamics Approach. Journal of Physical Chemistry C, 2007. **111**: p. 2759-2769.
130. Brunello, G., et al., *A molecular dynamics simulation study of hydrated sulfonated poly(ether ether ketone) for application to polymer electrolyte membrane fuel cells: Effect of water content.* Journal of Renewable and Sustainable Energy, 2009. **1**(3): p. 033101.
131. Brunello, G.F., et al., *Effect of temperature on structure and water transport of hydrated sulfonated poly(ether ether ketone): A molecular dynamics simulation approach.* Journal of Renewable and Sustainable Energy, 2011. **3**(4): p. 043111.
132. Han, K.W., et al., *Molecular Dynamics Simulation Study of a Polysulfone-Based Anion Exchange Membrane in Comparison with the Proton Exchange Membrane.* Journal of Physical Chemistry C, 2014. **118**(24): p. 12577-12587.
133. Verma, A. and S. Basu, *Direct alkaline fuel cell for multiple liquid fuels: Anode electrode studies.* Journal of Power Sources, 2007. **174**(1): p. 180-185.
134. Coutanceau, C., L. Demarconnay, and J.-M.L. C. Lamy, *Development of electrocatalysts for solid alkaline fuel cell (SAFC).* Journal of Power Sources, 2006. **156**(1): p. 14-19.
135. Nordin, N. *Limitations of Commercializing Fuel Cell Technologies*. in *10th Asian International Conference on Fluid Machinery*. 2010. Univ Teknologi Malaysia, Kuala Lumpur, MALAYSIA.
136. Tripković, A.V., et al., *Methanol electrooxidation on supported Pt and PtRu catalysts in acid and alkaline solutions.* Electrochimica Acta, 2002. **47**(22-23): p. 3707-3714.
137. Varcoe, J.R. and R.C.T. Slade, *Prospects for alkaline anion-exchange membranes in low temperature fuel cells.* Fuel Cells, 2005. **5**(2): p. 187-200.
138. Tuckerman, M.E., A. Chandra, and D. Marx, *Structure and dynamics of OH-(aq).* Accounts of Chemical Research, 2006. **39**(2): p. 151-158.
139. Marx, D., A. Chandra, and M.E. Tuckerman, *Aqueous Basic Solutions: Hydroxide Solvation, Structural Diffusion, and Comparison to the Hydrated Proton.* Chemical Reviews, 2010. **110**(4): p. 2174-2216.
140. Lee, S.G., et al., *Effect of monomeric sequence on transport properties of D-glucose and ascorbic acid in poly(VP-co-HEMA) hydrogels with various water contents: molecular dynamics simulation approach.* Theoretical Chemistry Accounts, 2012. **131**(4).
141. Lee, S.G., et al., *Effect of Monomeric Sequence on Mechanical Properties of P(VP-co-HEMA) Hydrogels at Low Hydration.* Journal of Physical Chemistry B, 2009. **113**(19): p. 6604-6612.
142. Lee, S.G., et al., *Molecular dynamics simulation study of P (VP-co-HEMA) hydrogels: Effect of water content on equilibrium structures and mechanical properties.* Biomaterials, 2009. **30**(30): p. 6130-6141.
143. Jang, S.S., W.A. Goddard, III, and Y. Kalani, *Mechanical and Transport Properties of Poly (Ethylene Oxide) - Poly (Acrylic Acid) Double Network Hydrogel: Molecular Dynamic Simulation Approach.* J. Phys. Chem. B, 2007. **111**: p. 1729-1737.
144. Jang, S.S., et al., *Mechanical and transport properties of the poly(ethylene oxide)-poly(acrylic acid) double network hydrogel from molecular dynamic Simulations*

(vol 111B, pg 1729, 2007). Journal of Physical Chemistry B, 2007. **111**(51): p. 14440-14440.
145. Jang, S.S. and W.A. Goddard, *Structures and properties of newton black films characterized using molecular dynamics simulations.* Journal of Physical Chemistry B, 2006. **110**(15): p. 7992-8001.
146. Jang, S.S., et al., *Structures and Properties of Self-Assembled Monolayers of Bistable [2]Rotaxanes on Au (111) Surfaces from Molecular Dynamics Simulations Validated with Experiment.* Journal of the American Chemical Society, 2005. **127**: p. 1563-1575.
147. Verlet, L., Phys. Rev., 1967. **159**: p. 98-103.
148. Dasgupta, S., T. Yamasaki, and W.A. Goddard, *The Hessian biased singular value decomposition method for optimization and analysis of force fields.* Journal of Chemical Physics, 1996. **104**(8): p. 2898-2920.
149. Dasgupta, S. and W.A. Goddard, *HESSIAN-BIASED FORCE-FIELDS FROM COMBINING THEORY AND EXPERIMENT.* Journal of Chemical Physics, 1989. **90**(12): p. 7207-7215.
150. Markovitch, O. and N. Agmon, *Structure and energetics of the hydronium hydration shells.* Journal of Physical Chemistry A, 2007. **111**(12): p. 2253-2256.
151. Smiechowski, M. and J. Stangret, *Hydroxide ion hydration in aqueous solutions.* Journal of Physical Chemistry A, 2007. **111**(15): p. 2889-2897.
152. Kreuer, K.D., *Proton conductivity: materials and applications.* Chem. Mater., 1996. **8**: p. 610-641.
153. Kreuer, K.D., *On the development of proton conducting materials for technological applications.* Solid state ionics, 1997. **97**: p. 1-15.
154. Kreuer, K.D., *On the complexity of proton conduction phenomena.* Solid state ionics, 2000. **136-137**: p. 149-160.
155. Verbrugge, M.W. and R.F. Hill, *Ion and solvent transport in ion-exchange membranes: II. A radiotracer study of the sulfuric-acid, Nafion-117 system.* J. Electrochem. Soc., 1990. **137**: p. 893-899.
156. Verbrugge, M.W. and R.F. Hill, *Analysis of promising perfluorosulfonic acid membranes for fuel-cell electrolytes.* J. Electrochem. Soc., 1990. **137**(12): p. 3770-3777.
157. Zawodzinski, T.A., et al., *Determination of water diffusion coefficients in perfluorosulfonate ionomeric membrane.* Journal of Physical Chemistry, 1991. **95**: p. 6040-6044.
158. Jo, W.H. and S.S. Jang, *Monte Carlo simulation of the order-disorder transition of a symmetric cyclic diblock copolymer system.* J. Chem. Phys., 1999. **111**(4): p. 1712-1720.
159. Kreuer, K.D., *On the development of proton conducting polymer membranes for hydrogen and methanol fuel cell.* Journal of Membrane Science, 2001. **185**: p. 29-39.
160. Schuster, M., K.D. Kreuer, and J. Maier. *Proton, Water and methanol transport in Nafion and sulfonated polyether ketone based membranes: A microstructural approach*. in *14th international conference on solid state ionics*. 2003. Monterey, USA.

161. Agel, E., J. Bouet, and J.F. Fauvarque, *Characterization and use of anionic membranes for alkaline fuel cells.* Journal of Power Sources, 2001. **101**: p. 267-274.
162. Park, D.-Y., P.A. Kohl, and H.W. Beckham, *Anion-Conductive Multiblock Aromatic Copolymer Membranes: Structure-Property Relationships.* Journal of Physical Chemistry C, 2013. **117**(30): p. 15468-15477.
163. Liu, L., et al., *Anion conducting multiblock copolymer membranes with partial fluorination and long head-group tethers.* Journal of Materials Chemistry A, 2016. **4**(41): p. 16233-16244.
164. Black, S.B., et al., *FTIR Characterization of Water–Polymer Interactions in Superacid Polymers.* The Journal of Physical Chemistry B, 2013. **117**(50): p. 16266-16274.